Coherent Control of Atomic Systems for various Applications: A Theoretical Exploration

A Thesis Submitted
in Partial Fulfillment of the Requirements for the
Degree of Doctor of Philosophy

by

Abdelsalam Hassan Muhammad Abdelaziz

Thesis Supervisor: **Prof. Amarendra Kumar Sarma**

to

Department of Physics
Indian Institute of Technology Guwahati
Guwahati - 781039, India

December, 2021

Dedication

To my mother and my brother

You left me!

But, you left behind beautiful memories everywhere

I miss you

Statement

The work contained in the thesis entitled "**Coherent Control of Atomic Systems for various Applications: A Theoretical Exploration**" has been carried out at the Department of Physics, Indian Institute of Technology Guwahati, India by me under the supervision of Prof. Amarendra Kumar Sarma. The material of this thesis has not been submitted elsewhere for any other degree. Works presented in the thesis are all my own unless referenced to the contrary in the text.

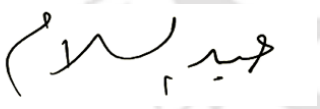

(Abdelsalam Hassan Muhammad Abdelaziz) December 1, 2021
Department of Physics
Indian Institute of Technology Guwahati
Guwahati - 781039, India

Disclaimer

The bibliography included in this thesis is, by no means complete but contains the ones which are consulted thoroughly by me. I apologize for inadvertently missing out some of the research papers, review articles and other scientific documents pertaining to the focus of this thesis which should also have been cited. For illustration purpose some of the figures in this thesis are taken from other sources and properly cited.

Certificate

It is certified that the work contained in the thesis entitled "**Coherent Control of Atomic Systems for various Applications: A Theoretical Exploration**" by Abdelsalam Hassan Muhammad Abdelaziz (Roll No. 166121021), a Ph.D. student of the Department of Physics, Indian Institute of Technology Guwahati is carried out under my supervision and has not been submitted elsewhere for the award of any other degree.

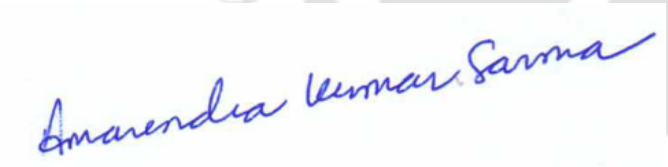

(Prof. Amarendra Kumar Sarma) December 1, 2021
Professor
Department of Physics
Indian Institute of Technology Guwahati
Guwahati - 781039, India

Acknowledgment

I would like to express my earnest gratitude to my supervisor Prof. Amarendra Kumar Sarma for his guidance and constant support, for his patience and kindness, and for being a constant source of motivation throughout my research work. I admire the way he is motivating his students to do hard work through a judicious mix of freedom, responsibility, and accountability!

I would like to express sincere appreciation to my Doctoral Committee Chairman Dr. Kanhaiya Pandey and Doctoral Committee Members Dr. Pankaj Kumar Mishra and Dr. Tapan Mishra for their useful suggestions, feedback and positive criticism which helped me to improve the quality of my research work.

I would like to acknowledge the Indian Council for Cultural Relations (ICCR), Government of India and the Ministry of Higher Education (MoHE), Egypt for support through a research scholarship. This opportunity to do Ph.D. at the Indian institute of Technology Guwahati opened the way for me to learn new things in my career and improve my skills, and most importantly introduced me to the culture of India.

I would like to thank all the HoDs and other faculty members of the Physics department for their friendly behavior and help, whenever it was needed. I would like to thank all the technical and administrative staff of the Physics department for their valuable help whenever it was needed.

I would like to thank our research group members Dr. Parvendra, Dr. Kaushik, Dr. Bijita, Dr. Jyoti, Dr. Monika, Dr. Subhadeep, Dipti, Sampreet, Roson, and Dr. Ambaresh for their support and assistance.

I would like to thank my seniors, and all my 2016 batch mates Dr. Dibyendu, Dr. Sayandeep, Dr. Ogaro, Dr. Suman, Kajal, Mousumi, Abhilasha, Apurba, Dangka, Lopamudra, Abhisek, Nilamoni, Ritupan, Priyanka, Mahananda, Dipti, Sayan, Rakesh, Manvendra, and Rajesh for creating a positive work environment.

I would like to thank my family for their constant love and support during my entire career, especially my son Khalid who was born during my Ph.D. journey at IIT Guwahati bringing joy to our life!

I would like to thank Allah for giving me the opportunity and the strength to accomplish this work.

December 1, 2021 Abdelsalam Hassan Muhammad Abdelaziz

Abstract

Coherent control is a promising technique for manipulating atomic and molecular systems. It has found numerous applications in a wide range of areas such as, ultracold physics, laser cooling, Bose-Einstein condensates, quantum information processing, attosecond physics and high precision spectroscopy. Coherent control of atomic and other quantum systems using laser pulses remains at the forefront of research in physics, chemistry and even in biological sciences. In this thesis, we use laser pulse induced coherent control methods for exploiting atomic systems for some interesting applications. We have proposed a scheme for effective control of optical multistability in a three-level V-type atomic system, which could find applications in optical switching. Also, we put forward a strategy to achieve slow and fast light in a four-level ultracold atomic systems via coherent control. In the last part of the thesis, we propose a novel scheme to obtain effective focusing of a diverging atomic beam using femtosecond laser pulse. All the proposed schemes are analyzed with experimentally realistic parameters, making them to be realized within current state-of-the-art experimental setups.

List of Publications

Journal Publications

[1] **Abdelaziz, Abdelsalam H. M.**, Parvendra Kumar, and Amarendra K. Sarma, "Effective focusing of a diverging atomic beam by a sequence of alternatively chirped few-cycle pulsed laser fields", Phys. Rev. A **99**, 023408 (2019).

[2] **Abdelaziz, Abdelsalam H. M.** and Amarendra K. Sarma, "Effective control and switching of optical multistability in a three-level V-type atomic system", Phys. Rev. A **102**, 043719 (2020).

[3] **Abdelaziz, Abdelsalam H. M.** and Amarendra K. Sarma, "Coherent Control of Hyperfine States and Slow and Fast Light Switching in Ultracold Atoms", arXiv:2107.08897 (2021); The article is under review in Physical Review A.

Conference Publication

[1] **Abdelaziz, Abdelsalam H. M.**, Parvendra Kumar, and Amarendra K Sarma, *Effective focusing of the diverging atomic beam by a sequence of engineered few-cycle pulsed laser fields,* IIT Patna, Dec. 2018.

Conference, School, and Workshop attended

[1] *International Conference on Quantum and Atom Optics, "ICQAO-2018",* IIT Patna, Dec. 2018.

[2] *SERB School on Frontiers in Quantum Optics,* IIT Guwahati, Dec. 2017.

[3] *One-Day Workshop on Vacuum Technology and its Application in Optical Science,* IIT Guwahati, Aug. 2017.

Contents

1 Introduction **1**

1.1 The topics and aim of research 4

1.2 Outline of the thesis 6

2 Coherent Control: Theoretical Background **9**

2.1 Density Matrix Formalism 9

2.2 Field Dynamics Inside the Atomic Medium 15

2.3 Coherent Population Transfer 17

2.4 Electromagnetically Induced Transparency (EIT) 21

2.5 Slow Light 25

2.6 Fast Light 25

2.7 Optical Force 27

2.8 Optical Bistability (OB) 29

3 Effective Control of Optical Multistability **35**

3.1 Brief overview 36

3.2 Model and theory 39

3.3 Results and Discussions 42

3.4 Summary 50

4 Slow and Fast Light in Ultracold Atoms **53**
4.1 Brief overview 53
4.2 Model and theory 56
4.3 Results and Discussions 58
4.4 Summary 66

5 Effective Focusing of an Atomic Beam **67**
5.1 Brief overview 68
5.2 Model and Theory 70
5.3 Results and Discussions 73
5.4 Summary 81

6 Conclusions **83**

A Analytical form of ρ_{31} **87**

Bibliography **91**

List of Figures

2.1 Schematic diagram of a two-level atom interacting with a classical field. 10

2.2 Schematic diagram of a three-level Λ-type atomic system for realizing CPT. 18

2.3 Schematic diagram of a three level Λ-type atomic system for realizing EIT. 21

2.4 $a(\omega_p)$ (in units of $N\omega_p|\mu_{13}|^2/(\varepsilon_0\hbar c)$) vs Δ/γ_{13} as given by Eq. 2.30 for $\gamma_{12}/\gamma_{13} = 0.02$ (a) $\Omega_c = 0$ and (b) $\Omega_c = 3\gamma_{13}$. 24

2.5 Fabry-Pérot resonator. 30

2.6 Illustration of Input-output relations under different cooperation parameter C_0 32

2.7 Schematic illustration of Optical Bistability phenomenon 33

3.1 (a) Three-level V-type atomic system, (b) Unidirectional ring cavity. 40

3.2 Output Characteristics as a function of the normalized parameters: the input field $|y|$ and the susceptibility components χ' and χ''. for different values of probe field detuning Δ_p/γ_{31}: (a) 0.5, (b) 1.0, (c) 1.3, and (d) 2.6. Other parameters are: $\Delta_c = 0$, $\Omega_c = 2.2\gamma_{31}$, and C=100. 45

3.3 Input-Output Characteristics under different control field detunings, Δ_c, with blue-detuning the probe field, Δ_p/γ_{31} : (a) 0.5, (b) 1.0, (c) 1.3, and (d) 2.6. The remaining parameters are: $\Omega_c = 2.2\gamma_{31}$, and C=100. 47
3.4 Input-Output Characteristics under different control field intensities Ω_c. Other parameters: $\Delta_p = 1.0\gamma_{31}$, $\Delta_c = 0.0\gamma_{31}$, and C=100. . 48
3.5 Input-Output Characteristics under different cooperation parameters C. Other parameters: $\Delta_p = 1.0\gamma_{31}$, $\Delta_c = 0.0\gamma_{31}$, and $\Omega_c = 2.2\gamma_{31}$. 48
3.6 Input-Output Characteristics under the combined effect of blue-detuned probe field and red-detuned control field. (a) $\Delta_p/\gamma_{31} = 2.5$ and (b) $\Delta_p/\gamma_{31} = 3.6$. Other parameters are, $\Omega_c = 1.0\gamma_{31}$ and C=100. 49

4.1 Schematic diagram of a four-level atomic system. 58
4.2 Population transfer as a function of field detuning for the Raman transition between the two hyperfine: (a) ground-, (b) excited- states. 60
4.3 Spectra of the real and imaginary components of polarization for the optical transitions between $|3\rangle \leftrightarrow |1\rangle$ [(a) and (b)] and $|4\rangle \leftrightarrow |1\rangle$ [(c) and (d)] 62
4.4 Spectra of the real and imaginary components of the induced polarization for the Raman transitions between the two hyperfine: (a) and (b) ground-, (c) and (d) excited- states. 65

5.1 (a) Three-level laddered atomic system, (b) time dependent frequency of the pulse train in the standard scheme, and in (c) the alternating scheme, for a train of eight pulses. 71
5.2 Spatiotemporal profile of the optical dipole force under standard and alternating chirped pulse excitations for $N = 2$. 75
5.3 Temporal evolution of populations under standard or alternating chirped pulse excitations (RWA) for $N = 2$. 76

5.4 Temporal evolution of phase angle of u and v under standard chirped pulse excitation (RWA) for $N = 2$. 77
5.5 Temporal evolution of phase angle of u and v under alternating chirped pulse excitation (RWA) for $N = 2$. 79
5.6 Temporal evolution of radial distance under standard alternatively chirped pulse excitation for different initial transverse velocities. . 80
5.7 Temporal evolution of radial distance under alternating up-chirped (solid lines) and down-chirped (dash-dot lines) pulse excitations for various order of the super-Gaussian pulse train and initial transverse velocities (a) 100 m/s (b) 1000 m/s. 81

Chapter 1

Introduction

RESEARCH in the manipulation of quantum systems using laser light continues at an ever-increasing pace, since the advent of Laser in 1960. As a matter of fact, in the last one decade, owing to extraordinary developments in femtosecond lasers and attosecond lasers, there is explosive growth of both theoretical and experimental studies envisaged at controlling atomic as well as molecular systems at its most fundamental level. In this context, various coherent control techniques have been developed and experimentally validated [1–5].

Quantum coherence and interference, which led to the observation of the phenomena such as, coherent population trapping (CPT) and electromagnetically induced transparency (EIT), are at heart of manipulation of the properties of an atomic medium and have been studied extensively in past decades and continues to remain a major area of research in various contexts [6–17]. This has enabled the realization of a plethora of novel phenomena such as Bose-Einstein condensation, laser cooling and trapping, deflection of atoms, optical bistability (OB), optical tristability (OT), and slow and fast light. These breakthroughs are now paving the ways for many diverse applications ranging from quantum metrology to quantum information [18–32] and, even in the context of

cold atoms [33, 34]. Optical bistability and multistability are interesting phenomena in which the cooperative nature of the interaction between a collection of atoms and laser fields tune system nonlinearity [35]. Such nonlinearity could be escalated further by inserting the atomic system inside a cavity to employ its feedback mechanism. Initially, OB has been demonstrated experimentally for saturable absorber, Ruby crystal, and Sodium vapor as a nonlinear medium inside in an optical resonator [36–38]. Then by developing the basic theoretical model of OB for two-level atoms coupled by a single cavity mode [38–41], it was realized that OB arises due to intensity-dependent absorption or dispersion, or hybridization of both; henceforth, OB is classified as absorptive or dispersive, or hybrid respectively. A decade later, OT has been demonstrated for Λ-type three-level atomic system comprising an excited state and two ground state sublevels driven by two cavity modes [42–44]. Soon it was proposed that OB (OT) is more definitive with multi-level atoms than in two (three) level atoms as a nonlinear medium inside in an optical resonator. This is owing to the fact that absorption, dispersion, and nonlinearity could be greatly modified by quantum coherence and interference in multilevel atoms for increased pathways. In this regard, coherent control by electromagnetic field induced transparency (EIT) in three level atomic systems was demonstrated theoretically and experimentally to reduce OB threshold intensity and give rise to a new type of OT by adjusting the control laser field parameters [45–47].

The fact that laser is a monochromatic, intense, and coherent source of radiation resurrects the long awaited expectation to manipulate atomic quantum systems by realizing a tremendous optical force. The interaction of a single frequency light with single atomic transition gives rise to two kinds of optical forces namely the radiative force and the dipole force. The former occurs due to spontaneous emission, while the later is due to stimulated emission [4, 48]. These two kinds of optical forces could be understood as a result of phase and

intensity gradients in a beam of light [49, 50]. The physical effects of both dipole and radiative forces induced by a CW laser were demonstrated through the focusing, defocusing, and steering of neutral sodium atoms [51]. Similar effects were also observed by utilizing the optical forces induced by pulsed laser fields instead of CW lasers. The ability of pulsed laser induced optical forces to beat the saturation limit of spontaneous force makes them much more favorable and increasingly attractive tools.

While atomic systems are being manipulated using intense laser light, it is interesting to note that the velocity of a laser light could be controlled in an extreme way using the atomic system itself, and applying various coherent control schemes. The possibility to engineer the group velocity of light pulses propagating through atomic medium has led to the emergence of slow and fast light. Slow light, also known as subluminality, stands for light propagation with a group velocity v_g less than the velocity of light in vacuum c, while fast light, also known as superluminality, refers to light propagation with $v_g > c$ or $v_g < 0$. It was thought that superluminal velocities are generally unphysical in the sense that light wave traveling with superluminal velocity does not transmit any information through the medium otherwise the causality principle of relativity theory would be violated [52]. Accordingly, subluminal group velocity can be regarded as signal velocity, which is not the case for superluminal group velocity [53, 54]. It is well known, from Kramers–Kronig relations which satisfy causality principle, that the dispersion changes sign steeply about absorption line (or closely-spaced absorption doublet), equivalent to dip in gain profile; where the steep anomalous (negative) dispersion near absorption line center results in fast light and the normal (positive) dispersion in the wings of absorption line results in slow light; likewise, slow light, associated with normal dispersion, is expected near the center of gain line (or closely-spaced gain doublet), equivalent to dip in absorption profile which is also known as spectral

hole, and fast light, associated with anomalous dispersion, is expected in the wings of gain line [32, 53, 55–60]. The observation of EIT, a quantum destructive interference effects in which a transparency window is generated between two absorption peaks, a dip in absorption profile, opens the way for slow light demonstration in Bose-Einstein condensate of sodium atoms and even in rubidium vapor [61–63].

1.1 The topics and aim of research

In this thesis, we report our theoretical explorations of various applications involving coherent control of atomic systems, briefly discussed below:

(a) ***Effective control and switching of optical multistability*:** OB and OT in three-level Λ-type atomic system have been extensively studied while less attention has been paid to investigate OB and OT in three-level V-type atomic system. This may be owing to the coherence relaxation of upper-levels by spontaneous emission which is not the case for Λ-type atomic system [64, 65]. Hence, available studies on OB and OT in three-level V-type atomic system are attempting to circumvent this effect by incorporating coherent control using incoherent pump field, or microwave field, or spontaneously generated coherence (SGC) [65–72]. In this work, by assuming that three-level atomic system should be sufficient for reliable obtainment of single OB, double OB, and OT, we investigate the criteria for achieving the same, without considering coherent control by incoherent pump field, or microwave field, or SGC.

(b) ***Coherent control of ultracold atom for slow and fast light phenomena*:** Taking advantage of the sharp spectral features offered by atomic vapors to obtain extreme values of the group velocity of light has been a topic of immense research interest for quite some time [31]. Sometime back, the experimental observation of electromagnetically induced transparency (EIT) [11, 73], a

quantum destructive interference effects in which a transparency window is generated between two absorption peaks, a dip in absorption profile, opens the way for slow light demonstration in Bose-Einstein condensate of sodium atoms with $v_g = 17\ \mathrm{m\,s^{-1}}$ [61], and the observation of $v_g = 90\ \mathrm{m\,s^{-1}}$ [62] and $8\ \mathrm{m\,s^{-1}}$ [63] in rubidium vapor. It was shown that slow light of EIT medium can be switched to fast light by driving the transition between the ground states using an additional control field in a closed system [74], or by tuning the phase of one of the fields in an open system [75]. On the other hand, fast light of single absorption line can be switched to slow light by controlling the coupling field intensity [76]. Again, copropagating slow and fast light manifested by EIT-assisted nonlinear gain and absorption has been observed experimentally [77]. In our work, we investigate various issues of slow and fast light effects through the coherent manipulation of the D_1 transition of ^{23}Na atoms. In addition, the coherent population transfer between the hyperfine states of the atom have been investigated.

(c) ***Effective focusing of a diverging atomic beam*:** Recently, the optical dipole induced by a unidirectional sequence of linearly chirped pulses has been investigated and showed to change its sign between odd and even number of pulses in the pulse train [78]. This results in oscillatory optical dipole force, making the time-averaged optical force to vanish. The physics behind the nature of the oscillating forces was not discussed and therefore still remains open for further investigations. Hence, we not only investigate and clarify physics behind the nature of the oscillating forces but also propose a strategy to overcome this issue, thereby realizing the effective time average focusing and defocusing dipole force. For this, we propose for the use of a sequence of alternatively chirped pulses instead of either positively or negatively chirped pulses.

1.2 Outline of the thesis

In the following, we present the outline of the thesis by including a description of the various problems that have been tackled in the form of different chapters of the thesis. There are a total of six chapters. **Chapter 1** has already provided an adequate introduction to the thesis and, discussed briefly the recent developments pertinent to the problems considered in the thesis.

We present a brief description about the content of the rest of the chapters below.

Chapter 2: This chapter is devoted to familiarize the reader with relevant concepts and phenomena introduced in this thesis. This chapter would be immensely helpful for readers to comprehend the research problems addressed in later chapters. Here, we discuss the density matrix formalism, the rotating wave approximation, the concept of EIT, slow and fast light phenomenon, and finally the notion of optical bistability.

Chapter 3: In this chapter, we theoretically analyze the behavior of single optical bistability (OB), double OB, and tristability (OT) in a three-level V-type atomic system confined in a unidirectional optical ring cavity. The physics behind the emergence of various bistable and tristable states, and switching from the absorptive to the dispersive characteristics, are explored. The role of probe- and control-field detunings on the input-output characteristics is probed. Further, it is found that the switching between various bistable phenomena is defined by the ratio between the absolute peak values of the parameters describing dispersion and absorption, respectively. This ratio sets a criterion for obtaining absorptive OB, OT, double OB, and dispersive OB. The role of control-field intensity and detuning as well as the cooperation parameter on the input-output characteristics are explored. Finally, a scheme is discussed to control the width of the middle branch of double OB and OT as well as single OB.

Chapter 4: In this chapter, we theoretically analyze the role of field detuning on both the population transfer and the induced polarization for the D_1 transition of Bose-Einstein condensate of ^{23}Na atoms. We have observed complete population transfer between the two hyperfine ground states at small field intensity. It is shown that slow and fast light, with large bandwidth at intermediate field intensity could be realized with our proposed scheme. In addition, we find that switching between slow and fast light, with large bandwidth is achievable via controlling the field intensity. Moreover, slow light associated with gain (loss) is found to co-propagate with fast-light, associated with loss (gain). Apart from these, we report our study on maximum attainable coherence for optical and Raman transitions.

Chapter 5: Coherent manipulation of atomic systems using few-cycle-pulsed light has garnered lots of attention recently. In this chapter, we theoretically show how the effective focusing and defocusing of a diverging atomic beam can be realized using an appropriate sequence of linearly chirped few-cycle pulsed laser fields. First, we investigate and show that the time averaged optical dipole force induced by the sequence of either positively or negatively chirped pulses vanishes due to the periodic oscillations of the phases of in-phase components of atomic dipole moments. Then, we demonstrate that this issue could be overcome by utilizing a sequence of alternatively chirped pulses instead of either positively or negatively chirped pulses. It is shown that for such a sequence of pulses, the phases of in-phase components of atomic dipole moments does not oscillate periodically and in fact remain constant at either 0 or π depending on the chirping direction of the initial pulse, resulting in either an effective focusing or defocusing optical dipole force. The trajectory of atoms under an optical dipole force is also investigated to actually show the focusing and defocusing. Finally, the role of beam shape on the proposed scheme is investigated and it turns out that a super-Gaussian pulse of order $m = 2$ shows more efficacy

compared to the normal Gaussian pulse.

Chapter 6: Here we provide the conclusions of the thesis. In this chapter, we conclude with an outline of the results obtained in the thesis. We also provide a future plan based on the work that we present in the thesis.

Chapter 2

Coherent Control: Theoretical Background

THIS chapter is devoted to familiarize the reader with the relevant concepts and phenomena related to the research problems discussed in this thesis.

2.1 Density Matrix Formalism

Density matrix formalism is a powerful tool in quantum as well as nonlinear optics. This tool is particularly suited for dealing with coherence in isolated or interactive systems. The density matrix permits us to ignore parts of a problem that appear to be irrelevant and to focus mathematically on the system of our interest.

To understand the density matrix formalism, let us begin by considering a two-level atomic system (TLS) interacting with a classical monochromatic field with angular frequency ω, amplitude E_0, and unit polarization vector $\hat{\eta}$. The model is schematically depicted in Fig. 2.1. The ground state and the excited state of the atom is labeled by $|1\rangle$ and $|2\rangle$, respectively. The resonant frequency of the atom is denoted by ω_0.

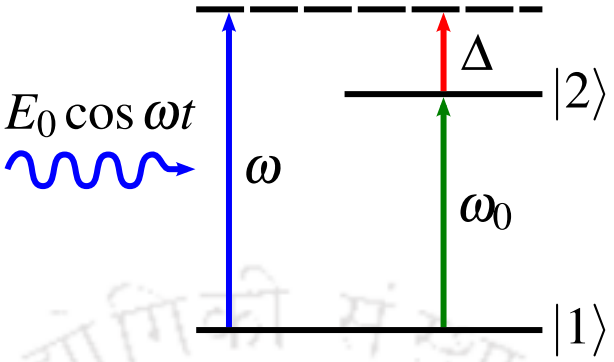

Figure 2.1: Schematic diagram of a two-level atom interacting with a classical field.

From elementary quantum mechanics, we know that the system could be described by the so called Schrödinger equation, as given below:

$$i\hbar \frac{\partial |\psi\rangle}{\partial t} = \hat{\mathbf{H}} |\psi\rangle \ . \tag{2.1}$$

Here $|\psi\rangle$ is the state of the atom, and it can be written as:

$$|\psi\rangle = c_1(t)|1\rangle + c_2(t)|2\rangle \ , \tag{2.2}$$

where $c_1(t)$ and $c_2(t)$ are the respective probability amplitudes for the ground and the excited states. We know that $|c_1(t)|^2$ and $|c_2(t)|^2$ give us the probability of finding the atom in the ground and the excited states respectively, with the condition $|c_1(t)|^2 + |c_2(t)|^2 = 1$.

On the other hand, the total Hamiltonian of the system, $\hat{\mathbf{H}}$ is

$$\hat{\mathbf{H}} = \hat{\mathbf{H}}_0 + \hat{\mathbf{V}} \ ,$$

$\hat{\mathbf{H}}_0$ being the Hamiltonian describing the isolated atom, such that:

$$\begin{aligned} \hat{\mathbf{H}}_0 |1\rangle &= E_1 |1\rangle \\ \hat{\mathbf{H}}_0 |2\rangle &= E_2 |2\rangle \end{aligned} \ ,$$

with $E_2 - E_1 = \hbar\omega_0$. On the other hand, $\hat{\mathbf{V}} = \hat{\vec{\mu}} \cdot \vec{\mathbf{E}}$ refers to the atom-field interaction. $\hat{\vec{\mu}}$ is the so-called atom-dipole operator, given in terms of the atomic electron position $\vec{\mathbf{r}}_e$ as $\hat{\vec{\mu}} = -e\vec{\mathbf{r}}_e$. We assume the two-level atom to contain a single electron, for simplicity. The operator $\hat{\vec{\mu}}$ could be expressed in terms of the eigenstates $|1\rangle$ and $|2\rangle$ as follows:

$$\hat{\vec{\mu}} = \langle 1|\hat{\vec{\mu}}|2\rangle\,|1\rangle\langle 2| + \langle 2|\hat{\vec{\mu}}|1\rangle\,|2\rangle\langle 1| \ .$$

This is written, considering the fact that $\hat{\vec{\mu}}$ has odd parity, while both $|1\rangle$ and $|2\rangle$ has definite parity. Now, we can write, taking $\langle 1|\hat{\vec{\mu}}|2\rangle$ to be real:

$$\hat{\vec{\mu}} = \langle 1|\hat{\vec{\mu}}|2\rangle\,(\sigma + \sigma^+)\ , \tag{2.3}$$

where $\sigma = |1\rangle\langle 2|$ is the atomic lowering operator and $\sigma^+ = |2\rangle\langle 1|$ is the atomic raising operator.

We can thus write the total atom-field Hamiltonian as :

$$\begin{aligned}\hat{\mathbf{H}} &= \hat{\mathbf{H}}_0 + \hat{\mathbf{V}} \\ &= \hbar\omega_0\sigma^+\sigma - \langle 1|\hat{\vec{\mu}}|2\rangle \cdot \vec{\mathbf{E}}(\sigma + \sigma^+).\end{aligned} \tag{2.4}$$

In writing the above Hamiltonian, we take the ground state energy $E_1 = 0$, without loss of any generality. It is straightforward to show that, in the unperturbed state, the expectation value of $\sigma = |1\rangle\langle 2|$ has the time dependence of $e^{-i\omega_0 t}$, while σ^+ has the time dependence of $e^{+i\omega_0 t}$. Keeping this in mind, we get

$$\begin{aligned}\hat{\mathbf{V}} &= -\hat{\vec{\mu}} \cdot \vec{\mathbf{E}} \\ &= -\langle 1|\hat{\vec{\mu}}|2\rangle \cdot \hat{\eta} E_0 \cos(\omega t)(\sigma + \sigma^+) \\ &= -\langle 1|\hat{\vec{\mu}}|2\rangle \cdot \hat{\eta}\frac{E_0}{2}\left(e^{i\omega t} + e^{-i\omega t}\right)(\sigma + \sigma^+)\end{aligned} \ .$$

Now let us examine the product term $\left(e^{i\omega t} + e^{-i\omega t}\right)(\sigma + \sigma^+)$:

$$\begin{aligned}\left(e^{i\omega t} + e^{-i\omega t}\right)(\sigma + \sigma^+) &= \sigma e^{i\omega t} + \sigma e^{-i\omega t} + \sigma^+ e^{i\omega t} + \sigma^+ e^{-i\omega t} \\ &\approx \sigma(0)e^{i(\omega-\omega_0)t} + \sigma^+(0)e^{-i(\omega+\omega_0)t} \\ &\quad + \sigma^+(0)e^{i(\omega+\omega_0)t} + \sigma^+(0)e^{-i(\omega-\omega_0)t}.\end{aligned} \ .$$

It is clear that the second and third terms of the above expression oscillates rapidly as $e^{\pm i(\omega+\omega_0)t}$ while the other two terms oscillate slowly as $e^{\pm i\Delta t}$, with $\Delta = \omega - \omega_0$. Now considering $|\omega - \omega_0| \ll \omega + \omega_0$, we can make the so-called rotating-wave approximation (RWA). "*This approximation focuses on slow dynamics, replacing terms rotating at optical frequencies are replaced by their zero-average value, which amounts to a coarse-graining on* fs *time scales. This is reasonable since optical detectors do not respond on* fs *time scales anyway.*" [79]. Because of RWA, we can neglect the highly oscillating terms, and we write:

$$\begin{aligned}\hat{\mathbf{H}} &= \hbar\omega_0\sigma^+\sigma - \frac{E_0\langle 1|\hat{\vec{\mu}}|2\rangle}{2}\cdot\hat{\eta}(\sigma e^{i\omega t} + \sigma^+ e^{-i\omega t}) \\ &= \hbar\omega_0\sigma^+\sigma + \frac{\hbar\Omega}{2}(\sigma e^{i\omega t} + \sigma^+ e^{-i\omega t}),\end{aligned} \tag{2.5}$$

where $\Omega = -\frac{\langle 1|\hat{\vec{\mu}}\cdot\hat{\eta}|2\rangle}{\hbar}E_0$ is termed as the Rabi frequency.

Now, the Schrödinger equation, $i\hbar\frac{\partial|\psi\rangle}{\partial t} = \hat{\mathbf{H}}|\psi\rangle$ leads to the following set of coupled differential equations:

$$\begin{aligned}\frac{\partial c_1}{\partial t} &= -i\frac{\Omega}{2}c_2 e^{i\omega t} \\ \frac{\partial c_2}{\partial t} &= -i\omega_0 c_2 - i\frac{\Omega}{2}c_1 e^{-i\omega t}\end{aligned}. \tag{2.6}$$

The explicit time dependency in the above equations could be get rid of if we make a transformation into the rotating frame of the laser field by the following unitary transformation, $U = e^{i\omega t|2\rangle\langle 2|}$. Then the Schrödinger equation, in this new frame, gives us:

$$\begin{aligned}\frac{\partial c_1}{\partial t} &= -i\frac{\Omega}{2}\tilde{c}_2 \\ \frac{\partial \tilde{c}_2}{\partial t} &= -i\Delta\tilde{c}_2 - i\frac{\Omega}{2}c_1\end{aligned} \tag{2.7}$$

where $\tilde{c}_2 = c_2 e^{i\omega t}$. The full Hamiltonian is now expressed as,

$$\hat{\mathbf{H}} = -\hbar\Delta|2\rangle\langle 2| + \frac{\hbar\Omega}{2}(\sigma + \sigma^+)\,. \tag{2.8}$$

Thus, to summarize, the TLS interacting with a classical field is described by the state vector, under RWA and in the rotating frame, $|\tilde{\psi}\rangle = c_1|1\rangle + \tilde{c}_2|2\rangle$. The Hamiltonian is given by Eq. 2.8.

Now, interestingly the state of the TLS can also be represented by an operator, defined as follows:

$$\rho = |\psi\rangle\langle\psi| \ . \tag{2.9}$$

This is the so-called density matrix. Soon, we will explain its significance. Using $|\psi\rangle = c_1|1\rangle + \tilde{c}_2|2\rangle$, we can write:

$$\rho = |c_1|^2|1\rangle\langle 1| + c_1\tilde{c}_2^*|1\rangle\langle 2| + \tilde{c}_2 c_1^*|2\rangle\langle 1| + |\tilde{c}_2|^2|2\rangle\langle 2| \ . \tag{2.10}$$

We can express the above in the following matrix form:

$$\rho = \begin{bmatrix} c_1c_1^* & c_1\tilde{c}_2^* \\ \tilde{c}_2c_1^* & \tilde{c}_2\tilde{c}_2^* \end{bmatrix} \equiv \begin{bmatrix} \rho_{11} & \rho_{12} \\ \rho_{21} & \rho_{22} \end{bmatrix} \ ,$$

where $\rho_{11} = |c_1|^2$ and $\rho_{22} = |\tilde{c}_2|^2$ give us probabilities in level $|1\rangle$ and $|2\rangle$ respectively.

On the other hand, $\rho_{12} = c_1\tilde{c}_2^*$ and $\rho_{21} = \tilde{c}_2 c_1^*$ denotes the coherence between the two energy levels. In fact, $\rho_{ij} = c_i c_j^* \neq 0 \Rightarrow$ that it is possible to have a coherent superposition between the energy levels $|i\rangle$ and $|j\rangle$. Because $|c_1|^2 + |\tilde{c}_2|^2 = 1$, it is clear that $\mathrm{Tr}(\rho) = 1$, an essential property for a density matrix! Now, using Eq. 2.7 and Eq. 2.9, it is straightforward to obtain the following evolution equations for the density matrix elements:

$$\begin{aligned}
\frac{\partial\rho_{22}}{\partial t} &= i\frac{\Omega}{2}(\rho_{21} - \rho_{12}) \\
\frac{\partial\rho_{11}}{\partial t} &= -i\frac{\Omega}{2}(\rho_{21} - \rho_{12}) \\
\frac{\partial\rho_{12}}{\partial t} &= -i\Delta\rho_{12} - i\frac{\Omega}{2}(\rho_{22} - \rho_{11}) \\
\frac{\partial\rho_{21}}{\partial t} &= i\Delta\rho_{21} + i\frac{\Omega}{2}(\rho_{22} - \rho_{11})
\end{aligned} \ . \tag{2.11}$$

It is clear that $\rho_{21} = \rho_{12}^*$. In fact, $\rho_{ij} = \rho_{ji}^*$ is true in general. This leads us to the property that, $\rho = \rho^\dagger \Rightarrow$ the density matrix is hermitian.

Now, please note that Eq. 2.11 do not reflect the existence of relaxation arising from spontaneous emissions and other collisional processes. However, it is not difficult to incorporate these processes phenomenologically in the density matrix equations. To a significant accuracy, it works. For example, we can incorporate spontaneous emissions as follows. With $\Delta = 0 = \Omega$, we can add a couple of extra-terms into Eq. 2.11:

$$\begin{aligned} \frac{\partial \rho_{22}}{\partial t} &= -\Gamma \rho_{22} \\ \frac{\partial \rho_{11}}{\partial t} &= \Gamma \rho_{22} \\ \frac{\partial \rho_{12}}{\partial t} &= -\gamma_\perp \rho_{12} \\ \frac{\partial \rho_{21}}{\partial t} &= -\gamma_\perp \rho_{21} \end{aligned} \quad . \tag{2.12}$$

Here, Γ is called the longitudinal decay rate. The excited population decays at a rate of Γ, and a similar term is added to compensate for this decayed population into the ground states. In the context of TLS, sometimes Γ is also denoted as A_{21}. The coherence also damp at the rate $\gamma_\perp$, which could be justified using quantum theory of damping. In general, $\gamma_\perp > \frac{\Gamma}{2}$ and one can write:

$$\gamma_\perp = \frac{\Gamma}{2} + \gamma_c \, ,$$

where γ_c models dephasing effects such as atom-atom collisions that do not affect the populations. γ_c is called the transverse decay rate. Including these

relaxation processes, we obtain the so-called optical Bloch equations:

$$\begin{aligned}
\frac{\partial \rho_{22}}{\partial t} &= i\frac{\Omega}{2}(\rho_{21}-\rho_{12}) - \Gamma\rho_{22} \\
\frac{\partial \rho_{11}}{\partial t} &= -i\frac{\Omega}{2}(\rho_{21}-\rho_{12}) + \Gamma\rho_{22} \\
\frac{\partial \rho_{12}}{\partial t} &= -(\gamma_\perp + i\Delta)\rho_{12} - i\frac{\Omega}{2}(\rho_{22}-\rho_{11}) \\
\frac{\partial \rho_{21}}{\partial t} &= -(\gamma_\perp - i\Delta)\rho_{21} + i\frac{\Omega}{2}(\rho_{22}-\rho_{11}).
\end{aligned} \tag{2.13}$$

2.2 Field Dynamics Inside the Atomic Medium

The optical Bloch equations describe a wide variety of coherent atom-field interactions. However, it is unable to describe propagation effects induced by an applied electric field, strong enough to stimulate substantial population exchange between levels $|1\rangle$ and $|2\rangle$. This issue could be addressed by coupling the optical Bloch equations to Maxwell's wave equation:

$$\nabla^2\vec{\mathbf{E}} - \frac{1}{c^2}\frac{\partial^2\vec{\mathbf{E}}}{\partial t^2} = \frac{1}{\varepsilon_0 c^2}\frac{\partial^2\vec{\mathbf{P}}}{\partial t^2}\,. \tag{2.14}$$

Here $\vec{\mathbf{P}}$ is the polarization density, i.e., the electric dipole moment per unit volume, and ε_0 is the permittivity of free space.

Let us consider a plane wave propagating in the z-direction:

$$\vec{\mathbf{E}}(\vec{\mathbf{z}},t) = \hat{\eta}E(z,t)e^{i(kz-\omega t)}\,,$$

where $E(z,t)$ is complex amplitude of the electric field, to be determined. $k = \frac{\omega}{c}$ is the magnitude of the wave vector. We assume that the magnitude $E(z,t)$ varies slowly compared to the carrier wave $e^{i(kz-\omega t)}$, justifying the following

inequalities:

$$\begin{aligned} \left| \frac{\partial E}{\partial z} \right| &\ll k \mid E \mid \\ \left| \frac{\partial^2 E}{\partial z^2} \right| &\ll k \left| \frac{\partial E}{\partial z} \right| \\ \left| \frac{\partial E}{\partial t} \right| &\ll \omega \mid E \mid \end{aligned} \tag{2.15}$$

Physically, these assumptions imply that $E(z,t)$ represent a smooth envelope in both space and time. These approximations are popularly known as slowly-varying envelope approximation (SVEA).

In the plane wave and slowly-varying envelope approximations for $\vec{\mathbf{E}}(\vec{\mathbf{z}},t)$, one can easily obtain the following:

$$\nabla^2 \vec{\mathbf{E}} - \frac{1}{c^2}\frac{\partial^2 \vec{\mathbf{E}}}{\partial t^2} = 2i\frac{\omega}{c}\left(\frac{\partial E}{\partial z} + \frac{1}{c}\frac{\partial E}{\partial t}\right)\hat{\eta}\, e^{i(kz-\omega t)} \,. \tag{2.16}$$

We now need to find out $\vec{\mathbf{P}}$. Here, we are considering a two-state atom. Each atom is assumed to have an electric moment, $\langle\hat{\vec{\mu}}\rangle$, given by:

$$\begin{aligned} \langle\hat{\vec{\mu}}\rangle &= \langle 1|\hat{\vec{\mu}}|2\rangle \, \langle(\sigma + \sigma^+)\rangle \\ &= \hat{\vec{\mu}}_{12}(\langle\sigma\rangle + \langle\sigma^+\rangle). \end{aligned}$$

As we discussed earlier, σ has the time dependence $e^{-i\omega_0 t}$, while σ^+ has the time dependence $e^{i\omega_0 t}$. Moreover, we can show that, $\langle\sigma\rangle = \tilde{c}_2 c_1^*$ and $\langle\sigma^+\rangle = c_1\tilde{c}_2^*$. Again taking $\omega_0 \approx \omega$, we can write, using the explicit time dependence,

$$\langle\hat{\vec{\mu}}\rangle = \hat{\vec{\mu}}_{12}\left[\tilde{c}_2 c_1^* e^{-i\omega t} + c_1\tilde{c}_2^* e^{i\omega t}\right] \,.$$

To account for the spatial variations of the plane wave acting on the atom located at z, we simply replace $e^{-i\omega t}$ by $e^{i(kz-\omega t)}$. Thus for an atom at z:

$$\langle\hat{\vec{\mu}}\rangle = \hat{\vec{\mu}}_{12}\left[\rho_{21} e^{i(kz-\omega t)} + \rho_{12} e^{-i(kz-\omega t)}\right] \,.$$

If there is a uniform distributions of N atoms per unit volume, the polarization $\vec{\mathbf{P}}$ is,

$$\vec{\mathbf{P}}(z,t) = N\hat{\vec{\mu}}_{12}\rho_{21}e^{i(kz-\omega t)} \ .$$

Since ρ_{21} varies much slowly in time than $e^{-i\omega t}$,

$$\frac{\partial^2\vec{\mathbf{P}}}{\partial t^2} = -N\omega^2\hat{\vec{\mu}}_{12}\rho_{21}e^{i(kz-\omega t)} \ . \tag{2.17}$$

Now using Eq. 2.16 and Eq. 2.17 in Eq. 2.14 and writing $\hat{\vec{\mu}}_{12} = \hat{\eta}\mu_{12}$, we obtain:

$$\begin{aligned} 2i\frac{\omega}{c}\left(\frac{\partial E}{\partial z}+\frac{1}{c}\frac{\partial E}{\partial t}\right) &= -\frac{1}{\varepsilon_0 c^2}N\omega^2\mu_{12}\rho_{21} \\ \Rightarrow \frac{\partial E}{\partial t}+c\frac{\partial E}{\partial z} &= \frac{i\omega}{2\varepsilon_0}N\mu_{12}\rho_{21} \\ \Rightarrow \frac{\partial E}{\partial t}+c\frac{\partial E}{\partial z} &= \frac{i\omega}{2\varepsilon_0}P(\omega), \end{aligned}$$

where $P(\omega) = N\mu_{12}\rho_{21}$. This equation describes the propagation of the electric field inside the atomic medium.

2.3 Coherent Population Transfer

Let us discuss the phenomenon of coherent population transfer (CPT) using the density matrix formalism we just discussed. It is a relevant topic for this thesis. Consider a three-level atomic system as depicted in Fig. 2.2.

Our goal is to transfer population in the most efficient way from the state $|1\rangle$ to $|2\rangle$. The symmetry of the states is assumed to be such that the electric dipole transitions are allowed between $|1\rangle \leftrightarrow |3\rangle$ and $|3\rangle \leftrightarrow |2\rangle$, but not between $|1\rangle \leftrightarrow |2\rangle$. Thus, $V_{12} = \langle 1|\hat{\mathbf{V}}|2\rangle = -\langle 1|\hat{\vec{\mu}}\cdot\vec{\mathbf{E}}|2\rangle = -\hat{\vec{\mu}}_{12}\cdot\vec{\mathbf{E}} = 0 = V_{21}$. ω_{31} and ω_{32} are the respective atomic transition frequencies between $|3\rangle \rightarrow |1\rangle$ and

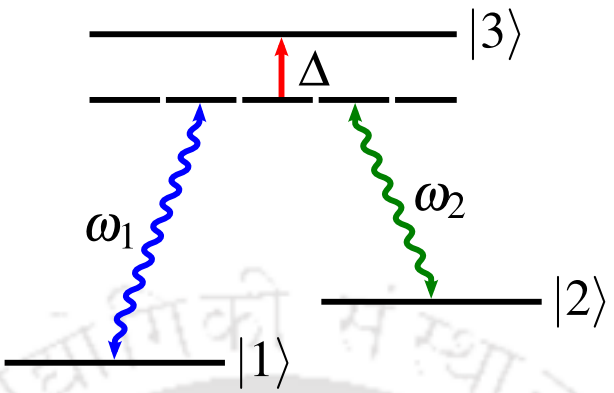

Figure 2.2: Schematic diagram of a three-level Λ-type atomic system for realizing CPT.

$|3\rangle \rightarrow |2\rangle$, respectively.

$$|\psi\rangle = c_1|1\rangle + c_2|2\rangle + c_3|3\rangle \ ,$$

where c_i is the probability amplitude of the eigenstate $|i\rangle$. Two monochromatic laser fields $\vec{\mathbf{E}}_1 = \hat{\eta} E_{1_0} \cos(\omega_1 t)$ and $\vec{\mathbf{E}}_2 = \hat{\eta} E_{2_0} \cos(\omega_2 t)$ are applied between $|1\rangle \leftrightarrow |2\rangle$ and $|3\rangle \leftrightarrow |2\rangle$, respectively. Starting with the Schrödinger equation, $i\hbar \frac{\partial|\psi\rangle}{\partial t} = (\hat{\mathbf{H}}_0 + \hat{\mathbf{V}})|\psi\rangle$, we can obtain the following evolution equations for the density matrix elements:

$$\begin{aligned}
i\hbar \frac{\partial \rho_{11}}{\partial t} &= V_{13}\rho_{31} - V_{31}\rho_{13} \\
i\hbar \frac{\partial \rho_{22}}{\partial t} &= V_{23}\rho_{32} - V_{32}\rho_{23} \\
i\hbar \frac{\partial \rho_{33}}{\partial t} &= V_{31}\rho_{13} - V_{13}\rho_{31} + V_{32}\rho_{23} - V_{23}\rho_{32} \\
i\hbar \frac{\partial \rho_{12}}{\partial t} &= \hbar\omega_{12}\rho_{12} + V_{13}\rho_{32} - V_{32}\rho_{13} \\
i\hbar \frac{\partial \rho_{13}}{\partial t} &= \hbar\omega_{13}\rho_{13} + V_{13}(\rho_{33} - \rho_{11}) - V_{23}\rho_{12} \\
i\hbar \frac{\partial \rho_{32}}{\partial t} &= \hbar\omega_{32}\rho_{32} + V_{31}\rho_{12} + V_{32}(\rho_{22} - \rho_{33})
\end{aligned} \tag{2.18}$$

It should be noted that $\rho_{31} = \rho_{13}^*$, $\rho_{32} = \rho_{23}^*$, and $\rho_{12} = \rho_{21}^*$. Again, $V_{13} = -\hat{\vec{\mu}}_{13} \cdot \vec{\mathbf{E}}_1$, $V_{32} = -\hat{\vec{\mu}}_{32} \cdot \vec{\mathbf{E}}_3$ and so on. In fact, we can express V_{13} in the following form: $V_{13} = -\frac{1}{2}\hbar\Omega_1 e^{i\omega_1 t} + c.c.$, where $\Omega_1 = \frac{-\hat{\vec{\mu}}_{13} \cdot \hat{\eta} E_{1_0}}{\hbar}$. Similarly, we can express others. We assume that, the density matrix elements describing the coherence has slowly-varying envelope and we write:

$$\begin{aligned} \rho_{12} &= \tilde{\rho}_{12} e^{i\omega_{12} t} \\ \rho_{13} &= \tilde{\rho}_{13} e^{i\omega_1 t} \\ \rho_{32} &= \tilde{\rho}_{32} e^{-i\omega_2 t} \end{aligned} , \tag{2.19}$$

where $\tilde{\rho}_{ij}$ refers to the slowly varying envelope. Putting Eq. 2.19 in Eq. 2.18, under the so-called rotating wave approximation (RWA), we can obtain the following set of coupled differential equations:

$$\begin{aligned} \dot{\tilde{\rho}}_{12} &= \frac{i}{2}\Omega_1 \tilde{\rho}_{32} - \frac{i}{2}\Omega_2 \tilde{\rho}_{13} \\ \dot{\tilde{\rho}}_{13} &= -i\Delta\tilde{\rho}_{13} + \frac{i}{2}\Omega_1(\rho_{33} - \rho_{11}) - \frac{i}{2}\Omega_2 \tilde{\rho}_{12} \\ \dot{\tilde{\rho}}_{32} &= -i\Delta\tilde{\rho}_{32} + \frac{i}{2}\Omega_1 \tilde{\rho}_{12} + \frac{i}{2}\Omega_2(\rho_{22} - \rho_{33}) \\ \dot{\rho}_{11} &= \frac{i}{2}\Omega_1(\tilde{\rho}_{31} - \tilde{\rho}_{13}) \\ \dot{\rho}_{22} &= \frac{i}{2}\Omega_2(\tilde{\rho}_{32} - \tilde{\rho}_{23}) \\ \dot{\rho}_{33} &= \frac{i}{2}\Omega_1(\tilde{\rho}_{13} - \tilde{\rho}_{31}) + \frac{i}{2}\Omega_2(\tilde{\rho}_{23} - \tilde{\rho}_{32}) \end{aligned} . \tag{2.20}$$

In writing the above equations we have employed the two-photon resonance condition: $\Delta = \omega_{31} - \omega_1 = \omega_{32} - \omega_2$. Eq. 2.20 could be written in the following compact form:

$$i\hbar\frac{\partial\tilde{\rho}}{\partial t} = \left[\hat{\mathbf{H}}_{eff}, \tilde{\rho}\right] , \tag{2.21}$$

where,

$$\hat{\mathbf{H}}_{eff} = -\frac{\hbar}{2}\begin{bmatrix} 0 & 0 & \Omega_1 \\ 0 & 0 & \Omega_2 \\ \Omega_1 & \Omega_2 & 2\Delta \end{bmatrix}, \tag{2.22}$$

and

$$\tilde{\rho} = \begin{bmatrix} \rho_{11} & \tilde{\rho}_{12} & \tilde{\rho}_{13} \\ \tilde{\rho}_{21} & \tilde{\rho}_{22} & \rho_{23} \\ \tilde{\rho}_{31} & \rho_{32} & \tilde{\rho}_{33} \end{bmatrix}. \tag{2.23}$$

It is an easy exercise to find the eigenvalues of Eq. 2.22. The eigenvalues of $\hat{\mathbf{H}}_{eff}$ are as follows: $\lambda_1(t) = 0$, $\lambda_2(t) = \Delta + \sqrt{\Delta^2 + \Omega_1^2 + \Omega_2^2}$, and $\lambda_3(t) = \Delta - \sqrt{\Delta^2 + \Omega_1^2 + \Omega_2^2}$. Clearly, the eigenvector corresponding to $\lambda_1 = 0$ does not evolve in time. Defining a mixing angle, θ, as $\tan(\theta) = \frac{\Omega_1(t)}{\Omega_2(t)}$, we can write the eigenvector corresponding to $\lambda_1 = 0$ as follows:

$$|\lambda_1\rangle = \cos\theta(t)\,|1\rangle - \sin\theta(t)\,|2\rangle\ .$$

With a little introspection, it is easy to see that, complete population transfer from $|1\rangle$ to $|2\rangle$ occurs, provided:

$$\left.\frac{\Omega_1(t)}{\Omega_2(t)}\right|_{t=-\infty} \to 0\,, \tag{a}$$

and

$$\left.\frac{\Omega_1(t)}{\Omega_2(t)}\right|_{t=+\infty} \to \infty\,. \tag{b}$$

Eq. a implies that the system starts in the state $|1\rangle$, since $\left.|\langle 1|\lambda_1(t)\rangle|^2\right|_{t=-\infty} = 1$, while Eq. b assumes that the final state is $|2\rangle$, since $\left.|\langle 2|\lambda_1(t)\rangle|^2\right|_{t=+\infty} = 1$.

We can observe that for complete population transfer to occur, the second transition (i.e., $|3\rangle \leftrightarrow |2\rangle$) must precede the first transition (i.e., $|3\rangle \leftrightarrow |1\rangle$) initially. It should be noted that initially, there is no population in the state $|2\rangle$

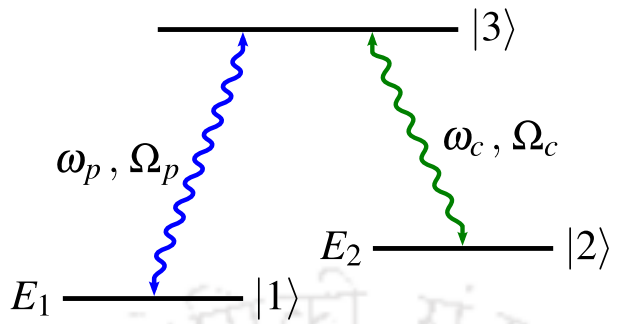

Figure 2.3: Schematic diagram of a three level Λ-type atomic system for realizing EIT.

to respond in the usual way to the pulse at ω_2. Nevertheless, the system does respond by establishing a coherence at this frequency. This counter-intuitive technique for population transfer is widely used in physics and chemistry, for coherent population transfer of atoms or molecules [3].

2.4 Electromagnetically Induced Transparency (EIT)

EIT is an important coherent-control phenomenon. We are not discussing EIT in this thesis, but referring to it at many places in the thesis. Moreover, some of the problems discussed here could be explored in the context of EIT as well.

Simply put, EIT is a phenomenon by which a weak field (called 'probe'), which is absorbed in an atomic media while passing through it, become transparent or propagate without getting absorbed within the media when a strong field (called 'pump') is applied. Of course, EIT to occur, appropriate conditions need to be fulfilled. We can understand this phenomenon by considering the three-level atomic system schematically shown in Fig. 2.3. Transitions are allowed between states $|1\rangle$ and $|3\rangle$ and between $|2\rangle$ and $|3\rangle$. $|1\rangle$ to $|2\rangle$ tran-

sition is not allowed. $\omega_p \approx (E_3 - E_1)/\hbar$ is the probe-field frequency, while $\omega_c \approx (E_3 - E_2)/\hbar$ is the coupling-field (or pump field) frequency. Ω_p and Ω_c are the Rabi frequencies corresponding to $|3\rangle \leftrightarrow |1\rangle$ and $|3\rangle \leftrightarrow |2\rangle$ transition respectively. The system could be described by the Schrödinger equation:

$$i\hbar\frac{\partial|\psi\rangle}{\partial t} = (H_0 + V)|\psi\rangle \ ,$$

where $|\psi\rangle = c_1|1\rangle + c_2|2\rangle + c_3|3\rangle$.

Following a similar procedure as discussed in Section 2.3, we can obtain the following equations for the density matrix elements describing coherence in the system under RWA and SVEA:

$$\begin{aligned}\frac{\partial\rho_{12}}{\partial t} &= i\Delta\rho_{12} - i\Omega_c\rho_{13} \\ \frac{\partial\rho_{13}}{\partial t} &= i\Delta\rho_{13} - i\Omega_c^*\rho_{12} - i\Omega_p^*\rho_{11}\end{aligned} \ . \tag{2.24}$$

Here, we have taken, $\Delta_1 = \omega_{21} - (\omega_p - \omega_c) = \Delta_2 = \omega_{31} - \omega_p = \Delta$.

Under weak excitation approximation:

$$\rho_{11}(t) \approx 1,\ \rho_{22}(t) \approx 0,\ \rho_{32}(t) = \rho_{22}(t) = \rho_{33}(t) = 0 \ .$$

So, we do not require density matrix equations for other elements. Taking damping effects into account, we write:

$$\begin{aligned}\frac{\partial\rho_{12}}{\partial t} &= i(\Delta + i\gamma_{12})\rho_{12} - i\Omega_c\rho_{13} \\ \frac{\partial\rho_{13}}{\partial t} &= i(\Delta + i\gamma_{13})\rho_{13} - i\Omega_c^*\rho_{12} - i\Omega_p^*\rho_{11}\end{aligned} \ . \tag{2.25}$$

γ_{12} and γ_{13} are the decay rates for coherences ρ_{12} and ρ_{13}, respectively. The steady state solutions of the above Eq. 2.25 for times $t \gg \gamma_{12}^{-1}$, γ_{13}^{-1} could be obtained very easily. We obtain the expression for the density matrix element ρ_{13} as follows:

$$\rho_{13} = \frac{\Omega_p^*(\Delta + i\gamma_{12})}{(\Delta + i\gamma_{12})(\Delta + i\gamma_{12}) - |\Omega_c|^2} \ . \tag{2.26}$$

It should be noted that ρ_{13} is complex; its real part is responsible for dispersive effect, and the imaginary part is responsible for the absorption, as experienced by the probe field in the medium. From Eq. 2.26, we can easily see that the presence of the pump field manipulates the coherence between $|3\rangle \leftrightarrow |1\rangle$, which eventually results in transparency of the probe field.

The steady-state electric dipole moment at the probe-field is given by:

$$\vec{\mathbf{p}} = \vec{\mu}_{13}\rho_{13}e^{-i\omega_p t} + c.c. \,. \tag{2.27}$$

We can write $\vec{\mathbf{p}}$ in terms of complex polarizability $\alpha(\omega_p)$ at the probe frequency ω_p as follows:

$$\vec{\mathbf{p}} = \hat{\eta}\,\alpha(\omega_p)E_p e^{-i\omega_p t} + c.c. \,. \tag{2.28}$$

Now, writing $\Omega_p = \frac{\vec{\mu}_{31}\cdot\hat{\eta}E_p}{\hbar}$, and comparing Eq. 2.27 and Eq. 2.28, after some algebra we get:

$$\alpha(\omega_p) = \frac{|\mu_{13}|^2}{\hbar}\frac{\Delta + i\gamma_{12}}{(\Delta + i\gamma_{12})(\Delta + i\gamma_{13}) - |\Omega_c|^2} \,. \tag{2.29}$$

We can define the complex refractive index, as seen by the probe field, using $n^2(\omega_p) = 1 + N\alpha(\omega_p)/\varepsilon_0$, where N is the atomic density. Assuming the atomic medium to be dilute, we can write:

$$n(\omega_p) = 1 + \frac{N}{2\varepsilon_0}\alpha(\omega_p) = n_R(\omega_p) + in_I(\omega_p) \,,$$

where n_R and n_I are the real and imaginary parts of n. It is straightforward to get the power attenuation coefficient, $a(\omega_p)$, and the real refractive index, $n_R(\omega_p)$, at the probe frequency, for a plane probe field propagating through the atomic medium. They are given as follows:

$$a(\omega_p) = \frac{N\omega_p}{\varepsilon_0 c}\frac{|\mu_{13}|^2}{\hbar}\frac{\gamma_{12}\left(\gamma_{12}\gamma_{13} + |\Omega_c|^2\right) + \Delta^2\gamma_{13}}{\left(\Delta^2 - \gamma_{12}\gamma_{13} - |\Omega_c|^2\right)^2 + \Delta^2(\gamma_{12} + \gamma_{13})^2} \,, \tag{2.30}$$

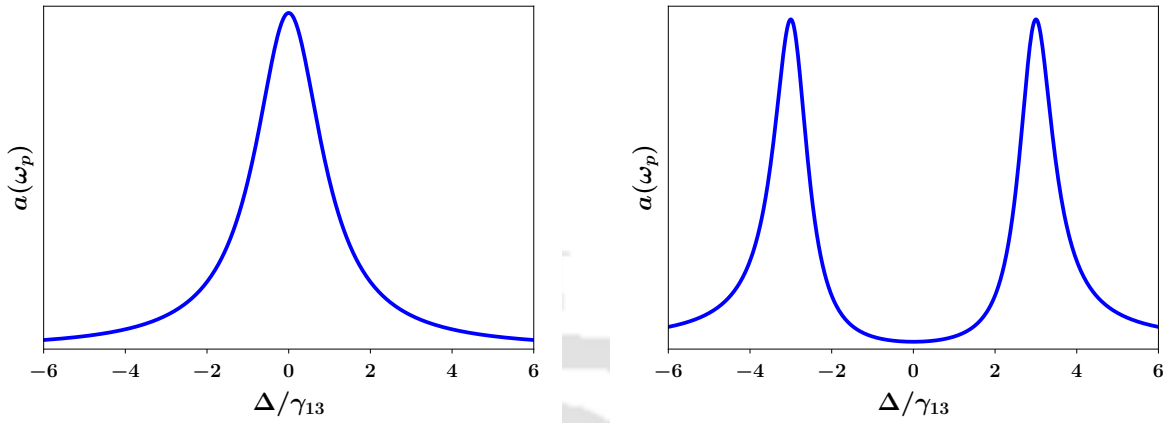

Figure 2.4: $a(\omega_p)$ (in units of $N\omega_p|\mu_{13}|^2/(\varepsilon_0\hbar c)$) vs Δ/γ_{13} as given by Eq. 2.30 for $\gamma_{12}/\gamma_{13} = 0.02$ (a) $\Omega_c = 0$ and (b) $\Omega_c = 3\gamma_{13}$.

and

$$n_R(\omega_p) = 1 + \frac{N|\mu_{13}|^2}{2\varepsilon_0\hbar} \frac{\Delta\left(\Delta^2 + \gamma_{12}^2 - |\Omega_c|^2\right)}{\left(\Delta^2 - \gamma_{12}\gamma_{13} - |\Omega_c|^2\right)^2 + \Delta^2(\gamma_{12} + \gamma_{13})^2}. \tag{2.31}$$

Now, if $\Delta = 0$, it implies the probe frequency is tuned exactly to the $|3\rangle \leftrightarrow |1\rangle$ transition. Then $n(\omega_p(t)) = 1$ and,

$$a(\omega_p) = \frac{N\omega_p|\mu_{13}|^2}{\varepsilon_0\hbar c} \frac{\gamma_{12}}{\gamma_{12}\gamma_{13} + |\Omega_c|^2}. \tag{2.32}$$

If $|\Omega_c|^2 \gg \gamma_{12}\gamma_{13}$, then the absorption coefficient $a(\omega_p)$ can be very small. Thus, a sufficiently intense coupling field can induce transparency at the probe frequency. Fig. 2.4 illustrates how a transparency window is generated because of presence of Ω_c, i.e., the pump field.

EIT could also be understood as a quantum interference phenomena as follows. The absorption of the probe field is defined by the transition from $|1\rangle$ to $|3\rangle$, refer to Fig. 2.3. Now, the fields can drive population from $|1\rangle$ to $|3\rangle$

by two pathways. One, directly from $|1\rangle \rightarrow |3\rangle$, and the other via the path, $|1\rangle \rightarrow |3\rangle \rightarrow |2\rangle \rightarrow |3\rangle$. EIT results, if the probability amplitudes for the different paths interfere destructively. If $|3\rangle$ has relatively long lifetime, then the transparency window would be completely inside the $|1\rangle \rightarrow |3\rangle$ absorption line.

2.5 Slow Light

For realization of EIT, it is necessary that the decoherence rate γ_{13} to be very small and consequently, EIT has been observed primarily in dilute gases. Now, for $|\Omega_c|^2 \gg \Delta^2,\ \gamma_{12}^2,\ \gamma_{12}\gamma_{13},\ |\Delta|\gamma_{13}$ we obtain:

$$n(\omega_p) \approx 1 - \frac{N}{2\varepsilon_0\hbar}\frac{|\mu_{13}|^2}{|\Omega_c|^2}\Delta\,.$$

Then, it could be shown that the group velocity, $v_g = \frac{c}{n+\omega\frac{\mathrm{d}n}{\mathrm{d}\omega}}$, at the probe frequency is: $v_g(\omega_p) \approx \frac{2c\hbar\varepsilon_0|\Omega_c|^2}{N\omega_p|\mu_{13}|^2}$, for $N\omega_p|\mu_{13}|^2/(2\varepsilon_0\hbar) \gg |\Omega_c|^2$. We can thus, conclude that the group velocity in EIT can be extremely small—on the order of few meters per second. Hence, exploiting EIT one can obtain slow light. In fact, we can estimate the group velocity for a probe field at the sodium D_2 line frequency ($\lambda = 589$ nm), taking atomic density $N = 3 \times 10^{12}$ cm^{-3} and pump field intensity of 12 mW/m^2. Assuming $|\mu_{23}|^2/|\mu_{13}|^2 \approx 1$, from our treatment, we obtain $v_g(\omega_p) \approx 120$ m/s.

For an excellent treatment on the topic of EIT, readers are referred to Refs. [80, 81].

2.6 Fast Light

We have touched upon the idea of slow light in the context of EIT in the previous section.

When a light pulse of frequency ω and bandwidth $\Delta\omega$ propagate through a dispersive medium having refractive index $n(\omega)$, the light velocity in the medium is described by the group velocity, $v_g = \frac{c}{n_g}$, where

$$n_g = n(\omega) + \omega \frac{\mathrm{d}n(\omega)}{\mathrm{d}\omega}\,, \tag{2.33}$$

is termed as the group index. c is the speed of light in vacuum. Now, based on Eq. 2.33, we can think of the following situations:

Case 1: The group index n_g remains constant over the pulse bandwidth $\Delta\omega$. Then the pulse maintains its shape during propagation.

Case 2: One can have a situation, where $\frac{\mathrm{d}n(\omega)}{\mathrm{d}\omega} > 0$. This is what happens in EIT. The group index is significantly enhanced in the lossless normal dispersion region between two closed spaced absorption lines [61, 82]. In experiments, it is shown that the group velocity of light is getting reduced to as low as 8 m/s [63].

Case 3: There are situations, where it is possible to get, $\frac{\mathrm{d}n(\omega)}{\mathrm{d}\omega} < 0$. For example, between two closely spaced gain lines, there appears an anomalous dispersion region where $\omega\frac{\mathrm{d}n(\omega)}{\mathrm{d}\omega} < 0$ and its magnitude could be very large. Clearly, in such a situation, the group velocity of light can exceed the speed c, and v_g can even be negative! At first, it may look like an impossibility. However, it turns out that, superluminal light pulse propagation ($v_g > c$) is not in conflict with the so-called causality principle of physics. Superluminal light is a direct consequence of classical interference between its different frequency components in an anomalous dispersion region [31, 82].

As discussed in [82], we can understand the idea of negative group velocity as follows. Consider a dispersive medium of length L. Light takes time, $t = \frac{L}{v_g} = \frac{Ln_g}{c}$ to propagate through it. Now compare the time $t_0 = \frac{L}{c}$, the time required by the light pulse to propagate the same distance in vacuum. It is evident that the light pulse that enters the medium will exit at a moment delayed

by a time difference $\Delta t = t - t_0 = \frac{L}{c} n_g - \frac{L}{c} = \frac{L}{c}(n_g - 1)$. Now, when $n_g < 1$ the delay time Δt is negative, resulting in advancement of the pulse compared to vacuum. Thus, a light incident on a medium with $n_g < 1$, the light appears to be on the other side of the medium sooner, if it had traversed the same distance in a vacuum. For more details on the topic, readers are referred to [31, 59].

2.7 Optical Force

Since the advent of laser, the mechanical effects of laser beams on particles such as atoms, molecules, ions, etc., have been successfully exploited in a variety of areas, such as Bose-Einstein condensate [83], laser cooling and trapping [84], quantum information [85], optical tweezers [86], and optomechanics [87]. At the core of most of these applications is the so-called radiation-pressure force, or simply called optical force. One of the important applications of optical force is towards manipulation of an atomic beam.

In this section, we briefly discuss optical force in the context of a two-level atom. The forces on two-level atoms are generally calculated by using the steady-state solutions of the so-called optical Bloch equations within the rotating-wave approximation (RWA) [88]. However, the validity of RWA and the SVEA is questionable when one uses intense femtosecond and attosecond optical pulses, rather than CW laser [89]. In this thesis, we discuss the problem of manipulation of an atomic beam using a femtosecond laser pulse. Hence, in the following, we explain optical force without taking RWA into consideration. The treatment is based on the Ref. [88].

Let us consider the interaction between a system of two-level atoms with a superimposed and copropagating collimated few-cycle laser pulse, given by:

$$\vec{\mathbf{E}} = \hat{\eta} A(\vec{\mathbf{r}}, t) \cos(\phi(z) - \omega t) \,, \tag{2.34}$$

where $A(\vec{\mathbf{r}},t)$ is the envelope, $\hat{\eta}$ is the polarization direction, $\phi(z)$ is the phase, and ω is the operating frequency of the laser field. The average optical force on the atoms is as follows:

$$\vec{\mathbf{F}} = \left\langle \vec{\nabla}(\vec{\mu}\cdot\vec{\mathbf{E}}) \right\rangle . \tag{2.35}$$

Using Eq. 2.34 in Eq. 2.35, it is straightforward to get:

$$\vec{\mathbf{F}} = \langle \vec{\mu}\cdot\hat{\eta}\rangle \left[\nabla A(\vec{\mathbf{r}},t)\cos\left(\phi(z)-\omega t\right) - \nabla\phi(z)A(\vec{\mathbf{r}},t)\sin\left(\phi(z)-\omega t\right) \right] . \tag{2.36}$$

Now, we know,

$$\langle \vec{\mu}\cdot\hat{\eta}\rangle = \mu(\rho_{12}+\rho_{21}) , \tag{2.37}$$

where ρ_{12} and ρ_{21} are the off-diagonal elements of the density matrix with $|1\rangle$ and $|2\rangle$ referring to the ground and the excited state of the two-level atom, respectively. Writing, $u = \rho_{12}+\rho_{21}$, the well-known Bloch vector component which accounts for the dispersive effects of the two-level atomic medium, we obtain:

$$\vec{\mathbf{F}} = \mu u \left[\nabla A(\vec{\mathbf{r}},t)\cos\left(\phi(z)-\omega t\right) - \nabla\phi(z)A(\vec{\mathbf{r}},t)\sin\left(\phi(z)-\omega t\right) \right] . \tag{2.38}$$

Now let us consider a few-cycle-pulse Gaussian laser field propagating along the z direction described by the following equation:

$$\vec{\mathbf{E}}(\vec{\mathbf{r}},t) = \hat{\eta}E_0 e^{-\left(\frac{r^2}{w_0^2}+\frac{t^2}{\tau^2}\right)}\cos(kz-\omega t) . \tag{2.39}$$

Thus, $A(\vec{\mathbf{r}},t) = E_0 e^{-\left(\frac{r^2}{w_0^2}+\frac{t^2}{\tau^2}\right)}$ and $\phi(z) = kz$.

Here, E_0 is the peak amplitude, w_0 is the beam waist, $r^2 = x^2+y^2$, and k is the wave vector of the Gaussian laser field. τ is the temporal pulse width, related to the full width at half maximum (FWHM) of the laser field. From

Eqs. 2.38 and 2.39, we obtain the expression for the optical force as follows:

$$\vec{\mathbf{F}} = \mu u \Bigg[-\frac{2r}{w_0^2} E_0 e^{-\left(\frac{r^2}{w_0^2}+\frac{t^2}{\tau^2}\right)} \cos(kz-\omega t)\hat{\mathbf{r}} \\ -kE_0 e^{-\left(\frac{r^2}{w_0^2}+\frac{t^2}{\tau^2}\right)} \sin(kz-\omega t)\hat{\mathbf{z}} \Bigg] \quad . \tag{2.40}$$

This could be decomposed into two parts, a transverse component, F_T, and the longitudinal component, F_z, of the light force, as given below:

$$F_T = -\frac{2\mu u E_0 r}{w_0^2} e^{-\left(\frac{r^2}{w_0^2}+\frac{t^2}{\tau^2}\right)} \cos(kz-\omega t) \\ F_z = -\mu u k E_0 e^{-\left(\frac{r^2}{w_0^2}+\frac{t^2}{\tau^2}\right)} \sin(kz-\omega t) \quad . \tag{2.41}$$

It is evident that the transverse component of the optical force could be used for trapping or focusing the atoms while the longitudinal one could be exploited for steering the atoms. The optical force in the non-RWA regime has been explored extensively in the last decade [2, 90–92].

2.8 Optical Bistability (OB)

OB refers to the situation in which two different output intensities are possible for a given input intensity. OB has found applications in optical communication and optical computing.

To understand OB phenomenon, let us consider a nonlinear medium placed inside a Fabry-Pérot resonator as shown in Fig. 2.5. Let the amplitude reflectance be ρ and transmittance be τ, then intensity reflectance R and transmittance T are given by:

$$R = |\rho|^2 \\ T = |\tau|^2 \quad , \tag{2.42}$$

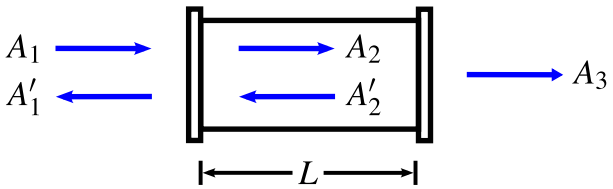

Figure 2.5: Fabry-Pérot resonator.

with, $R+T=1$.

The incident and internal fields are related to each other through boundary conditions of the form:

$$\begin{aligned} A_2' &= \rho(A_2 e^{ikl})e^{ikl}e^{-\alpha l} \\ &= \rho A_2 e^{2ikl}e^{-\alpha l} \\ A_2 &= \tau A_1 + \rho A_2' \end{aligned} \quad , \tag{2.43}$$

where the field amplitudes are measured at the left-hand mirror.

The propagation constant $k = \frac{\omega}{c}n$, and the absorption coefficient α include both linear and nonlinear contributions. These quantities are taken to be real. Solving the above equations, we obtain

$$A_2 = \tau A_1 + \rho^2 A_2 e^{i2kl-\alpha l} = \frac{\tau A_1}{1-\rho^2 A_2 e^{i2kl-\alpha l}} \, . \tag{2.44}$$

If k or α (or both) is a sufficiently nonlinear function of the intensity of light within the interferometer, this equation predicts bistability in the intensity of the transmitted wave.

Absorptive Bistability

Say, the absorptive coefficient α depends nonlinearly on the field intensity, and k is a constant. Assume that the mirror separation l is adjusted so that the cavity is tuned to resonance with the applied field. Then, $\rho^2 e^{2ikl} = R$. Also assume

that $\alpha l \ll 1$, so that we can ignore the spatial variation of the intensity of the field inside the cavity.

Thus,

$$A_2 = \frac{\tau A_1}{1 - R(1-\alpha l)} \,. \tag{2.45}$$

Using $I_i = 2n\varepsilon_0 |A_i|^2$, we get

$$I_2 = \frac{T I_1}{[1 - R(1-\alpha l)]^2} \,.$$

Now, introducing a dimensionless parameter C, called the cooperation number, defined as:

$$C = \frac{R\alpha l}{1-R} \,, \tag{2.46}$$

we can write:

$$I_2 = \frac{T I_1}{[T(1+C)]^2} = \frac{I_1}{T(1+C)^2} \,, \tag{2.47}$$

where C depends on intensity of light within the interferometer through α.

Let us assume that, $\alpha = \frac{\alpha_0}{1+I/I_s}$, an expression valid for two level saturable absorber, where I is the local field inside the interferometer. Taking $I = I_2 + I_2' \approx 2I_2$, the parameter C could be written as,

$$C = \frac{R\alpha l}{1-R} = \frac{R\alpha_0 l}{(1+I/I_s)(1-R)} = \frac{C_0}{(1+2I/I_s)} \,,$$

with $C_0 = \frac{R\alpha_0 l}{1-R}$. Thus,

$$I_1 = T I_2 (1+C)^2 = T I_2 \left(1 + \frac{C_0}{(1+2I/I_s)}\right)^2 \,. \tag{2.48}$$

Finally, we have the output intensity,

$$I_3 = T I_2 \,. \tag{2.49}$$

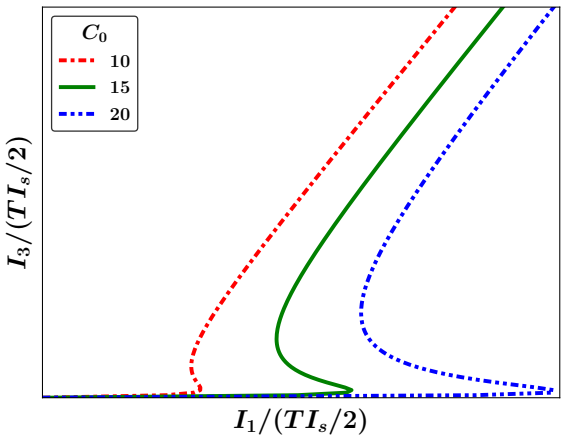

Figure 2.6: Illustration of Input-output relations under different cooperation parameter C_0

The input-output relations, as given by Eq. 2.48 and Eq. 2.49, is illustrated in Fig. 2.6. It is clear that, for C_0 greater than 8, more than one output intensity can occur for certain values of the input intensity, showing that the system posses multiple solutions. The mechanism of OB phenomena is illustrated in Fig. 2.7. Let us imagine that the input intensity I_1 is initially zero and is slowly increased: as I_1 is increased from zero to I_h (the high jump point), the output intensity is given by the lower branch of the solution, i.e., by the segment terminated by points a and b. As the input intensity is increased still further, the output intensity must jump to the point c and trace out the portion of the curve labeled $c-d$. If the intensity is now slowly decreased, the system will remain on the upper branch and the output intensity will be given by the curve segment $e-d$. As the input intensity passes through the value I_l, the system makes a transition to the point f and traces out the curve $f-a$ as the input intensity is decreased to zero. One can use such systems as an optical switch as illustrated in Fig. 2.7. Let us say the input intensity is fixed at the value I_b (the bias intensity). Two stable output points indicated by the filled dots are

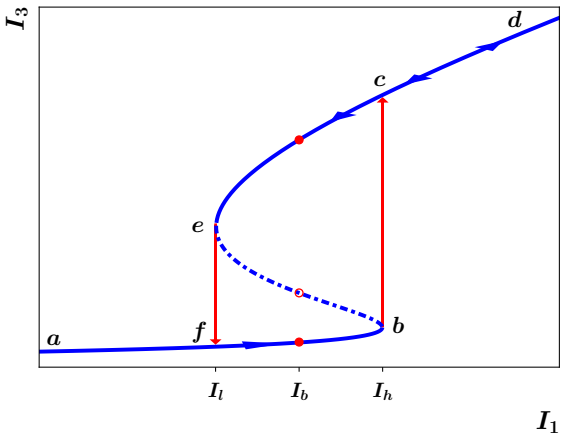

Figure 2.7: Schematic illustration of Optical Bistability phenomenon

possible. The state of the system can be used to store binary information. The system can be forced to make a transition to the upper state by injecting a pulse of light so that the total input intensity exceeds I_h; the system can be forced to make a transition to the lower state by momentarily blocking the input beam.

For more detailed exposition on the topic, readers are referred to Ref. *Nonlinear Optics*, Boyd [81], Ch. 7, on which this section is based.

There are excellent review articles and books on the topic of coherent control. Some of these are cited in: [1, 3, 93–95].

Chapter 3

Effective Control of Optical Multistability

In this chapter, we theoretically analyze the behavior of single optical bistability (OB), double OB, and tristability (OT) in a three-level V-type atomic system confined in a unidirectional optical ring cavity. The physics behind the emergence of various bistable and tristable states, and switching from the absorptive to the dispersive characteristics are explored. The role of probe- and control-field detunings on the input-output characteristics is probed. Further, it is found that the switching between various bistable phenomena is defined by the ratio between the absolute peak values of the parameters describing dispersion and absorption respectively. This ratio sets a criterion for obtaining absorptive OB, OT, double OB and dispersive OB. The role of control-field intensity and detuning as well the cooperation parameter on the input-output characteristics are explored. Finally, a scheme is discussed to control the width of the middle branch of double OB and OT as well single OB.

The contents of this chapter are published in **Abdelaziz, Abdelsalam H. M.** and Amarendra K. Sarma, "Effective control and switching of optical multistability in a three-level V-type atomic system", Phys. Rev. A **102**, 043719 (2020).

3.1 Brief overview

The possibility to modify linear absorption, dispersion, and nonlinearity of atomic medium ceaselessly pushes the research in optical sciences for half a century till now. Quantum coherence and interference, which led to the observation of the phenomena such as, coherent population trapping (CPT) and electromagnetically induced transparency (EIT), are at heart of manipulation of the properties of an atomic medium and have been studied extensively in past decades and continues to remain a major area of research in various contexts [6–17]. Among a plethora of phenomena, optical bistability (OB) and optical tristability (OT) have drawn much attention due to their numerous applications such as all-optical switching, optical transistors, optical memories, logical gates [23–26] and, even in the context of cold atoms [33, 34]. Initially, OB has been demonstrated experimentally for saturable absorber, Ruby crystal, and Sodium vapor as a nonlinear medium inside in an optical resonator [36–38]. Then by developing the basic theoretical model of OB for two-level atoms coupled by a single cavity mode [38–41], it was realized that OB arises due to intensity-dependent absorption or dispersion, or hybridization of both; henceforth, OB is classified as absorptive or dispersive, or hybrid respectively. A decade later, OT has been demonstrated for Λ-type three-level atomic system comprising an excited state and two ground state sublevels driven by two cavity modes [42–44]. Soon it was proposed that OB (OT) is more definitive with multi-level atoms than in two- (three-) level atoms as a nonlinear medium inside in an optical resonator. This is owing to the fact that absorption, dispersion, and nonlinearity could be greatly modified by quantum coherence and interference in multilevel atoms for increased pathways. In this regard, coherent control by electromagnetic field induced transparency (EIT) in three-level atomic systems was demonstrated theoretically and experimentally to reduce OB thresh-

old intensity and give rise to a new type of OT by adjusting the control laser field parameters [45–47]. Also by considering spontaneously generated coherence (SGC), the possibility of obtaining small cooperative parameter with low threshold intensity for OB, and OT in three level atomic systems was demonstrated [65, 67, 71, 96, 97]. Moreover, the optical bistability (OB) behavior of a three-level V-type atomic system inside a unidirectional ring cavity was demonstrated using a microwave field driving a hyperfine transition between two upper excited states. It was illustrated that, with the increase of the intensity of the coherent microwave driving field, the bistable threshold intensity increases and the hysteresis loop becomes wider [69]. Recently, incorporating coherent control by incoherent pumping in Λ-type three-level atomic system was demonstrated to reduce OB threshold intensity [98]. Furthermore, hybrid absorptive-dispersive optical bistability (OB) behavior in an open Λ-type three-level atomic system by using a microwave field to drive the hyperfine transition between two lower states, along with the consideration of incoherent pumping and SGC has been analyzed and demonstrated to reduce OB threshold intensity over closed three-level atomic system [99]. On the other hand, the consideration of coherent control by incoherent pumping and SGC in open Ξ-type three-level atomic system was shown to affect the OB threshold intensity, and give rise to OT by adjusting the detuning of the control laser field [100]. Alongside closed and open three level schemes, four- and five-level atomic systems were proposed as a promising alternatives to control OB and OT. In this context, considering SGC in four level atomic system was illustrated to decrease the threshold intensity for OB [101]. On the other hand, without considering SGC, OB and OT in open and closed four level atomic system inside a standing-wave cavity were theoretically and experimentally studied [102, 103]. Also, coherent control of nonlinear absorption of a probe field by both the coupling and control fields was shown to affect OB threshold intensity in Ξ-type four-level

atomic system [104]. Moreover, coherent control of the two sublevels in the ground state was shown to manipulate the OB threshold intensity, and change OB to OT in inverted Y-type four level atomic system by switching the two orthogonally polarized cavity modes was reported [105]. Furthermore, coherent control by a microwave field driving two lower states and relative phase of the applied fields was demonstrated to control OB behavior, and change OB to OT in four-level systems [106, 107]. Again, coherent control by the probe and the control field was shown to affect OB behavior, and switch OB to OT in five-level EIT atomic system [108]. As previously mentioned, OB and OT in three-level Λ-type atomic system have been extensively studied while less attention has been paid to investigate OB and OT in three-level V-type atomic system. This may be owing to the coherence relaxation of upper-levels by spontaneous emission which is not the case for Λ-type atomic system [64, 65]. Hence, to the best of our knowledge, available studies on OB and OT in a three-level V-type atomic system are attempting to circumvent this effect by incorporating coherent control using incoherent pump field, or microwave field, or SGC [65–72]. In passing, it is worthwhile to note that various studies, including optical bistability, continues in V-type atomic systems. For example, very recently, experimental studies on optical bistability and nonlinear dynamics in a three-level V-type cold Yb-atomic system have been reported [109]. In this work, by assuming that three-level atomic system should be sufficient for reliable obtainment of single OB, double OB, and OT, we investigate the criteria for achieving the same, without considering coherent control by incoherent pump field, or microwave field, or SGC. In addition, we propose a method to control the width of the middle branch of double OB and OT even at small cooperation parameter. We find that our proposed scheme for obtaining OB and OT in three-level V-type atomic system, even amidst coherence relaxation of upper-levels by spontaneous emission, is comparable or even better than that of

ones reported with three-level Λ-type atomic system, where coherent control is done by making use of incoherent pump field, or microwave field, or SGC [25, 26, 45, 46, 96].

3.2 Model and theory

We consider a three-level V-type atomic system, as depicted in Fig. 3.1(a). The transition $|1\rangle \leftrightarrow |3\rangle$ with frequency ω_{31} is coupled by a coherent probe laser field of frequency ω_p and amplitude E_p. The transition $|1\rangle \leftrightarrow |2\rangle$ with frequency ω_{21} is coupled by coherent laser field of frequency ω_c and amplitude E_c. The total electric field can be written as: $\mathbf{E} = (\mathbf{E_c}e^{i\omega_c t} + \mathbf{E_p}e^{i\omega_p t} + c.c)/2$. Under the dipole and the rotating-wave approximations, the Hamiltonian of a three-level V-type atomic system is given by:

$$\mathbf{H}/\hbar = \begin{bmatrix} 0 & \Omega_c^*/2 & \Omega_p^*/2 \\ \Omega_c/2 & -\Delta_c & 0 \\ \Omega_p/2 & 0 & -\Delta_p \end{bmatrix}, \tag{3.1}$$

where $\Omega_c = -\mu_{21}E_c/\hbar$ and $\Omega_p = -\mu_{31}E_p/\hbar$ are Rabi frequencies for the transitions with electric dipole moments μ_{21} and μ_{31} respectively. $\Delta_c = \omega_c - \omega_{21}$ and $\Delta_p = \omega_p - \omega_{31}$ are the detunings of control and probe fields respectively. It should be noted that $\omega_{ij} = \omega_i - \omega_j$. The density matrix equations describing the atomic system dynamics are given by:

$$\begin{aligned}
\dot{\rho}_{11} &= \gamma_{21}\rho_{22} + \gamma_{31}\rho_{33} - i[\Omega_c^*\rho_{21} + \Omega_p^*\rho_{31} - c.c]/2 \\
\dot{\rho}_{22} &= -\gamma_{21}\rho_{22} + i[\Omega_c^*\rho_{21} - c.c]/2 \\
\dot{\rho}_{33} &= -\gamma_{31}\rho_{33} + i[\Omega_p^*\rho_{31} - c.c]/2 \\
\dot{\rho}_{21} &= \Gamma_{21}\rho_{21} - i\left[\Omega_c\left(\rho_{11} - \rho_{22}\right) - \Omega_p\rho_{23}\right]/2 \\
\dot{\rho}_{31} &= \Gamma_{31}\rho_{31} - i\left[-\Omega_c\rho_{32} + \Omega_p\left(\rho_{11} - \rho_{33}\right)\right]/2 \\
\dot{\rho}_{32} &= \Gamma_{32}\rho_{32} - i\left[-\Omega_c^*\rho_{31} + \Omega_p\rho_{12}\right]/2
\end{aligned}, \tag{3.2}$$

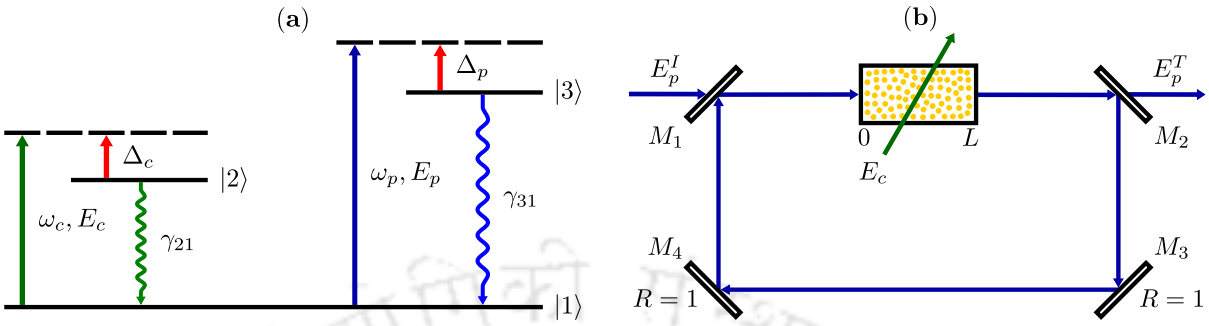

Figure 3.1: (a) Three-level V-type atomic system, (b) Unidirectional ring cavity.

with $\rho_{ij} = \rho_{ji}^*$ and $\sum_{i=1}^{3} \rho_{ii} = 1$. γ_{ij} denotes the spontaneous decay rate from state $|i\rangle$ to $|j\rangle$. $\Gamma_{21} = i\Delta_c - \gamma_{21}/2$, $\Gamma_{31} = i\Delta_p - \gamma_{31}/2$, and $\Gamma_{32} = i(\Delta_p - \Delta_c) - (\gamma_{21} + \gamma_{31})/2$.

In a unidirectional ring cavity, a three-level V-type atomic medium with number density N and length L is inserted as shown in Fig. 3.1(b). For simplicity, the mirrors M_3 and M_4 are assumed to be perfect, whereas R (T) is the intensity reflection (transmission) coefficient of mirrors M_1 and M_2, provided that $R+T=1$. The probe field E_p circulates in the cavity, while the control field E_c does not. The incident coherent probe field E_p^I entering the cavity through semi-silvered mirror M_1 induces polarization $P(\omega_p)$ in the atomic medium and then transmitted partially from the mirror M_2 as E_p^T. Meanwhile, the control field can further modulate the induced polarization, which may modify the absorption and the dispersion of the atomic medium. Under the slowly varying envelope approximation and using Maxwell's equations, the equation describing the probe field dynamics could be expressed as follows:

$$\frac{\partial E_p}{\partial t} + c\frac{\partial E_p}{\partial z} = \frac{i\omega_p}{2\varepsilon_0} P(\omega_p), \tag{3.3}$$

where c is the speed of light, ε_0 is the permittivity of free space, and $P(\omega_p) =$

$N\mu_{13}\rho_{31}$ is the slowly oscillating term for the induced polarization in the transition $|1\rangle \leftrightarrow |3\rangle$. It is worthwhile to note that, it is possible to obtain an analytical expression for ρ_{31}, and thereby $P(\omega_p)$ [8, 10, 45]. The analytical expression for ρ_{31} is provided in App. A. However, rather than discussing this very complicated expression, we focus on our simplified model.

For a perfectly tuned ring cavity, in the steady state limit, the boundary conditions between the incident field E_p^I and the transmitted field E_p^T are given by:

$$\begin{aligned} E_p(L) &= E_p^T/\sqrt{T} \\ E_p(0) &= \sqrt{T}E_p^I + RE_p(L) \end{aligned} . \tag{3.4}$$

By considering the mean-field limit, and employing the boundary conditions, the steady state input-output relation for the probe field is written as [25, 41, 45]

$$y = x - iC\gamma_{31}\rho_{31}\,, \tag{3.5}$$

where $x = \mu_{13}E_p^T/(\hbar\sqrt{T})$, $y = \mu_{13}E_p^I/(\hbar\sqrt{T})$ are the normalized output and input field respectively, and $C = N\omega_p L\mu_{13}^2/(2\hbar\varepsilon_0 cT\gamma_{31})$ is the cooperation parameter. The input field y is complex while the transmitted amplitude x is assumed to be real [45].

The atomic system response to the applied fields is determined by the complex susceptibility parameter, $\chi = \chi_R + i\chi_I$, which is connected to ρ_{31}, which is again a complex quantity, via the following relation:

$$\chi(\omega_p) = \frac{N\mu_{13}}{\varepsilon_o E_p}\rho_{31}(\omega_p). \tag{3.6}$$

It is well known that the real part of susceptibility, i.e. χ_R is related to dispersion while the imaginary one, i.e. χ_I, is related to absorption of the atomic system

[81]. It is straightforward to show that:

$$\begin{aligned} \chi_R &= -\frac{N\mu_{13}}{C\gamma_{31}\varepsilon_o E_p} Im(y) \\ \chi_I &= \frac{N\mu_{13}}{C\gamma_{31}\varepsilon_o E_p} [Re(y) - x] \end{aligned} . \tag{3.7}$$

Thus, $Im(y)$ could be utilized to quantify dispersion, whereas $[Re(y) - x]$ could be used for enumeration of absorption. For the sake of brevity, in the rest of the work we will write, $\chi' = Im(y)$ and $\chi'' = [Re(y) - x]$, and they could respectively be referred to as the real part of susceptibility and imaginary part of susceptibility in normalized units.

3.3 Results and Discussions

We solve Eqs. 3.2 and their complex conjugates at the steady state, together with Eq. 3.5 numerically to study the input-output characteristics. As regards a real system, we may consider rubidium vapor as the cavity nonlinear medium to observe OB, double OB, and OT. The states $|1\rangle$, $|2\rangle$ and $|3\rangle$ respectively refer to $5S_{1/2}$, $6P_{1/2}$, and $6P_{3/2}$ quantum states of Rb atoms. $\omega_{21}/2\pi = 113.18$ and $\omega_{31}/2\pi = 113.56$ THz are the transition frequencies with electric dipole moments $\mu_{21} = 2.7427$ and $\mu_{31} = 4.4342 \times 10^{-30}$ C $\cdot$ m respectively [110]. The corresponding spontaneous decay rates are $\gamma_{21}/2\pi = 0.23873$ and $\gamma_{31}/2\pi = 0.28170$ MHz [111]. The vapor cell length L could be taken as 0.05 m, and the intensity transmission coefficient T of mirrors M_1 and M_2 is 0.05. The cooperation parameter C is an adjustable parameter, and could be changed by varying the vapor density inside the cell. However it is worthwhile to note that in order to set the cooperation parameter C to 100, the atomic number density N of 7×10^{15} m^{-3} is mandatory which corresponds to temperature ~ 292 K [112]. There is another possibility in which the probe and the control fields

interchange their roles. In that case, $C = 100$ is possible at slightly higher atomic number density N of 6×10^{16} m^{-3} which corresponds to temperature ~ 300 K.

For the sake of brevity and to keep the calculations clean, in the rest of the work, we assume $\gamma_{21} = \gamma_{31}$ and scale all figures in the unit of γ_{31}. Fig. 3.2 exhibits the effect of the probe field blue-detuning, Δ_P, on the output field, x, as a function of the normalized parameters, the input field $|y|$ and the susceptibility components χ' and χ''. It could be seen that for small Δ_P of $0.5\gamma_{31}$ [Fig. 3.2(a)], χ'' has a negative peak (absorption) at a small output field, while χ' after having a very small positive peak (positive refraction) at small output field, displays a negative peak (negative refraction) at intermediate output field. This feature may be used to explain the input-output characteristics, exhibiting OB, as shown by the blue-colored solid curve. Here, OB is of absorptive nature as its threshold intensity is mainly due to the absolute value of χ'', at small output field. On the other hand, for large Δ_P of $2.6\gamma_{31}$ [Fig. 3.2(d)], χ'' exhibits a small negative peak value compared to the previous case. Interestingly, χ' does not show any initial positive peak unlike the previous case. Rather, it displays a minor negative peak at small output field followed by a small negative peak at an intermediate output field. This results in disappearance of absorptive OB at small output field and the emergence of dispersive OB, where the threshold intensity could be owing to the absolute value of χ', at an intermediate output field.

In between these two extreme cases, say, for Δ_P of $1.0\gamma_{31}$ [Fig. 3.2(b)], we find that χ'' has a negative peak at small output field, whereas χ' has a negative peak at intermediate output field. These features results in the formation of OT, as could be seen joining the higher and lower branches of absorptive and dispersive hysteresis loops respectively into a middle branch. In fact, we find that OT will exist whenever the width of the middle branch does not exceed

the sum of respective widths of lower and higher branch. It is worthwhile to note that OT could be changed to double OB by increasing Δ_P to $1.3\gamma_{31}$, as illustrated in Fig. 3.2(c). In this case, the width of the middle branch exceeds the respective sum of the widths of lower and higher branch. The difference between double OB and OT is that double OB has two stable output fields for each of two input field regions while OT has three stable output fields for one input field region. Moreover, the threshold intensities of the absorptive and dispersive hysteresis loops increase with probe field detuning.

Furthermore, it is revealed that the threshold intensities of the dispersive OB, and that of both OT and double OB, in the middle branch, are predominantly due to the absolute peak value of χ' at intermediate output field. On the contrary, the threshold intensities of absorptive OB and that of both OT and double OB, in the lower branch, are due to the absolute peak value of χ'' and/or χ' at small output field. Thus it may be inferred that, the ratio between the absolute peak value of χ', at intermediate output field, and the absolute peak value of χ'' and/or χ', at small output field, defines the switching between various bistable phenomena. If this ratio is considerably less than unity, absorptive OB is attainable and when it is around unity, OT could be obtained. On the other hand, if it is slightly more than unity, double OB is achievable, while if it is considerably more than unity, dispersive OB is attainable. It is worthwhile to note that this ratio rely on the physical properties of the atomic system such as absorption and dispersion but not on the cavity feedback.

In Fig. 3.3 we show the effect of the control field detuning, Δ_c, on the behavior of single OB, double OB, and OT for a given blue-detuned probe-field, Δ_p. It is observed that, in Fig. 3.3(a), the hysteresis loop area of the absorptive OB could be enhanced by red-detuning the control field, say, by $0.15\gamma_{31}$, compared to the case without detuning. This results in the increment of the threshold intensity of the lower branch, while reduction in the threshold inten-

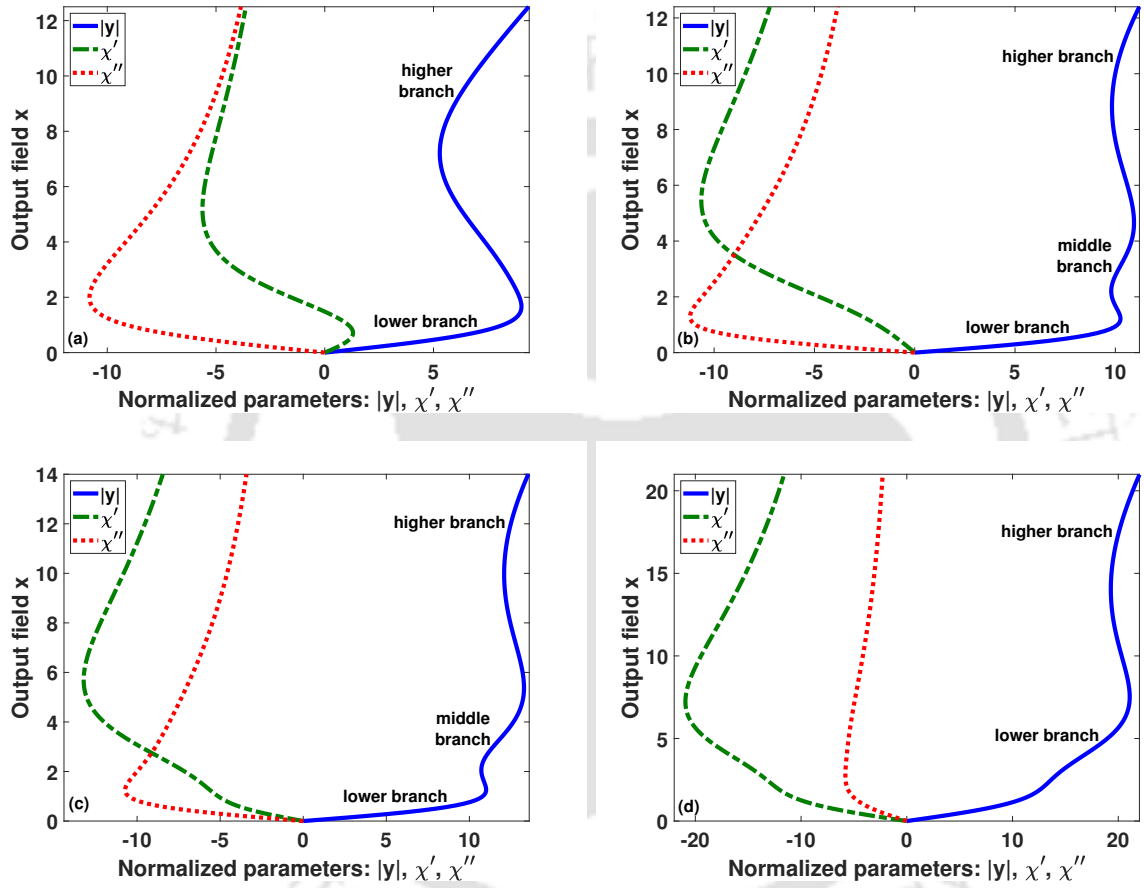

Figure 3.2: Output Characteristics as a function of the normalized parameters: the input field $|y|$ and the susceptibility components χ' and χ''. for different values of probe field detuning Δ_p/γ_{31}: (a) 0.5, (b) 1.0, (c) 1.3, and (d) 2.6. Other parameters are: $\Delta_c = 0$, $\Omega_c = 2.2\gamma_{31}$, and C=100.

sity of the higher branch. On the other hand, blue-detuning of the control field, by $0.15\gamma_{31}$, results in increase of the threshold intensity in both the lower and the higher branch. Again, as illustrated in Figs. 3.3(b) and 3.3(c) respectively, we find that the absorptive and dispersive hysteresis loop area/width for both OT and double OB could be manipulated by detuning the control field. The threshold intensity of both the lower and middle branch gets affected while that of the higher branch remains almost the same. Similar effect could also be seen for the case with highly detuned probe-field, as depicted in Fig. 3.3(d). However, in this case only the middle branch and the corresponding threshold intensity could be engineered by detuning the control field. It is worth mentioning that for a given red-detuned probe field, the resonant control field results in the same input-output characteristics as that of the blue-detuned one. But in this case, detuning of the control field yields opposite effects, i.e. the blue-detuned control field exhibits the results shown by the red-detuned one with blue-detuned probe-field and vice versa.

The effect of the control field intensity, Ω_c, on the input-output characteristics, for a given detuned probe-field, is illustrated in Fig. 3.4. It could be seen that for small Ω_c of $1.2\gamma_{31}$, only dispersive OB with very large area/width exists. However, as the control field intensity, Ω_c, is increased to $2.0\gamma_{31}$ and $2.2\gamma_{31}$, emergence of OT and double OB could be observed. If Ω_c is increased to $3.0\gamma_{31}$, the unfolding of OB alone could be seen. Thus it is possible to switch from dispersive OB to OT, double OB and so on with judicious choice of the control field intensity.

In Fig. 3.5 we show the effect of the cooperation parameter C on the input-output characteristics. It can be seen that, for small C of 75, only the absorptive hysteresis loop exists. Now, if C is increased to 100, the dispersive hysteresis loop emerges above the absorptive one. The threshold intensity of its lower branch is less than that of the middle branch, resulting in OT. Further increment

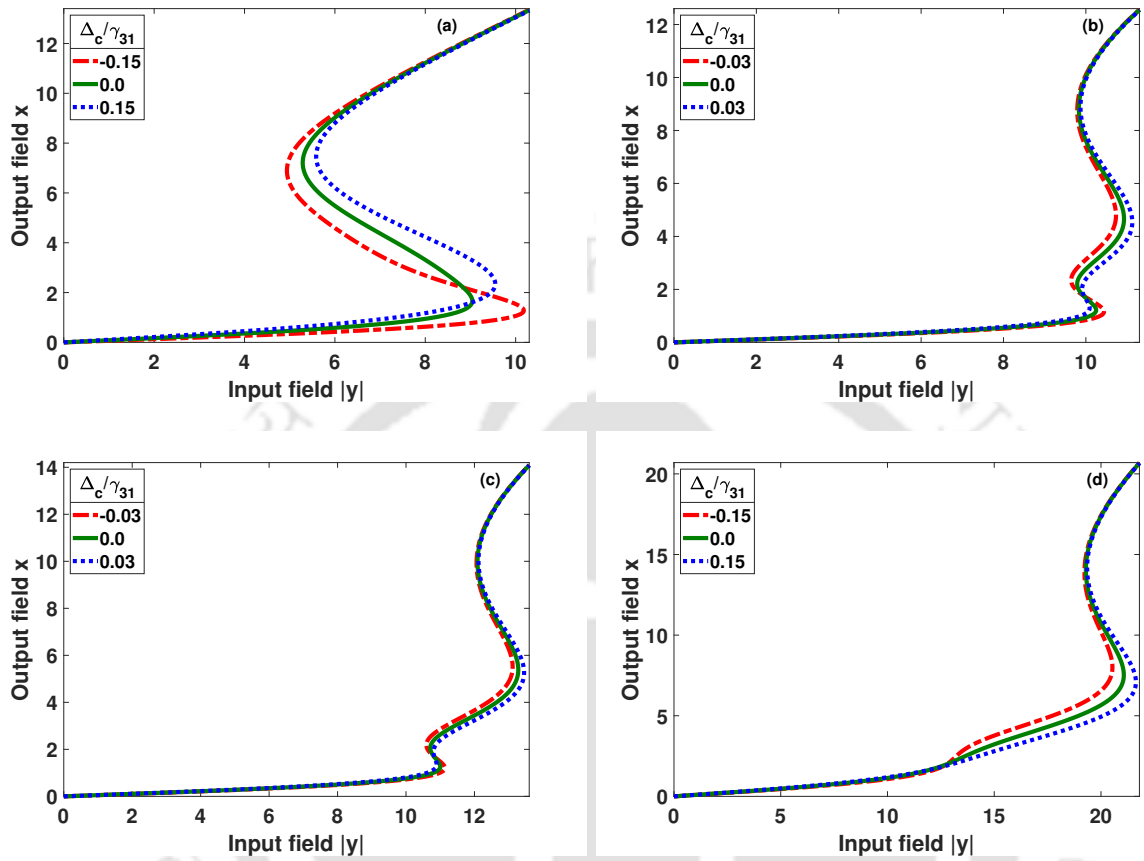

Figure 3.3: Input-Output Characteristics under different control field detunings, Δ_c, with blue-detuning the probe field, Δ_p/γ_{31} : (a) 0.5, (b) 1.0, (c) 1.3, and (d) 2.6. The remaining parameters are: $\Omega_c = 2.2\gamma_{31}$, and C=100.

of C to 175, results in significant decrease in the absorptive hysteresis loop area, which is again situated below the dispersive hysteresis loop. It is easy to see that the required input threshold intensity to obtain OB or OT is significantly increases with higher C. Hence, the cooperation parameter needs to be chosen sagaciously. Finally, in what follows, we discuss the attainability of OT and double OB using a small control field intensity, Ω_c. In Fig. 3.6, we depict the combined effect of blue-detuned probe field and red-detuned control field

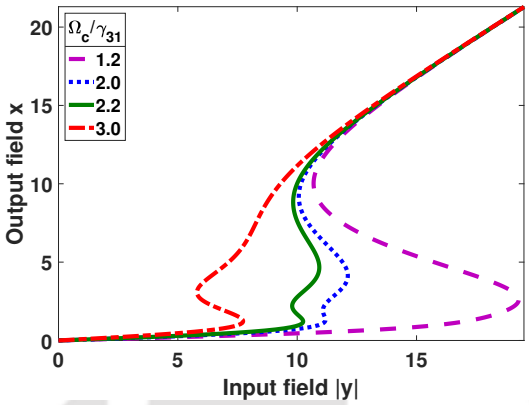

Figure 3.4: Input-Output Characteristics under different control field intensities Ω_c. Other parameters: $\Delta_p = 1.0\gamma_{31}$, $\Delta_c = 0.0\gamma_{31}$, and C=100.

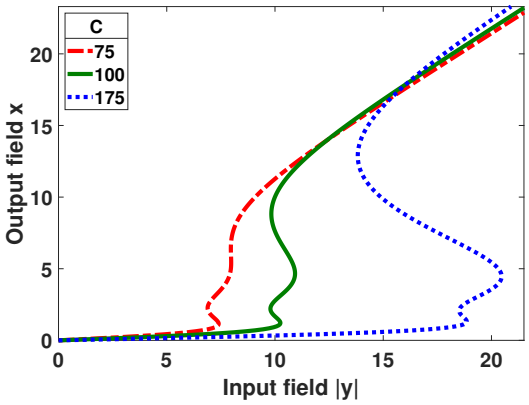

Figure 3.5: Input-Output Characteristics under different cooperation parameters C. Other parameters: $\Delta_p = 1.0\gamma_{31}$, $\Delta_c = 0.0\gamma_{31}$, and $\Omega_c = 2.2\gamma_{31}$.

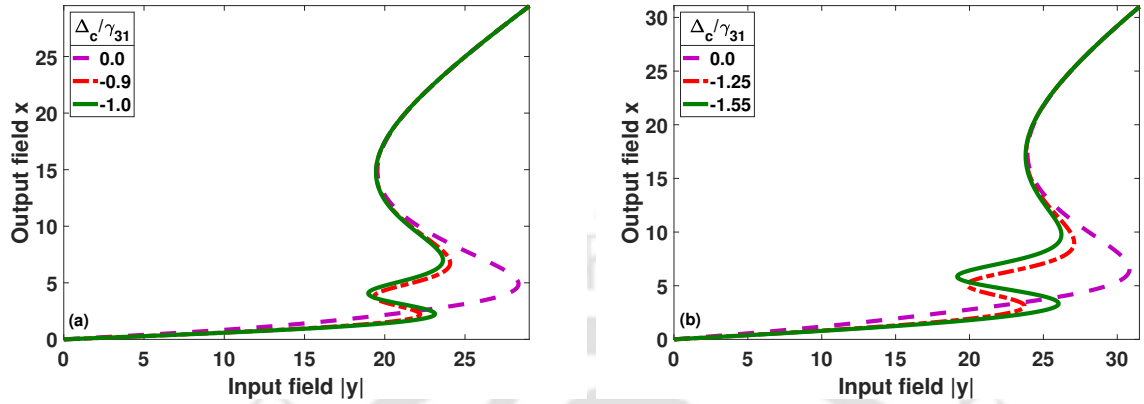

Figure 3.6: Input-Output Characteristics under the combined effect of blue-detuned probe field and red-detuned control field. (a) $\Delta_p/\gamma_{31} = 2.5$ and (b) $\Delta_p/\gamma_{31} = 3.6$. Other parameters are, $\Omega_c = 1.0\gamma_{31}$ and C=100.

on the input-output characteristics. Previously, we found that blue-detuning the control field, for a given blue-detuned probe field, shrinks the absorptive hysteresis loop area, while the one for the dispersive case is increased. On the other hand, opposite effect could be observed by red-detuning the control field, paving the way to control the width of the middle branch by adjusting the system parameters judiciously. Fig. 3.6(a) exhibits dispersive OB, for a given blue-detuned probe field with $2.5\gamma_{31}$, if the control field is resonant. Now, if the control field is red-detuned, say, by $0.9\gamma_{31}$, OT could be achieved. A slight increase in the detuning, say, to $1.0\gamma_{31}$, results in a smooth and wide OT characteristics. We find that in order to obtain double OB as well as OT, the probe field detuning, i.e. Δ_p needs to be increased, along with the control field detuning. This is clearly illustrated in Fig. 3.6(b). We observe that, blue detuning the probe field by $3.6\gamma_{31}$ and red-detuning the control field by $1.25\gamma_{31}$, unfolding of the double OB is achievable. Further increase in the detuning of the control field by $1.55\gamma_{31}$, gives rise to the ramification of OT. It may be noted

that, while we have proposed atomic vapor as the nonlinear medium to observe OB, double OB, and OT, it may be possible to test the proposed scheme in other nonlinear systems as well. For example, asymmetric quantum wells, or double quantum dot nanostructure, or even a hybrid semiconductor quantum dot–metal nanoparticle system could possibly be modeled as a V-type system for the observation of the aforementioned phenomena [113–115]. It may be useful to note that SGC is extremely difficult to obtain in atomic systems. An effect similar to that, such as Fano-type interference, is possible in solid-state systems, which has been employed in Ref. [113]. Our work shows that even with such a type of interference, while it reduces the threshold intensity, it is not mandatory to obtain OB, double OB, and OT.

3.4 Summary

In conclusion, we have theoretically analyzed single OB, double OB, and OT behavior in a V-type three-level atomic system, confined in a unidirectional optical ring cavity. Most importantly, we have tried to understand the physics behind the emergence of various bistable and tristable states, in particular switching from the absorptive to the dispersive characteristics. It is found that the switching between various bistable phenomena is defined by the ratio between the absolute peak values of the parameters describing dispersion and absorption respectively. This ratio sets a criterion for obtaining absorptive OB, OT, double OB and dispersive OB. It is interesting to note that this ratio is independent of the cavity feedback. However, the respective width of the lower, the middle and the higher branch of the hysteresis loop could be manipulated with judicious control of the detuning of the control and the probe fields. Further, we report that the threshold intensities of the absorptive and the dispersive hysteresis loops decrease with the control field intensity but increase with the

probe field detuning and the cooperation parameter, thereby paving the way for easy control of the width of the middle branch of double OB and OT as well single OB. These results are crucial and useful for many applications aiming towards fabrication of efficient all-optical switches and logic-gate devices for optical computing and quantum information processing.

Chapter 4

Slow and Fast Light in Ultracold Atoms

In this chapter, We propose a scheme for attaining slow and fast light via coherent control of the hyperfine ground and excited states of an ultracold atomic system. The proposed scheme is theoretically analyzed for the D_1 transition of ultracold ^{23}Na atoms. The role of field detuning and field intensity on both the population transfer and induced polarization is investigated. It is shown that slow and fast light, with large bandwidth could be obtained in the proposed system. It is inferred that both slow and fast light could co-propagate, pertaining to different optical and Raman transitions. Further, it is observed that switching between the slow and the fast light is achievable by controlling the field intensity, as well as the field detuning.

4.1 Brief overview

The possibility to control the group velocity of light pulses propagating through atomic medium has led to the emergence of slow and fast light. These effects

This chapter is based on the article **Abdelaziz, Abdelsalam H. M.** and Amarendra K. Sarma, "Coherent Control of Hyperfine States and Slow and Fast Light Switching in Ultracold Atoms", arXiv:2107.08897 (2021). The article is under review in Physical Review A.

are at the forefront of optical science research due to its promising applications in optical telecommunication, interferometry, and laser radar [27–32]. Apart from atomic media, slow and fast light phenomena is a topic of intense research in a variety of media, including optomechanics [116, 117], optical fibers [118] and photorefractive crystals [119, 120]. In fact, recently, slow and fast light is experimentally demonstrated even in a plasma medium [121]. Furthermore, storage and retrieval of optical pulse was reported, and recently implemented with a nonlinear metamaterial; where the concept of dark-state polariton, a combined atomic and optical excitation, clarifies how the quantum state of the probe is 'imprinted' in the atoms [12, 59, 122–124]. On the other hand, fast light in a medium with gain doublet, dip in gain profile, was proposed [125], then demonstrated by creating a Raman gain doublet using a bichromatic field [82]. Moreover, fast light was demonstrated by rendering a Raman gain peak into a doublet using a coherent control field [126]. Slow and fast light have been observed extensively in solid-state materials and realized in optical fibers utilizing coherent population oscillation, stimulated Brillouin and Raman scattering [30–32, 118, 127, 128].

Slow light, also known as subluminality, stands for light propagation with a group velocity v_g less than the velocity of light in vacuum c, while fast light, also known as superluminality, refers to light propagation with $v_g > c$ or $v_g < 0$. It was thought that superluminal velocities are generally unphysical in the sense that light wave traveling with superluminal velocity does not transmit any information through the medium otherwise the causality principle of relativity theory would be violated [52]. Accordingly, subluminal group velocity can be regarded as signal velocity, which is not the case for superluminal group velocity [53, 54].

The group velocity for a traveling optical pulse $v_g = c/n_g$, where the group index $n_g = n + \omega\, \mathrm{d}n/\mathrm{d}\omega$, depend on the refractive index n and its dependence

on frequency ω—the dispersion $\mathrm{d}n/\mathrm{d}\omega$. It is well known, from Kramers–Kronig relations which satisfy causality principle, that the dispersion changes sign steeply about absorption line (or closely-spaced absorption doublet), equivalent to dip in gain profile; where the steep anomalous (negative) dispersion near absorption line center results in fast light and the normal (positive) dispersion in the wings of absorption line results in slow light; likewise, slow light, associated with normal dispersion, is expected near the center of gain line (or closely-spaced gain doublet), equivalent to dip in absorption profile which is also known as spectral hole, and fast light, associated with anomalous dispersion, is expected in the wings of gain line [32, 53, 55–60]. The observation of electromagnetically induced transparency (EIT) [11, 73], a quantum destructive interference effects in which a transparency window is generated between two absorption peaks, a dip in absorption profile, opens the way for slow light demonstration in Bose-Einstein condensate of sodium atoms with $v_g = 17$ m/s [61], and the observation of $v_g = 90$ m/s [62] and 8 m/s [63] in rubidium vapor. Despite the near complete symmetry between slow and fast light effects, it was found that large fractional, delays is easily attainable than advances, on resonance. This may be attributed to the constraints imposed by both the maximum allowable loss or gain in a medium. The loss should not be too large, as the transmitted pulse would be too weak to be noticeable. Again, the gain should not also be too large at any frequency; otherwise the process of amplified spontaneous emission may occur resulting in the depletion of gain of the material [60, 129]. Slow light of EIT medium can be switched to fast light by driving the transition between the ground states using an additional control field in a closed system [74], or by tuning the phase of one of the fields in an open system [75]; conversely, fast light of single absorption line can be switched to slow light by controlling the coupling field intensity [76]. Copropagating slow and fast light manifested by EIT-assisted nonlinear gain and absorption has been observed

experimentally [77]. In this paper, we investigate the role of field detuning on both the population transfer and the induced polarization for optical and Raman transitions of the system. we observe slow and fast light, with large bandwidth at intermediate field intensity.

4.2 Model and theory

We consider a four-level atomic system, where two hyperfine ground states, $|1\rangle$ and $|2\rangle$, are coupled by a single coherent laser field of frequency ω and amplitude E to two hyperfine excited states, $|3\rangle$ and $|4\rangle$, as depicted in Fig. 4.1. This system can be realized by the hyperfine states associated with the D_1 transition of an alkali atom with a nuclear spin quantum number $I = 3/2$ (^{7}Li, ^{23}Na, ^{39,41}K, and ^{87}Rb), where the total angular momenta of the hyperfine ground and excited states are $F = 1, 2$ and $F' = 1, 2$, respectively. The electric field can be written as: $\mathbf{E} = (\hat{\varepsilon} E e^{i\omega t} + c.c)/2$. Under the dipole and the rotating-wave approximations, the Hamiltonian for the proposed four-level atomic system is given by:

$$\mathbf{H}/\hbar = \begin{bmatrix} 0 & 0 & \Omega_{13} & \Omega_{14} \\ 0 & \Delta_g & \Omega_{23} & \Omega_{24} \\ \Omega_{13} & \Omega_{23} & -\Delta & 0 \\ \Omega_{14} & \Omega_{24} & 0 & \Delta_e - \Delta \end{bmatrix}, \tag{4.1}$$

where $\Omega_{ij} = -\mu_{ij} E/2\hbar$ is one-half Rabi frequency for the transition with electric dipole moment μ_{ij}. $\Delta_g = \omega_{21}$ and $\Delta_e = \omega_{43}$ are ground and excited states hyperfine energy splittings, respectively. $\Delta = \omega - \omega_{32}$ is the laser field detuning. It should be noted that $\omega_{ij} = \omega_i - \omega_j$. The density matrix equations

describing the atomic system dynamics are given by:

$$\begin{aligned}
\dot{\rho}_{11} &= \gamma_{31}\rho_{33} + \gamma_{41}\rho_{44} + i[\Omega_{13}\rho_{13} + \Omega_{14}\rho_{14} - c.c] \\
\dot{\rho}_{22} &= \gamma_{32}\rho_{33} + \gamma_{42}\rho_{44} + i[\Omega_{23}\rho_{23} + \Omega_{24}\rho_{24} - c.c] \\
\dot{\rho}_{33} &= -(\gamma_{31} + \gamma_{32})\rho_{33} - i[\Omega_{13}\rho_{13} + \Omega_{23}\rho_{23} - c.c] \\
\dot{\rho}_{44} &= -(\gamma_{41} + \gamma_{42})\rho_{44} - i[\Omega_{14}\rho_{14} + \Omega_{24}\rho_{24} - c.c] \\
\dot{\rho}_{31} &= \Gamma_{31}\rho_{31} - i[\Omega_{13}(\rho_{11} - \rho_{33}) - \Omega_{14}\rho_{34} + \Omega_{23}\rho_{21}] \\
\dot{\rho}_{32} &= \Gamma_{32}\rho_{32} - i[\Omega_{13}\rho_{12} + \Omega_{23}(\rho_{22} - \rho_{33}) - \Omega_{24}\rho_{34}] \\
\dot{\rho}_{41} &= \Gamma_{41}\rho_{41} + i[\Omega_{13}\rho_{43} - \Omega_{14}(\rho_{11} - \rho_{44}) - \Omega_{24}\rho_{21}] \\
\dot{\rho}_{42} &= \Gamma_{42}\rho_{42} - i[\Omega_{14}\rho_{12} - \Omega_{23}\rho_{43} + \Omega_{24}(\rho_{22} - \rho_{44})] \\
\dot{\rho}_{21} &= \Gamma_{21}\rho_{21} + i[\Omega_{13}\rho_{23} + \Omega_{14}\rho_{24} - \Omega_{23}\rho_{31} - \Omega_{24}\rho_{41}] \\
\dot{\rho}_{43} &= \Gamma_{43}\rho_{43} + i[\Omega_{13}\rho_{41} - \Omega_{14}\rho_{13} + \Omega_{23}\rho_{42} - \Omega_{24}\rho_{23}]
\end{aligned} \quad , \tag{4.2}$$

with $\rho_{ij} = \rho^*_{ji}$ and $\sum_{i=1}^{4}\rho_{ii} = 1$. γ_{ij} denotes the spontaneous decay rate from state $|i\rangle$ to $|j\rangle$. $\Gamma_{21} = -i\Delta_g$, $\Gamma_{31} = i(\Delta - \Delta_g) - (\gamma_{31} + \gamma_{32})/2$, $\Gamma_{32} = i\Delta - (\gamma_{31} + \gamma_{32})/2$, $\Gamma_{41} = i(\Delta - \Delta_g - \Delta_e) - (\gamma_{41} + \gamma_{42})/2$, $\Gamma_{42} = i(\Delta - \Delta_e) - (\gamma_{41} + \gamma_{42})/2$ and $\Gamma_{43} = -i\Delta_e - (\gamma_{31} + \gamma_{32} + \gamma_{41} + \gamma_{42})/2$. As we are dealing with dense media, in which many atoms exist within a cubic resonance wavelength, the near-dipole-dipole interaction (NDD) needs to be considered by incorporating local-field correction resulting in the following relation: $\Omega_{ij} = \Omega - \varepsilon_{ij} Re(\rho_{ij})$, where $\varepsilon_{ij} = \frac{N\mu_{ij}^2}{3\varepsilon_0\hbar}$ provided that N is the atomic number density and ε_0 is the permittivity of free space [130, 131]. We choose the average of ground and excited states hyperfine energy splittings $\Delta_u = (\Delta_g + \Delta_e)/2$ as a unit scale for detuning, and define a new detuning $\Delta_c = \Delta - \Delta_u$ by raising the point of zero detuning by Δ_u.

It may be useful to be reminded, see Eq. 3.6, that the atomic system response to the applied fields is determined by the complex susceptibility parameter, $\chi = \chi_R + i\chi_I$, which is connected to ρ_{ij}, which is again a complex quantity,

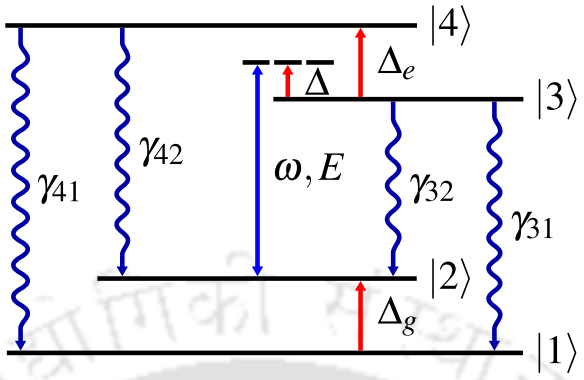

Figure 4.1: Schematic diagram of a four-level atomic system.

via the following relation [81]:

$$\chi_{ij} = \frac{N\mu_{ij}}{\varepsilon_o E}\rho_{ij} = -\frac{N|\mu_{ij}|}{\varepsilon_o E}\rho_{ij}\,. \tag{4.3}$$

It is well known that the real part of susceptibility, i.e. χ_R (which is again related to $Re(\rho_{ij})$), is related to dispersion while the imaginary one, i.e. χ_I (which in turn is associated to $Im(\rho_{ij})$), is related to absorption of the atomic system [81].

4.3 Results and Discussions

We solve Eqs. 4.2 and their complex conjugates at the steady state to investigate the role of field detuning on both the population transfer and the induced polarization for optical and Raman transitions of the system. We consider the D_1 transition of Bose-Einstein condensate of ^{23}Na atoms with atomic number density N of 1.5×10^{20} m^{-3} at a temperature of 2.0 μK [132]. Note that all hyperfine transitions have the same, spontaneous decay rate $\gamma/2\pi$ of 9.76 MHz and electric dipole moment μ of 21.1165×10^{-30} C$\cdot$m [133–135]. The ground and excited states hyperfine energy splittings are $\Delta_g/2\pi = 1771.62$

and $\Delta_e/2\pi = 188.88$ MHz, respectively. Accordingly, the unit scale for detuning is $\Delta_u/2\pi = 980.25$ MHz. Figure 4.2 exhibits the role of field detuning on population transfer for four different field intensities, namely 0.5γ, 5γ, 20γ, and 100γ which would be referred respectively as small, low-intermediate, high-intermediate, and large field intensities throughout the rest of the paper. Interestingly, we observe complete population transfer, for Raman transition, between the two hyperfine ground states [Fig. 4.2(a)] at small field intensity around the positive and negative peaks of $\Delta_c/\Delta_u \approx \pm 1$, i.e., the field is near resonant between $|4\rangle$ and $|1\rangle$ states, and $|3\rangle$ and $|2\rangle$ states respectively. As the field intensity is increased, the curve depicting population transfer gets flatten gradually leading to insignificant population transfer for large field intensity. Then the curve reverses its direction near about $\Delta_c = 0$ at high-intermediate field intensity of 20γ. For the other Raman transition between the two hyperfine excited states [Fig. 4.2(b)], partial population transfer occurs at intermediate field intensities with positive and negative peaks about $\Delta_c = 0$. It can be seen that there is insignificant population transfer for small and large field intensities. In view of these results, it could be concluded that population inversion for optical transitions does not occur.

In Fig. 4.3, we depict the effect of field detuning on the real and imaginary components of the induced polarization, which are correlated to dispersion and absorption respectively, for optical transitions, $|3\rangle \leftrightarrow |1\rangle$ and $|4\rangle \leftrightarrow |1\rangle$, under different field intensities. In the rest of the manuscript, for brevity and clarity of explanations, we refer the optical transitions, $|3\rangle \leftrightarrow |1\rangle$ and $|4\rangle \leftrightarrow |1\rangle$ as optical transitions I and II respectively. As could be seen from Fig. 4.3, the spectral range of the region of anomalous dispersion associated with the absorption line for the optical transition I and II at low-intermediate field intensity is approximately $2\,\Delta_u$. This region of (linear) anomalous dispersion is appropriate for realizing fast light with large bandwidth. On the other hand, the region of

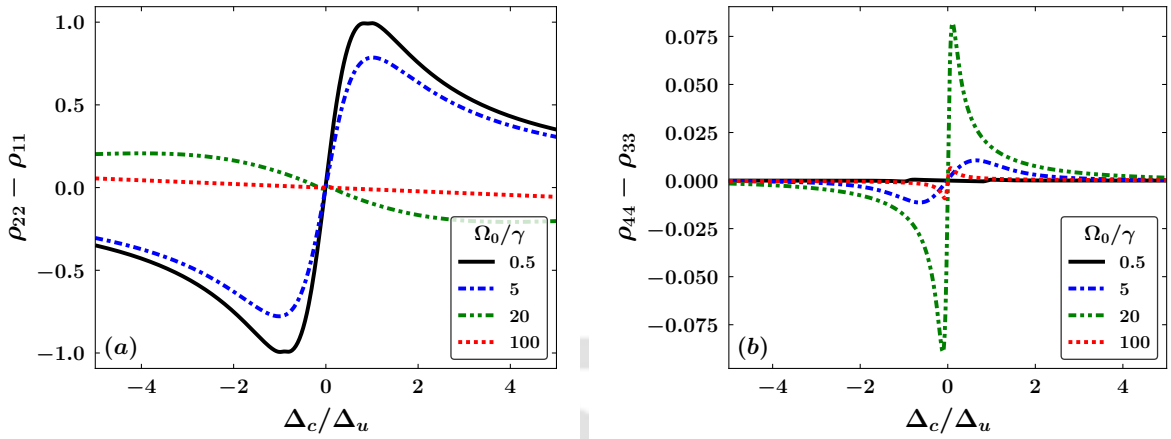

Figure 4.2: Population transfer as a function of field detuning for the Raman transition between the two hyperfine: (a) ground-, (b) excited- states.

normal dispersion of the red-detuned wing of absorption line, corresponding to intermediate field intensity, has a spectral range of approximately 4.5 Δ_u. This region could be split into two sub-regions of (nearly linear) small and large normal dispersion. The latter sub-region is appropriate for realizing slow light with large bandwidth. Interestingly, the large-linewidth absorption-profile changes to gain profile, for the optical transition I [Figs. 4.3(a) and 4.3(b)] at the high-intermediate field intensity. Now, the spectral range of the region of steep-normal dispersion associated with the gain line is found to be approximately 0.15 Δ_u. This region of dispersion, which is nearly linear, is appropriate for realizing slow light. It could be seen that the red-detuned wing of the gain line, which has a spectral range of approximately 4.9 Δ_u, exhibits anomalous dispersion. This region could be split into two sub-regions of (nearly linear) small and large normal dispersion. The latter sub-region is appropriate for realizing fast light with large bandwidth. Again, it could be observed that there is a steep but small anomalous dispersion regime, near $\Delta_c = 0$ and $\Delta_c > 0$, that could be utilized for attaining fast-light. Thus, by controlling the field intensity

or the field detuning, switching from slow to fast light or back, is feasible.

We can carry out a similar analysis for the optical transition II. Here, we observe that the absorption profile with large-linewidth, corresponding to intermediate field intensity, [Figs. 4.3(c) and 4.3(d)] transforms into an absorption profile with narrow-linewidth at high-intermediate field intensity. The spectral range of the region of very steep-anomalous dispersion associated with the absorption line is approximately 0.15 Δ_u. This linear dispersion region, near $\Delta_c = 0$ and $\Delta_c > 0$, is appropriate for realizing fast light. One could observe a steep normal dispersion region at the other side, i.e. near $\Delta_c = 0$ and $\Delta_c < 0$; this region could be used for slow-light. The region of dispersion corresponding to the red-detuned wing of the absorption line has a spectral range of approximately 4 Δ_u. This region could be further divided into two sub-regions of (nearly linear) small-anomalous and large-anomalous as indicated in Fig. 4.3(c). The latter sub-region is appropriate for realizing fast light with large bandwidth. Thus, by tuning the field intensity or the frequency of the external field, it is possible to attain switching from slow to the fast light or back. One of the advantages of the proposed scheme is that the switching mechanisms could be realized with large bandwidth for both the optical transitions.

In addition to these switching behaviors from the slow to the fast light or the reverse, it could be seen from Fig. 4.3 that, at high-intermediate field intensity, the slow light associated with optical transition I could co-propagate with the fast light related with the optical transition II. In passing, it is worthwhile to mention that the spectra of polarization for the optical transitions, $|4\rangle \leftrightarrow |2\rangle$ and $|3\rangle \leftrightarrow |2\rangle$ are not depicted as we find that these transitions are connected to optical transitions I and II, by dint of the following empirical relations:

$$\begin{aligned} \rho_{42}(\pm\Delta_c) + \rho_{31}^{*}(\mp\Delta_c) &= 0 \\ \rho_{32}(\pm\Delta_c) + \rho_{41}^{*}(\mp\Delta_c) &= 0 \end{aligned} . \tag{4.4}$$

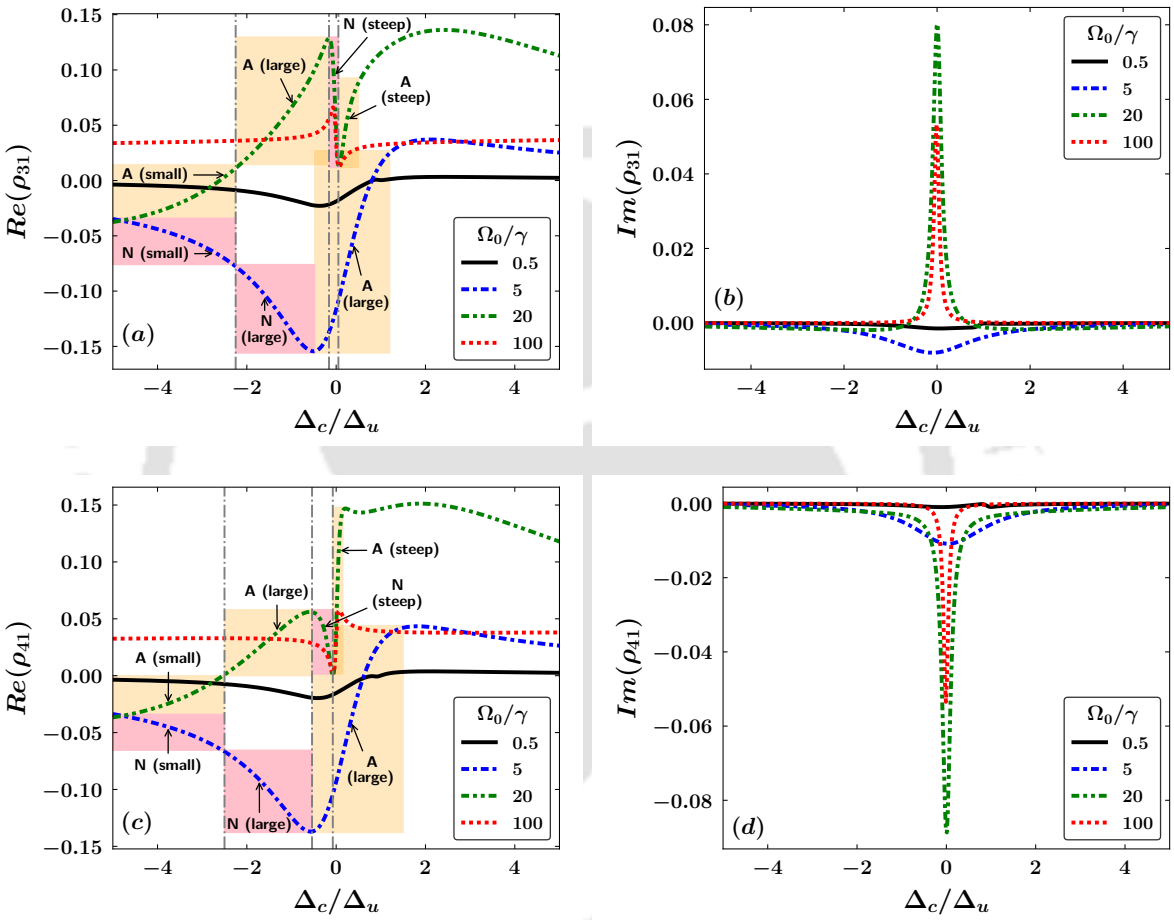

Figure 4.3: Spectra of the real and imaginary components of polarization for the optical transitions between $|3\rangle \leftrightarrow |1\rangle$ [(a) and (b)] and $|4\rangle \leftrightarrow |1\rangle$ [(c) and (d)]

We can also make few observations on maximum attainable coherences in the proposed system. It could be seen from Fig. 4.3(a) that for the transition I, we can obtain a coherence of ≈ 0.3 (on the scale of maximum attainable coherence of 0.5) at the low-intermediate intensity. On the other hand, the same is feasible at low- as well as, high-intermediate intensity for the transition II, as could seen from Fig. 4.3(c).

Now, as regards the Raman transitions, $|2\rangle \leftrightarrow |1\rangle$ and $|4\rangle \leftrightarrow |3\rangle$, are concerned, the behavior of the corresponding induced polarizations could be predicted from the optical transitions themselves, as follows. Let us consider the steady state solutions of the induced polarization for Raman transitions by setting $\dot{\rho}_{21}$ and $\dot{\rho}_{43}$ of Eqs. 4.2 to zero; this leads to the following equations:

$$\begin{aligned} \Gamma_{21}\rho_{21} &= -i\Omega[\rho_{23} + \rho_{24} - \rho_{31} - \rho_{41}] \\ \Gamma_{43}\rho_{43} &= -i\Omega[\rho_{41} - \rho_{13} + \rho_{42} - \rho_{23}] \end{aligned} . \tag{4.5}$$

Here, for simplicity we neglect the near dipole-dipole interaction, which may be of importance only at small field intensity. Using Eqs. 4.4, we can express Eqs. 4.5 as follows:

$$\begin{aligned} \Gamma_{21}\rho_{21} &= i\Omega[\rho_{31}^{R} + \rho_{41}^{R}] \\ \Gamma_{43}\rho_{43} &= i\Omega[\rho_{31}^{*R} - \rho_{41}^{R}] \end{aligned} , \tag{4.6}$$

where $\rho_{ij}^{R} = \rho_{ij}(\pm\Delta_c) + \rho_{ij}(\mp\Delta_c)$.

It is easy to infer directly from Eqs. 4.6, that the spectra of the induced polarization for Raman transitions is symmetric about $\Delta_c = 0$ axis, i.e. it is even function of Δ_c. Bearing that in mind, we depict the effect of field detuning on the real and imaginary components of the induced polarization for the Raman transitions under different field intensity in Fig. 4.4. For brevity of explanations, we split the spectra of the induced polarization into two regions, 1 and 2 as shown in Fig. 4.4. Each region has a spectral range of 5 Δ_u. Figs.

4.4(a) and 4.4(b) discuss the Raman transition $|2\rangle \leftrightarrow |1\rangle$, while Figs. 4.4(b) and 4.4(c) consider the one with $|4\rangle \leftrightarrow |3\rangle$. It could be seen from Fig. 4.4(a) that, at low-intermediate intensity near $\Delta_c = 0$, we have a linear anomalous dispersion region in 1 and a normal one in 2. These regions correspond to a broad-gain profile, as could be observed from Fig. 4.4(b). Thus just by a slight change in field detuning, one can switch from a fast to a slow light or back. It is interesting to observe that, at high-intermediate field intensity, the gain profile gets wider, and a very sharp spike appears at the gain line center. Now the corresponding dispersion curve exhibits, near $\Delta_c = 0$, very steep anomalous and normal dispersion in region 1 and 2 respectively. This could again be exploited for fast and slow light applications. Thus, by controlling the field intensity, switching from fast to the slow light could be achieved. However, it should be noted that the proposed scheme is not effective at very large intensity or at small intensity, as evident from Fig. 4.4.

Now, as regards the Raman transition, $|4\rangle \leftrightarrow |3\rangle$ is concerned, one can observe steep, normal and anomalous dispersion in region 1 and 2 respectively at high-intermediate intensity near $\Delta_c = 0$. In contrast, we can notice (near linear) anomalous and normal dispersion at low-intermediate intensity in the respective regions. It is worthwhile to note that, here, these dispersion curves pertain to absorption lines; while in the case of Raman transition,$|2\rangle \leftrightarrow |1\rangle$, discussed earlier, the dispersion curves are related to gain lines. Once again, we find that either by field detuning or changing the intensity we can switch from fast to slow light or back. One could have a larger band-width, and lower absorption, in the case of low-intermediate intensity compared to the high-intermediate one. Again, for reasons raised earlier, the Raman transition involving the hyperfine ground states is preferable for exploration of fast light phenomena over that of the excited ones. Further, it could be observed that, at high-intermediate field intensity, the fast (slow) light-associated with the gain line, corresponding

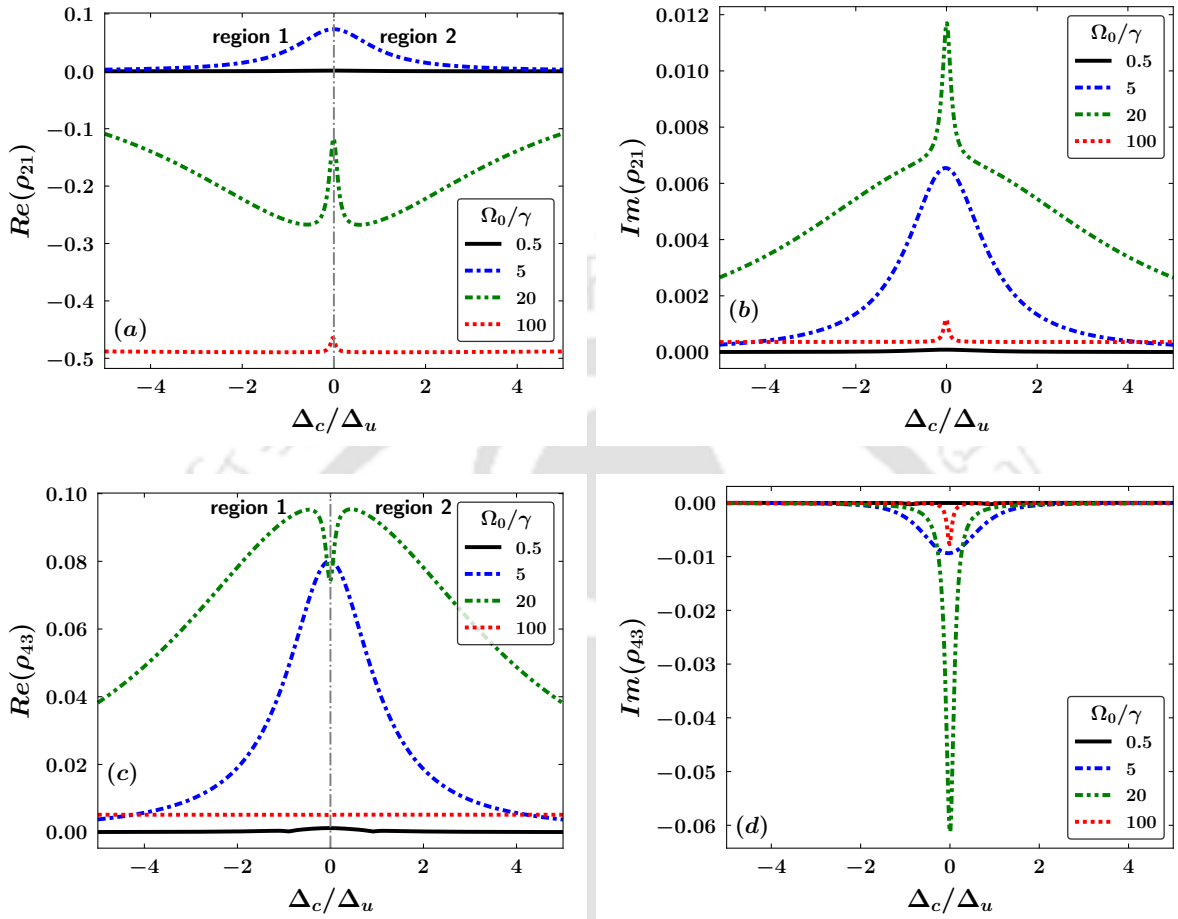

Figure 4.4: Spectra of the real and imaginary components of the induced polarization for the Raman transitions between the two hyperfine: (a) and (b) ground-, (c) and (d) excited- states.

to $|2\rangle \leftrightarrow |1\rangle$ Raman transition could co-propagate with the slow (fast) light associated with loss-line for the Raman transition $|4\rangle \leftrightarrow |3\rangle$. Finally, we observe that, while very little coherence is possible to attain between the hyperfine excited states, it is possible to obtain maximum coherence of ≈ 0.5 between the two hyperfine ground states, though, at large field intensity.

4.4 Summary

In conclusion, we have theoretically analyzed the role of field detuning on both the population transfer and the induced polarization for optical and Raman transitions in an ultracold atomic system. We have observed complete population transfer, for Raman transition, between the two hyperfine ground states at small field intensity when the field is near resonant between $|4\rangle$ and $|1\rangle$ states or $|3\rangle$ and $|2\rangle$ states. We have ascertained that slow and fast light, with large bandwidth are achievable at intermediate field intensity for the optical transitions, $|3\rangle \leftrightarrow |1\rangle$ and $|4\rangle \leftrightarrow |1\rangle$. In addition, by controlling the field intensity, switching from the slow to the fast light, with large bandwidth and the reverse are attainable. It is observed that at high-intermediate field intensity, the slow-light associated with gain for the optical transition $|3\rangle \leftrightarrow |1\rangle$ co-propagates with fast-light associated with loss for the optical transition $|4\rangle \leftrightarrow |1\rangle$. Similarly, we have observed that slow and fast light, with large bandwidth are feasible at intermediate field intensities for Raman transitions of the system. One could switch from fast to slow light, with large bandwidth, by tuning the field intensity for the Raman transition between the two hyperfine ground states. It is observed that the fast-light associated with the gain for the Raman transition between the two hyperfine ground states could co-propagate with the slow-light associated with loss for the Raman transition between the two hyperfine excited states. Finally, it should be noted that while our scheme is discussed in the context of the sodium D_1 transition, the proposed scheme should be applicable to other alkali atoms such as ^{7}Li, ^{39,41}K, and ^{87}Rb) or other molecular systems satisfying the required conditions.

Chapter 5

Effective Focusing of an Atomic Beam

In this chapter, we theoretically show how the effective focusing and defocusing of a diverging atomic beam can be realized using an appropriate sequence of linearly chirped few-cycle pulsed laser fields. First, we investigate and show that the time averaged optical dipole force induced by the sequence of either positively or negatively chirped pulses vanishes due to the periodic oscillations of the phases of in-phase components of atomic dipole moments. Then, we demonstrate that this issue could be overcome by utilizing a sequence of alternatively chirped pulses instead of either positively or negatively chirped pulses. It is shown that for such a sequence of pulses, the phases of in-phase components of atomic dipole moments does not oscillate periodically and in fact remain constant at either 0 or π depending on the chirping direction of the initial pulse, resulting in either an effective focusing or defocusing optical dipole force. The trajectory of atoms under an optical dipole force is also investigated to actually show the focusing and defocusing. Finally, the role of beam shape on the proposed scheme is investigated and it turns out

The contents of this chapter are published in **Abdelaziz, Abdelsalam H. M.**, Parvendra Kumar, and Amarendra K. Sarma, "Effective focusing of a diverging atomic beam by a sequence of alternatively chirped few-cycle pulsed laser fields", Phys. Rev. A **99**, 023408 (2019). Selected contents are reproduced with permission © American Physical Society.

that a super-Gaussian pulse of order $m = 2$ shows more efficacy compared to the normal Gaussian pulse.

5.1 Brief overview

Optical manipulation (OM) of atoms and molecules relying on laser induced optical forces has enabled the realization of many novel phenomena such as Bose-Einstein condensation, laser cooling, trapping, and deflection of atoms, molecules, and nanoparticles [136–144]. These breakthroughs are now paving the ways for many diverse applications ranging from quantum metrology to quantum information [18–22]. OM, being on the path of continuous improvements, is getting a tremendous boost and attention particularly due to the recent technological development in the generation of short laser pulses together with deterministic amplitude and frequency shaping techniques [145–147].

Generally, optical forces can be classified into two kinds: the dipole force, also known as the stimulated force, and the radiative force, also known as the spontaneous force [78, 148–150]. The dipole force could be understood to arise as a result of the intensity gradient while the radiative force could be owing to the phase gradient of the optical field [151]. For plane waves incident on neutral atoms, absorption of photons is followed most probably by spontaneous emission, i.e., the optical force is purely radiative. Hence focusing of neutral atoms using plane waves is not applicable. When it comes to non plane waves, absorption of photons is followed by either spontaneous or stimulated emission. The absorption of photons followed by the spontaneous emission gives rise to the radiative force which is dominant at resonant excitation of neutral atoms. On the other hand, the absorption of photons followed by stimulated emission gives rise to dipole force which is dominant at detuned excitation of neutral atoms [4, 152]. The physical effects of both dipole and radiative forces in-

duced by a CW laser were demonstrated through the focusing, defocusing, and steering of neutral sodium atoms [51]. Similar effects were also observed by utilizing the optical forces induced by pulsed laser fields instead of CW lasers. The ability of pulsed laser induced optical forces to beat the saturation limit of spontaneous force makes them much more favorable and increasingly attractive tools. Additionally, the broad spectrum of short laser pulses also allow us to access the systems with strong Doppler and Zeeman shifts. It is demonstrated that the magnitude of a counterpropagating *pi*-pulses induced force, termed as stimulated force, can be at least one order of magnitude greater than that of saturated spontaneous forces depending upon the pulse repetition rate [153]. Later on, bichromatic and polychromatic pulses have been employed for laser cooling through such stimulated forces [154–156]. Significant attention, recently, has been paid towards the stimulated forces induced by the linearly chirped pulses primarily because of their robustness [51, 157–162]. The laser cooling without spontaneous emission is also demonstrated through this scheme [160]. In all of these aforementioned works, stimulated forces by linearly chirped pulses are investigated but the equally important intensity gradient dependent dipole force has not received similar attention and is therefore rarely explored. In our previous work [78], partially we investigated the optical dipole induced by a unidirectional sequence of linearly chirped pulses and showed to change its sign between odd and even number of pulses in the pulse train. This results in an oscillatory optical dipole force, making the time-averaged optical force to vanish. The physics behind the nature of the oscillating forces was not discussed and therefore still remains open for further investigations. In this article we not only investigate and clarify physics behind the nature of the oscillating forces but also propose a strategy to overcome this issue, thereby realizing the effective time average focusing and defocusing dipole force. For this we propose the use of a sequence of alternatively chirped pulses instead of either

positively or negatively chirped pulses. It is shown that for such sequence of pulses, the phases of in-phase components of atomic dipole moments does not oscillate periodically and in fact remain constant at either 0 or π depending on the chirping direction of the initial pulse, resulting in either an effective focusing or defocusing optical dipole force. This could be in principle used in effective focusing and defocusing of the diverging atomic beam. Moreover, we investigate the role of the beam shape on the chirped pulsed excitation of atoms. We find that a super-Gaussian pulse with order $m = 2$ offers the best result in terms of effective focusing and defocusing in the proposed scheme.

5.2 Model and Theory

We consider a ladderlike atomic system interacting with a train of two few-cycle-pulsed laser fields. The atomic beam is considered to consist of sodium atoms, the schematic of the level structure of the atom is depicted in Fig. 5.1(a). The states $|1\rangle$, $|2\rangle$ and $|3\rangle$, respectively refer to $3S_{1/2}$, $3P_{3/2}$, and $4S_{1/2}$ quantum states of neutral sodium atoms. It is to be noted that the proposed scheme is similar to the one discussed earlier in Ref. [78]. However, in this work we consider a sequence of chirped pulse trains of alternating sign while the earlier work (i.e., Ref. [78]) considered chirped pulse trains of the same sign. For brevity and clarity, we refer to the former scheme as "alternating" while the later as the "standard" one in this work. This is illustrated in Figs. 5.1(b) and 5.1(c). The total electric field of the trains of a few-cycle linearly chirped pulsed laser fields is given by

$$\begin{aligned}\mathbf{E}_{i(i=1,2)}(t) = \sum_{n=0}^{N-1} \varepsilon_i A_i(t-nt_r)\cos[\omega_i(t-nt_r) \\ +(-1)^n \alpha_i(t-nt_r)^2/2 + \omega_{Di}(t-nt_r) + \phi_i(z)]\end{aligned}, \tag{5.1}$$

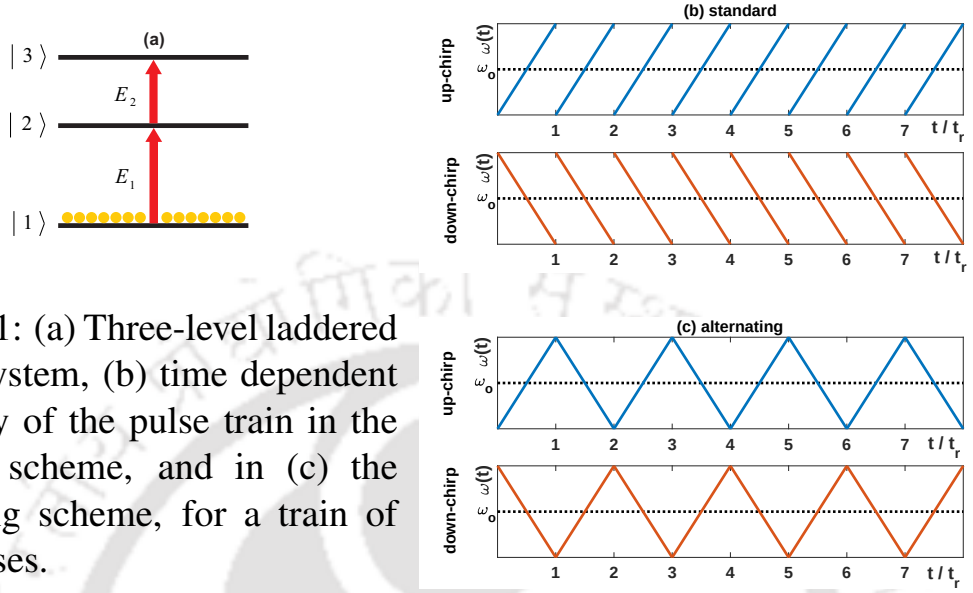

Figure 5.1: (a) Three-level laddered atomic system, (b) time dependent frequency of the pulse train in the standard scheme, and in (c) the alternating scheme, for a train of eight pulses.

where $A_i(t-nt_r) = E_{oi}\exp\{-[((t-nt_r)/\tau)^{2m}/2+(r/w_o)^{2m}]\}$. m is the order of the super-Gaussian-shaped pulse. In the first of this work we consider a super-Gaussian pulse of order $m=1$, which basically refer to the so called normal Gaussian pulse. Later, in order to investigate the role of the shape of the pulse train on the atomic beam, we consider super-Gaussian beams of different orders. It is assumed that the pulse train of electric field E_1 and the pulse train of electric field E_2 are interacting between the states $|1\rangle$ and $|2\rangle$, and $|2\rangle$ and $|3\rangle$, respectively. Here, $\omega_{Di} = -\mathbf{k}_i \cdot \mathbf{v}$ refers to the detuning of the transition lines of the atom moving with velocity $\mathbf{v}$ owing to the Doppler shift. τ is the temporal half-width of the pulse and it is related to the so-called full width at half maximum (FWHM) of the pulse by, $T_{FWHM} = 1.665\tau$. N is the number of pulses, t_r is the pulse repetition time, α_i is the chirp rate, r is the radial distance from the center axis of the beam, z is the axial distance from the beam waist, w_o is the beam waist radius, ω_i is the laser frequency, and $\phi_i(z) = k_i z$ represents the longitudinal phases. Here, $k_i (i = 1,2)$ is the wave vector of the corresponding electric fields.

The density matrix equations, without invoking the so-called rotating wave approximation, describing the temporal evolution of the density matrix elements, are as follows [78]:

$$\begin{aligned}
\frac{d\rho_{11}}{dt} &= i(\Omega_{12}\rho_{21} - \Omega_{21}\rho_{12}) \\
\frac{d\rho_{22}}{dt} &= i[\Omega_{12}(\rho_{12} - \rho_{21}) + \Omega_{23}(\rho_{32} - \rho_{23})] \\
\frac{d\rho_{33}}{dt} &= i(\Omega_{32}\rho_{23} - \Omega_{23}\rho_{32}) \\
\frac{d\rho_{21}}{dt} &= -i\omega_{21}\rho_{21} + i[\Omega_{21}(\rho_{11} - \rho_{22}) + \Omega_{23}\rho_{31}] \\
\frac{d\rho_{32}}{dt} &= -i\omega_{32}\rho_{32} + i[\Omega_{32}(\rho_{22} - \rho_{33}) - \Omega_{12}\rho_{31}] \\
\frac{d\rho_{31}}{dt} &= -i\omega_{31}\rho_{31} + i[\Omega_{23}\rho_{21} - \Omega_{21}\rho_{32}]
\end{aligned} \quad . \tag{5.2}$$

Here, $\Omega_{12} = \Omega_{21} = \mu_{12}\mathbf{E}_1(r,t)/\hbar$ and $\Omega_{23} = \Omega_{32} = \mu_{23}\mathbf{E}_2(r,t)/\hbar$ are the time-dependent Rabi frequencies for the transition with electric dipole moment μ_{12} and μ_{23} respectively. It should be noted that $\omega_{ij} = \omega_i - \omega_j$ and $\rho_{ij} = \rho^*_{ji}$. Using an approach based on the density matrix equations and the Ehrenfest's theorem, the optical dipole force, for $m = 1$, is derived as follows

$$\begin{aligned}
\mathbf{F}_t = \mu_{12} \sum_{n=0}^{N-1} u[\nabla A_1(t - nt_r)] \cos[\omega_1(t - nt_r) \\
+(-1)^n \alpha_1 (t - nt_r)^2/2 + \omega_{D1}(t - nt_r) + \phi_1(z)] \\
+\mu_{23} \sum_{n=0}^{N-1} v[\nabla A_2(t - nt_r)] \cos[\omega_2(t - nt_r) \\
+(-1)^n \alpha_2 (t - nt_r)^2/2 + \omega_{D2}(t - nt_r) + \phi_2(z)]
\end{aligned} \quad , \tag{5.3}$$

where $u = \rho_{12} + \rho_{21}$ and $v = \rho_{32} + \rho_{23}$.

5.3 Results and Discussions

We solve Eqs. (5.2) and (5.3) numerically using a standard Runge-Kutta algorithm. The atoms are assumed to be in the ground state $|1\rangle$ initially. The following typical parameters are used for simulations with regard to the temporal evolution of u and v phases, and populations: $\omega_{21} = \omega_1 = 3.19$ rad/fs, $\omega_{32} = \omega_2 = 1.65$ rad/fs, $\alpha_1 = \alpha_2 = 0.028$ and -0.028 fs^{-2} for up- and down-chirp pulse excitations respectively, $\Omega_{21}^{max} = \Omega_{32}^{max} = 1.30$ rad/fs, $\mu_{12} = \mu_{23} = 1.85 \times 10^{-29}$ C $\cdot$ m, $w_o = 10$ µm, $r = w_o/\sqrt{2} = 7.07$ µm. The pulse duration is taken to be 20 fs which corresponds to a pulse FWHM of 33.3 fs. In the current study, atoms with mass $M = 22.99$ u are considered for simulation.

In Fig. 5.2 the spatiotemporal profile of the optical dipole force under the standard and the alternating chirped pulse excitations is depicted. Figures 5.2(a) and 5.2(b) exhibit the spatiotemporal profile of optical force for the standard scheme with up- and down- chirped pulse excitations respectively. On the other hand, Figs. 5.2(c) and 5.2(d) refer to the corresponding cases for the alternating scheme. From the temporal evolution of optical dipole force under the standard chirped pulse excitation, it is evident that for the up-chirped pulse trains [Fig. 5.2(a)] the optical force is negative for an odd number of pulses in the pulse train and positive for an even number of pulses in the pulse train. On the other hand, for the down-chirped pulse trains [Fig. 5.2(b)], the contrary is observed. Hence the atoms in an atomic beam will experience an oscillating optical dipole force induced by the chirped few-cycle-pulse trains. While from the radial dependence of optical dipole force, it is obvious that for the up-chirped pulse trains, refer to Fig. 5.2(a), the optical force is maximum at $r = 0$, while it is minimum at $r = w_o/\sqrt{2} = 7.07$ µm for an odd number of pulses in the pulse train. Interestingly, it is minimum at $r = 0$ and maximum at $r = 7.07$ µm for an even number of pulses in the pulse train. On the other hand,

for the down-chirped pulse trains, refer to Fig. 5.2(b), the contrary is observed. Hence the atoms in an atomic beam will experience a radial dependent optical dipole force induced by the chirped few-cycle-pulse trains. Now from the temporal evolution of optical dipole force under the alternating chirped pulse excitation, it is clear that for the up-chirped pulse trains the optical force is negative while it is positive for down-chirped pulse trains. It should be noted that the nature of the force is independent of the number of pulses in the pulse train. Hence the atoms in an atomic beam will experience non-oscillating optical dipole force due to the alternating chirped few-cycle-pulse trains. Again, it is evident from Fig. 5.2(c) that for up-chirped pulse trains the optical force is maximum at $r = 0$ and minimum at $r = w_o/\sqrt{2} = 7.07$ µm. The contrary is observed for down-chirped pulse trains, refer to Fig. 5.2(d). This result is also independent of the number of pulses in the pulse train. Hence the atoms in an atomic beam will experience a radial dependent non-oscillating optical dipole force induced by the alternating chirped few-cycle-pulse trains.

In the following, we endeavor to understand the physics of both the standard and the alternating schemes for chirped pulse excitation of atoms. Figure 5.3 depicts the temporal evolution of the populations under the alternating chirped pulse excitation. The standard one also exhibits exactly the same behavior. Regardless of the nature of the chirp, it is observed that coherent population transfer occurs due to adiabatic rapid passage from state $|1\rangle$ to state $|3\rangle$ for an odd number of pulses in the pulse train and from state $|3\rangle$ to state $|1\rangle$ for an even number of pulses in the pulse train. Thus, we can conclude that the diagonal elements in the density matrix are not directly responsible for the oscillating nature of the force. It means that the off-diagonal elements of the density matrix, i.e. the relative phase between the probability amplitudes of the states, has a role to play.

In order to validate this assumption, in Fig. 5.4, we depict the temporal

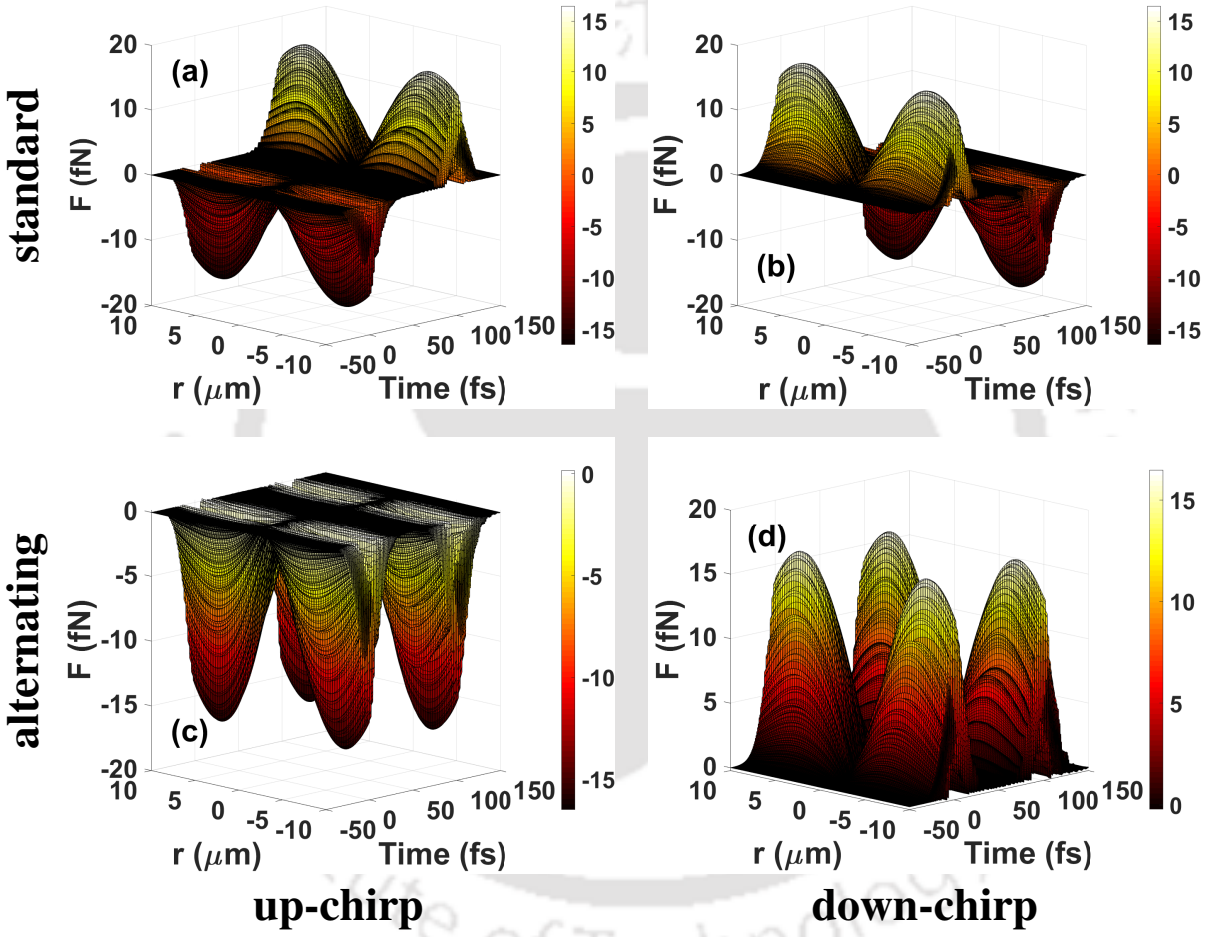

Figure 5.2: Spatiotemporal profile of the optical dipole force under standard and alternating chirped pulse excitations for $N = 2$.

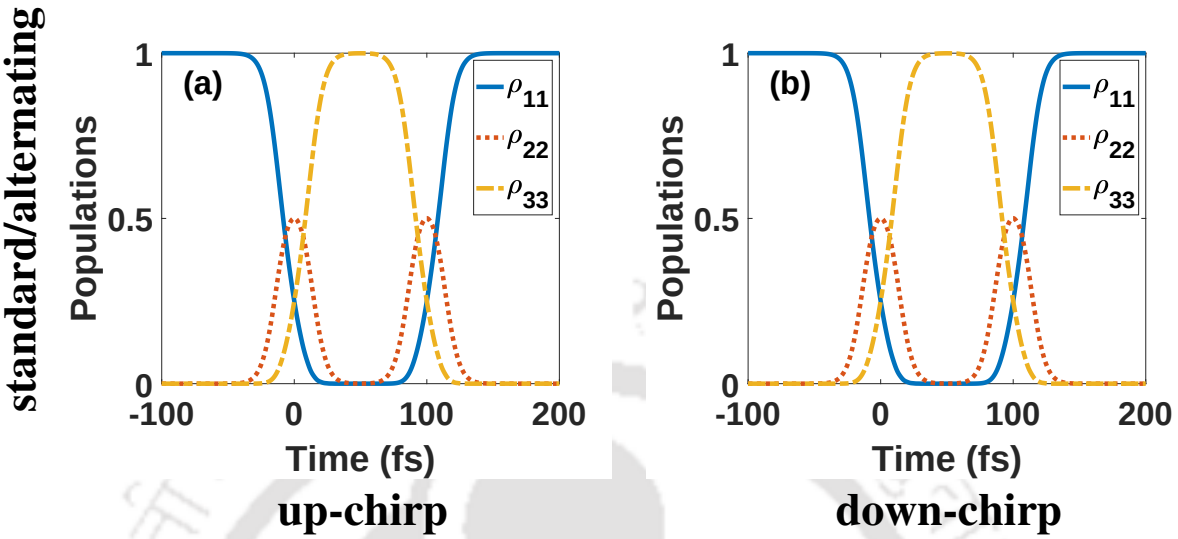

Figure 5.3: Temporal evolution of populations under standard or alternating chirped pulse excitations (RWA) for $N = 2$.

evolution for the phases of the Bloch vector components u and v under the standard chirped pulse excitation. It could be seen that for the up-chirped pulse trains, both u and v phases equal to zero for an odd number of pulses in the pulse train and equal to π for an even number of pulses in the pulse train. This means that the phases of the in-phase components of the atomic dipole moments oscillate periodically i.e. the average dipole moments $\langle \mu_{12} \rangle = \mu_{12} u$, and $\langle \mu_{23} \rangle = \mu_{23} v$ are positive for an odd number of pulses in the pulse train and negative for an even number of pulses in the pulse train. As a result, the optical dipole force is negative for an odd number of pulses in the pulse train and positive for an even number of pulses in the pulse train. On the other hand, for down-chirped pulse trains, the contrary is observed. Moreover, a comparison between u and v phases of the up-chirped pulse trains and the respective u and v phases of the down-chirped pulse trains reveal the existence of a time reversal symmetry. This asserts the equivalence of up- and down-chirped pulse excitation of atoms initially in states $|1\rangle$ and $|3\rangle$ respectively.

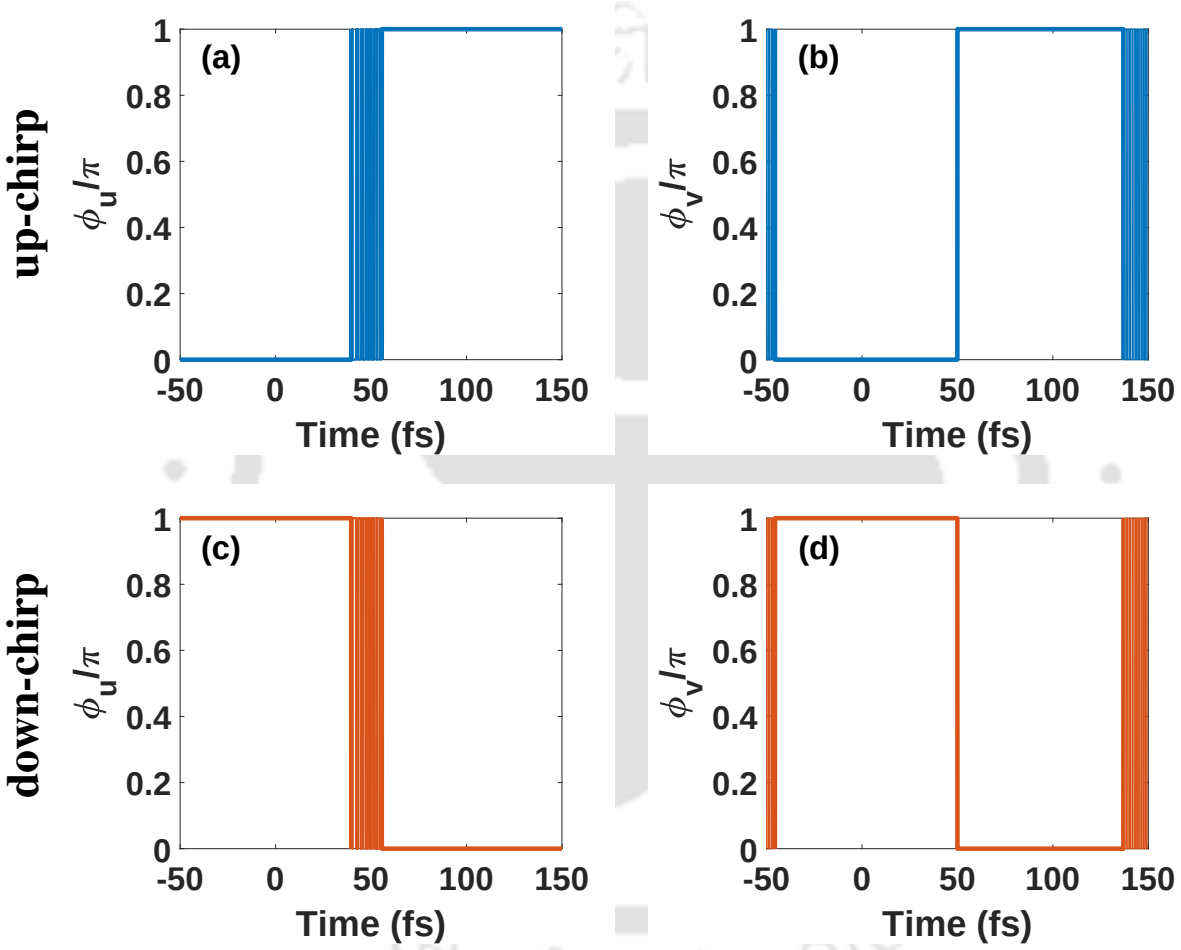

Figure 5.4: Temporal evolution of phase angle of u and v under standard chirped pulse excitation (RWA) for $N = 2$.

Next, in Fig. 5.5 we show the temporal evolution of u and v phases under alternating chirped pulse excitation scheme. It is apparent, regardless of the pulse number in the pulse train, that both u and v phases equal zero for up-chirped and equal π for down-chirped pulse trains i.e. the phases of the in-phase components of the atomic dipole moments does not oscillate periodically. As a result, the optical dipole force, irrespective of the pulse number in the pulse train, is negative for up-chirped and positive for down-chirped pulse trains.

It is evident that the alternating scheme should be useful, unlike the standard one (discussed in details in Ref. [78]), for focusing and defocusing of atoms owing to the non-oscillating nature of the force, resulting in a non-zero time-averaged force. In order to see it more clearly, in Fig. 5.6 we exhibit the temporal evolution of the radial distance under the standard and the alternating chirped pulse excitations for different initial transverse velocities. It is apparent that the alternating chirped pulse excitation is much more efficacious than the standard chirped pulse excitation in focusing and defocusing of moving atoms. It is obvious, for up-chirped pulse trains, that the efficacy of focusing of moving atoms decreases with increasing initial transverse velocity. On the other hand, for down-chirped pulse trains it is obvious that defocusing efficacy of moving atoms increases with increase in the initial transverse velocity.

Finally, we investigate the role of the beam shape on the chirped pulse excitation of atoms subjected to the optical dipole force via our proposed scheme. Figure 5.7 exhibits the temporal evolution of the radial distance under the alternating chirped pulse excitations for different order of the super-Gaussian pulse. The phenomena of focusing and defocusing are achieved with up-chirped (shown by solid lines) and down-chirped (shown by dash-dot lines) pulse excitations respectively. We observe that the super-Gaussian pulse with order $m = 2$ gives the best result and is more effective than the usual Gaussian one with $m = 1$

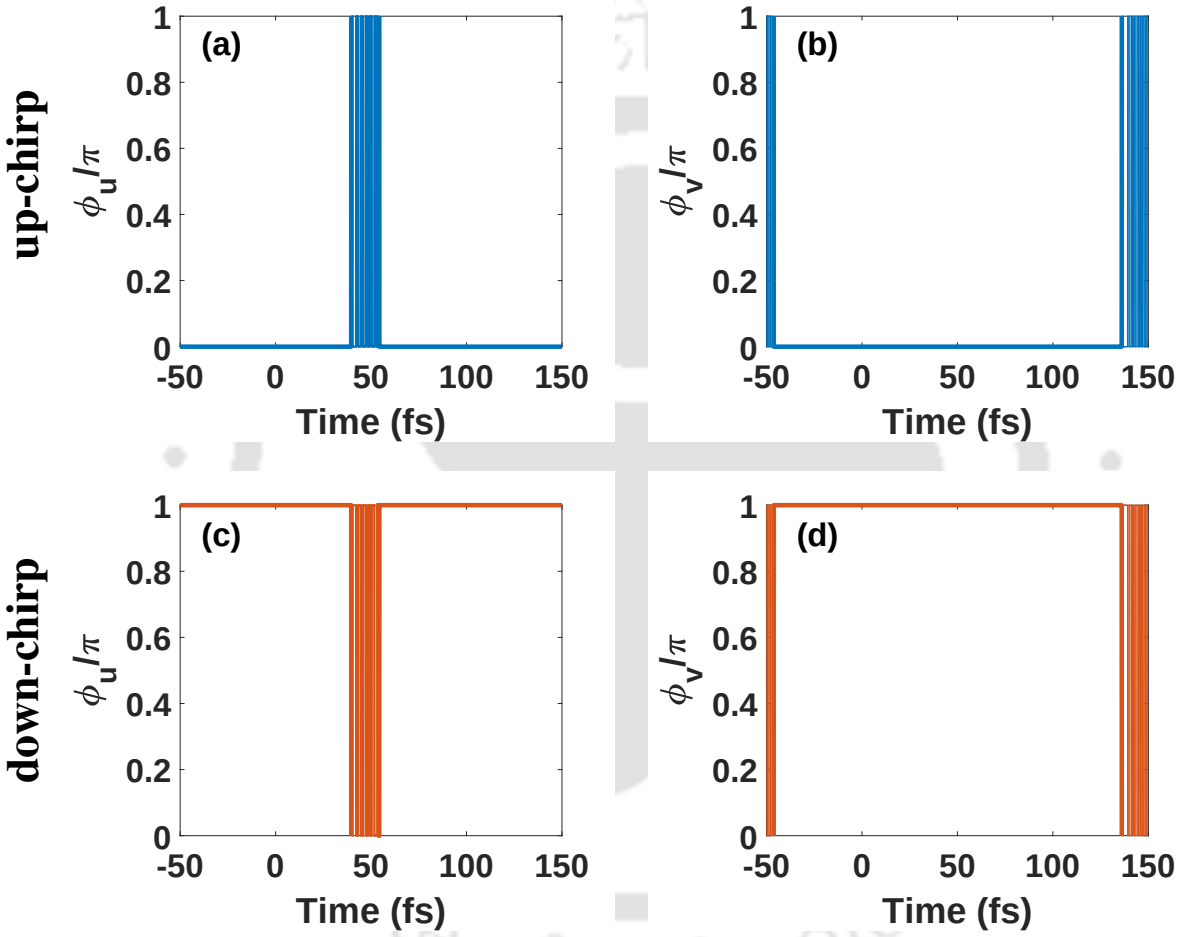

Figure 5.5: Temporal evolution of phase angle of u and v under alternating chirped pulse excitation (RWA) for $N = 2$.

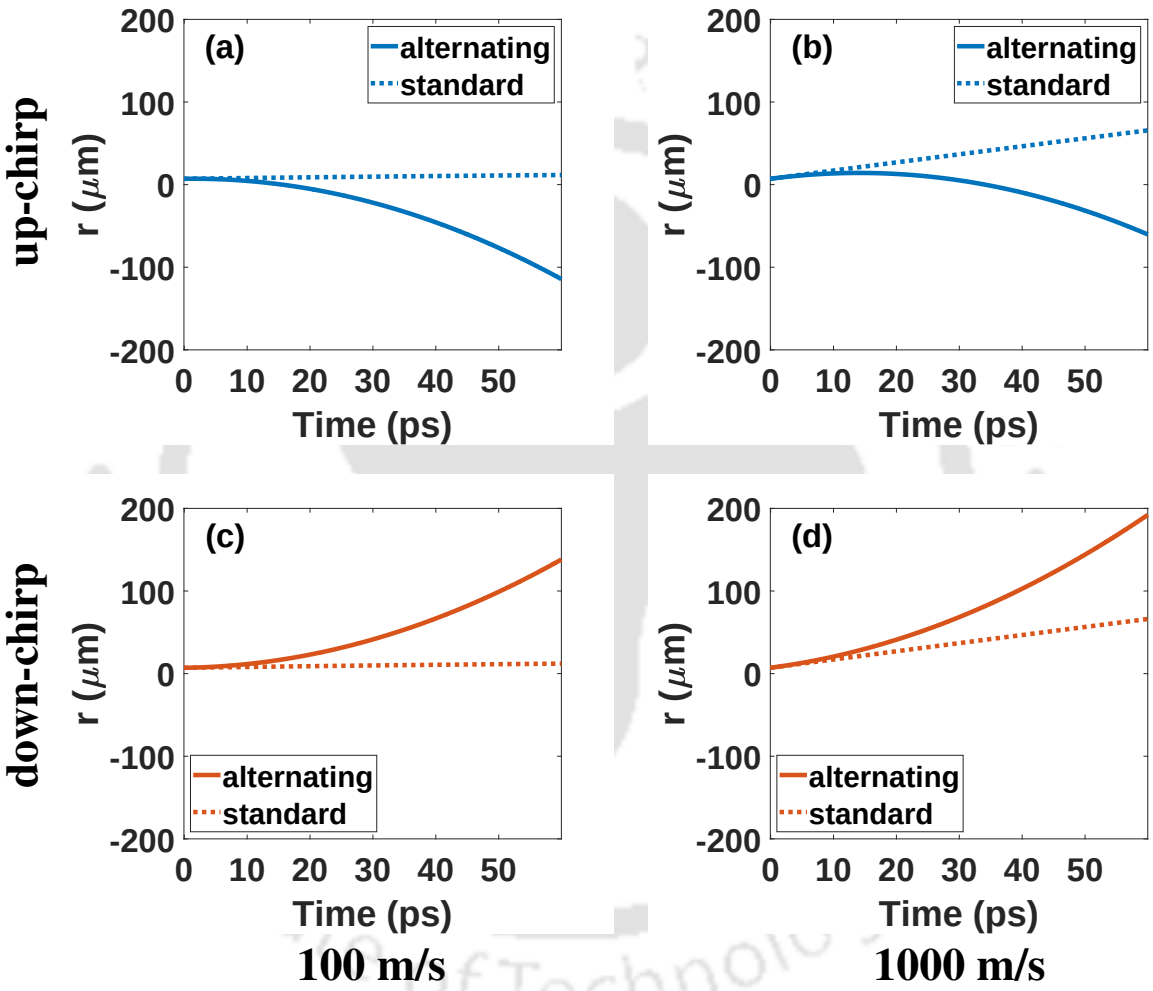

Figure 5.6: Temporal evolution of radial distance under standard alternatively chirped pulse excitation for different initial transverse velocities.

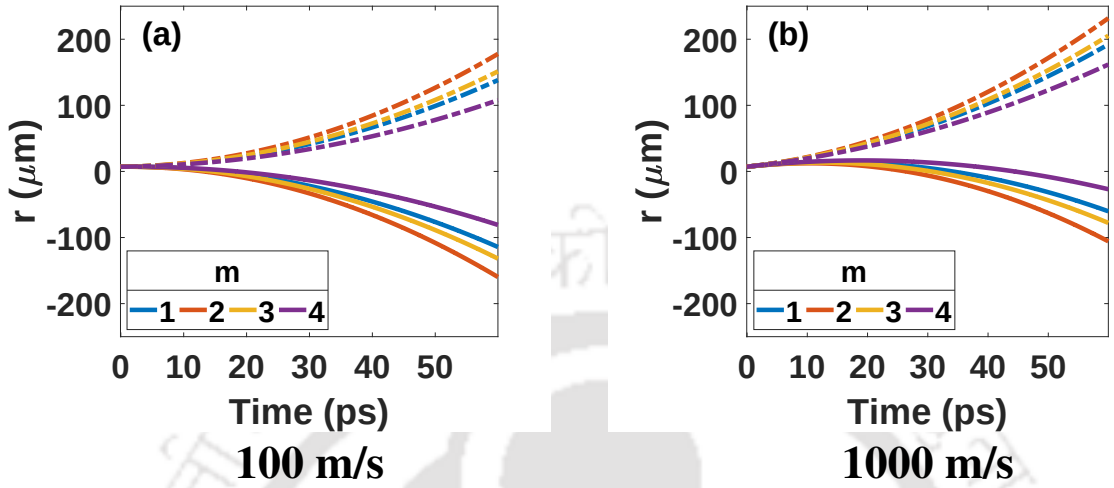

Figure 5.7: Temporal evolution of radial distance under alternating up-chirped (solid lines) and down-chirped (dash-dot lines) pulse excitations for various order of the super-Gaussian pulse train and initial transverse velocities (a) 100 m/s (b) 1000 m/s.

or even with pulses having $m > 2$. It is worthwhile to note that in the standard case, not shown here, the focusing and defocusing effects rise with increase in the order of the super-Gaussian pulse, though the enhancement is way below the proposed scheme and not very significant. Thus, it is clear that the proposed scheme has features that are much more improved and notable than the so-called standard scheme, and hence may turn out to be useful for many atomic physics related applications.

5.4 Summary

In conclusion, we have theoretically demonstrated how the effective focusing and defocusing of a diverging atomic beam could be realized using an appropriate sequence of linearly chirped few-cycle pulsed laser fields. It is shown that

the time averaged optical dipole force induced by the sequence of either positively or negatively chirped pulses vanishes due to the periodic oscillations of the phases of the in-phase components of the atomic dipole moments. We then show that this issue could be circumvented by utilizing a sequence of alternatively chirped pulses instead of either positively or negatively chirped pulses. It is demonstrated that for such a sequence of pulses, the phases of in-phase components of atomic dipole moments does not oscillate periodically and in fact remain constant at either 0 or π depending on the sign of the chirp (i.e., positive or negative) of the initial pulse. This results in either an effective focusing or defocusing optical dipole force. The trajectory of atoms under the optical dipole force is also investigated to actually exhibit the focusing and defocusing. The role of the beam shape is investigated and found that a super-Gaussian pulse with order $m = 2$ is more effective than the usual Gaussian pulse (with order $m = 1$). The proposed scheme may enable one to generate strong optical force.

Chapter 6

Conclusions

In this thesis, we have explored coherent control to manipulate atomic systems for various applications such as optical multistability, slow and fast light, and focusing of an atomic beam. In chapter 1, we presented a brief introduction and motivation of the research problems considered in the thesis, along with the recent developments pertinent to these problems. In chapter 2, we discussed, in details, the relevant concepts and phenomena related to the research problems addressed in this thesis.

In chapter 3, we analyzed single OB, double OB, and OT behavior in a V-type three-level atomic system, confined in a unidirectional optical ring cavity. We explored the physics behind the emergence of various bistable and tristable states, in particular switching from the absorptive to the dispersive characteristics. It is found that the switching between various bistable phenomena is defined by the ratio between the absolute peak values of the parameters describing dispersion and absorption respectively. This ratio sets a criterion for obtaining absorptive OB, OT, double OB and dispersive OB. It is interesting to note that this ratio is independent of the cavity feedback. However, the respective width of the lower, the middle and the higher branch of the hysteresis loop could be manipulated with judicious control of the detuning of the con-

trol and the probe fields. Further, we report that the threshold intensities of the absorptive and the dispersive hysteresis loops decrease with the control field intensity but increase with the probe field detuning and the cooperation parameter, thereby paving the way for easy control of the width of the middle branch of double OB and OT as well single OB.

In Chapter 4, we discussed our theoretical proposal for attaining slow and fast light via coherent control of the hyperfine ground and excited states of an ultracold atomic system. We observed complete population transfer, for Raman transition, between the two hyperfine ground states at small field intensity. We ascertained that slow and fast light, with large bandwidth could be obtained in the proposed system. It is inferred that both slow and fast light could co-propagate, pertaining to different optical and Raman transitions. Further, we observed that switching between the slow and the fast light is achievable by controlling the field intensity, as well as the field detuning.

In chapter 5, we demonstrated theoretically how the effective focusing and defocusing of a diverging atomic beam could be realized using an appropriate sequence of linearly chirped few-cycle pulsed laser fields. It is shown that the time averaged optical dipole force induced by the sequence of either positively or negatively chirped pulses vanishes due to the periodic oscillations of the phases of the in-phase components of the atomic dipole moments. We circumvented this issue by utilizing a sequence of alternatively chirped pulses instead of either positively or negatively chirped pulses. It is demonstrated that for such a sequence of pulses, the phases of in-phase components of atomic dipole moments does not oscillate periodically and in fact remain constant at either 0 or π depending on the sign of the chirp of the initial pulse. This results in either an effective focusing or defocusing optical dipole force. The trajectory of atoms under the optical dipole force is also investigated to actually exhibit the focusing and defocusing. We examined the role of the beam shape and found

that a super-Gaussian pulse with order $m = 2$ is more effective than the usual Gaussian pulse (with order $m = 1$).

Scopes of Future Work

In this thesis we have explored the problem of optical multistability using cw laser light. Clearly, it would be interesting to investigate the issue using pulsed laser light, in particular, the real-time behavior of the phenomena of optical multistability. The transient behavior of the system may put restriction on the attainability of optical multistability. Hence optimization of the system for optical multistability might be essential. Again, related to our work on the effects of slow and fast light, the role of field intensity on the switchability between slow and fast light effects in a system possessing a gain doublet could be probed. While the investigation of slow and fast light phenomena using a cw laser is the usual norm, it may be useful but challenging to come up with schemes where pulsed laser light could be used. As it is already known that a pulse contains a range of frequencies, not a single frequency, the steady-state solution may be questionable in that case. Here, the counter-intuitive mechanism of dark-sate polariton could be explored. The role of pulse shape, duration and bandwidth might also be attempted. Indeed, atomic systems are suffering from upper level relaxation. This is posing a limitation on the storage time of a pulse. In this regard, it may be a promising choice to explore various systems, such as quantum wells, quantum dots, optical fibers, and even optomechanics. Finally, in continuation of our work on optical force, the role of ground-state coherence on the optical force in a Λ-type three-level atomic systems under coherent population trapping conditions may be investigated.

Appendix A

Analytical form of ρ_{31}

THE steady state solution for the off-diagonal density matrix element ρ_{31} is found to be the ratio of two polynomials of order 5 and 6 in Ω_p

$$\rho_{31} = 4\Omega_p \frac{\sum_{i=0}^{2} [a_{2i} - i\gamma_{31} b_{2i}/2] \left|\Omega_p\right|^{2i}}{\sum_{i=0}^{3} d_{2i} \left|\Omega_p\right|^{2i}}, \tag{A.1}$$

where a_{2i}, b_{2i}, and d_{2i} are real parameters that depend on probe- and control-field detunings, spontaneous decay rates, and control-field intensity. To arrive at the familiar expression for two-level atomic system, simply set $i = 0$ and 1 in the numerator and denominator to retain the first order term, and up to the second order in Ω_p respectively, which result only in OB. While for three-level atomic system, judicious choice of the system parameters plays the key role behind the emergence of OB, double OB, and OT. The detailed expressions for a_{2i}, b_{2i}, and d_{2i} parameters are given as follows

$$
\begin{aligned}
a_0 &= \Delta_p \gamma^m I_c^s (4\Delta^2 + \gamma_s^2) + 16\gamma^m (\Delta_c - \Delta) |\Omega_c|^4 \\
&\quad + 4\gamma^m (\Delta_c (8\Delta\delta + \gamma_s^2) + \Delta_p (4\Delta^2 - \gamma_d \gamma_s)) |\Omega_c|^2 \\
a_2 &= 16(\gamma_{21}^2 (\Delta_c - \Delta) + \gamma_{31}^2 \Delta_p) |\Omega_c|^2 \\
&\quad + 8\gamma^m \Delta_p (4\Delta_c \Delta + \gamma_{21}\gamma_s) \\
a_4 &= 16\gamma^m \Delta_p
\end{aligned}
\quad , \tag{A.2}
$$

$$
\begin{aligned}
b_0 &= \gamma^m I_c^s (4\Delta^2 + \gamma_s^2) + 16\gamma^m |\Omega_c|^4 \\
&\quad + 4\gamma_{21} (-8\gamma_{31}\Delta_c\Delta + \gamma_s (4\Delta^2 + \gamma_s^2 - 2\gamma^m)) |\Omega_c|^2 \\
b_2 &= 16(\gamma_s^2 - 2\gamma^m) |\Omega_c|^2 + 8\gamma^m (4\Delta_c\Delta + \gamma_{21}\gamma_s) \\
b_4 &= 16\gamma^m
\end{aligned}
\quad , \tag{A.3}
$$

$$
\begin{aligned}
d_0 &= \gamma^m I_c^s I_p^s (4\Delta^2 + \gamma_s^2) + 128\gamma^m |\Omega_c|^6 \\
&\quad + 16\gamma^m (I_c^s - 16\Delta_p\Delta + 4\gamma_{31}\gamma_s) |\Omega_c|^4 \\
&\quad + 8\gamma^m (I_c^s (4\Delta_c\Delta_p + \gamma^m + 2\gamma_{31}^2) \\
&\quad + I_p^s (I_p^s - 8\Delta_c\Delta_p + 2\gamma^m)) |\Omega_c|^2 \\
d_2 &= 128(\gamma_s^2 - \gamma^m) |\Omega_c|^4 \\
&\quad + 32(3\gamma^m (4\Delta^2 + \gamma^m) - 4\Delta_c\Delta_p (\gamma_s^2 - 2\gamma^m) \\
&\quad + 2\gamma^m (\gamma_s^2 - 2\gamma^m) + \gamma_{21}^2 (I_c^s + 2\Delta_p^2) \\
&\quad + \gamma_{31}^2 (I_p^s + 2\Delta_c^2)) |\Omega_c|^2 + 8\gamma^m (I_p^s (4\Delta_c\Delta_p + \gamma^m + 2\gamma_{21}^2) \\
&\quad + I_c^s (I_c^s - 8\Delta_c\Delta_p + 2\gamma^m)) \\
d_4 &= 128(\gamma_s^2 - \gamma^m) |\Omega_c|^2 \\
&\quad + 16\gamma^m (I_p^s + 16\Delta_c\Delta + 4\gamma_{21}\gamma_s) \\
d_6 &= 128\gamma^m
\end{aligned}
\quad , \tag{A.4}
$$

where

$$\begin{aligned} &\gamma_s = \gamma_{21} + \gamma_{31}, \quad \gamma_d = \gamma_{21} - \gamma_{31}, \quad \gamma^m = \gamma_{21}\gamma_{31}, \\ &2\delta = (\Delta_p + \Delta_c), \quad \Delta = (\Delta_p - \Delta_c), \\ &I_p^s = (4\Delta_p^2 + \gamma_{31}^2), \quad I_c^s = (4\Delta_c^2 + \gamma_{21}^2) \end{aligned} \quad . \tag{A.5}$$

Bibliography

[1]Moshe Shapiro and Paul Brumer, *Quantum control of molecular processes*, Second (Wiley-VCH-Verl, Weinheim, 2012).

[2]Bruce W. Shore, "Picturing stimulated Raman adiabatic passage: a STIRAP tutorial", Adv. Opt. Photon **9**, 563–719 (2017).

[3]Bruce W. Shore, *Manipulating quantum structures using laser pulses*, First (Cambridge Univ. Press, Cambridge, 2011).

[4]Harold Metcalf, "*Colloquium* : Strong optical forces on atoms in multifrequency light", Rev. Mod. Phys. **89**, 041001 (2017).

[5]Wolfgang Demtröder, *Atoms, Molecules and Photons: An Introduction to Atomic-, Molecular- and Quantum Physics*, Graduate Texts in Physics (Springer Berlin Heidelberg, Berlin, Heidelberg, 2018).

[6]G. Alzetta, A. Gozzini, L. Moi, and G. Orriols, "An experimental method for the observation of r.f. transitions and laser beat resonances in oriented Na vapour", Nuovo Cimento B **36**, 5–20 (1976).

[7]E. Arimondo and G. Orriols, "Nonabsorbing atomic coherences by coherent two-photon transitions in a three-level optical pumping", Lett. Nuovo Cimento **17**, 333–338 (1976).

[8]F. T. Hioe and J. H. Eberly, "Nonlinear constants of motion for three-level quantum systems", Phys. Rev. A **25**, 2168–2171 (1982).

[9]G. P. Zhang and Thomas F. George, "Proposed Coherent Trapping of a Population of Electrons in a C 60 Molecule Induced by Laser Excitation", Phys. Rev. Lett. **109**, 257401 (2012).

[10]G P Zhang, "Hidden identity in a generic Λ system: applications to coherent population trapping", J. Phys. B **46**, 035504 (2013).

[11]K.-J. Boller, A. Imamoğlu, and S. E. Harris, "Observation of electromagnetically induced transparency", Phys. Rev. Lett. **66**, 2593–2596 (1991).

[12]M. D. Lukin and A. Imamoğlu, "Controlling photons using electromagnetically induced transparency", Nature **413**, 273–276 (2001).

[13]Michael Fleischhauer, Atac Imamoglu, and Jonathan P. Marangos, "Electromagnetically induced transparency: Optics in coherent media", Rev. Mod. Phys. **77**, 633–673 (2005).

[14]Benjamin Dive, Nikolaos Koukoulekidis, Stefanos Mousafeiris, and Florian Mintert, "Characterization of multilevel quantum coherence without ideal measurements", Phys. Rev. Research **2**, 013220 (2020).

[15]Klaus Hornberger, Stefan Gerlich, Philipp Haslinger, Stefan Nimmrichter, and Markus Arndt, "Colloquium: Quantum interference of clusters and molecules", Rev. Mod. Phys. **84**, 157–173 (2012).

[16]Shiue-Yuan Shiau and Monique Combescot, "Optical Signature of Quantum Coherence in Fully Dark Exciton Condensates", Phys. Rev. Lett. **123**, 097401 (2019).

[17]Bijita Sarma and Amarendra K. Sarma, "Quantum-interference-assisted photon blockade in a cavity via parametric interactions", Phys. Rev. A **96**, 053827 (2017).

[18]Chengyi Luo, Jiahao Huang, Xiangdong Zhang, and Chaohong Lee, "Heisenberg-limited Sagnac interferometer with multiparticle states", Phys. Rev. A **95**, 023608 (2017).

[19]Luca Pezzè, Augusto Smerzi, Markus K. Oberthaler, Roman Schmied, and Philipp Treutlein, "Quantum metrology with nonclassical states of atomic ensembles", Rev. Mod. Phys. **90**, 035005 (2018).

[20]M. J. Martin, M. Bishof, M. D. Swallows, X. Zhang, C. Benko, J. von-Stecher, A. V. Gorshkov, A. M. Rey, and Jun Ye, "A Quantum Many-Body Spin System in an Optical Lattice Clock", Science **341**, 632–636 (2013).

[21]M. D. Swallows, M. Bishof, Y. Lin, S. Blatt, M. J. Martin, A. M. Rey, and J. Ye, "Suppression of Collisional Shifts in a Strongly Interacting Lattice Clock", Science **331**, 1043–1046 (2011).

[22]Tomasz Wasak and Jan Chwedeńczuk, "Bell Inequality, Einstein-Podolsky-Rosen Steering, and Quantum Metrology with Spinor Bose-Einstein Condensates", Phys. Rev. Lett. **120**, 140406 (2018).

[23]Andy Brown, Amitabh Joshi, and Min Xiao, "Controlled steady-state switching in optical bistability", Appl. Phys. Lett. **83**, 1301–1303 (2003).

[24]Hong Chang, Haibin Wu, Changde Xie, and Hai Wang, "Controlled Shift of Optical Bistability Hysteresis Curve and Storage of Optical Signals in a Four-Level Atomic System", Phys. Rev. Lett. **93**, 213901 (2004).

[25]Jiteng Sheng, Utsab Khadka, and Min Xiao, "Realization of All-Optical Multistate Switching in an Atomic Coherent Medium", Phys. Rev. Lett. **109**, 223906 (2012).

[26]Jiteng Sheng, Junfeng Wang, and Min Xiao, "Synchronous control of dual-channel all-optical multistate switching", Opt. Lett. **38**, 5369 (2013).

[27]Jay E. Sharping, Yoshitomo Okawachi, James van Howe, Chris Xu, Yan Wang, Alan E. Willner, and Alexander L. Gaeta, "All-optical, wavelength and bandwidth preserving, pulse delay based on parametric wavelength conversion and dispersion", Opt. Express **13**, 7872–7877 (2005).

[28]Jay E. Sharping, Yoshitomo Okawachi, and Alexander L. Gaeta, "Wide bandwidth slow light using a Raman fiber amplifier", Opt. Express **13**, 6092–6098 (2005).

[29]Robert W. Boyd, Daniel J. Gauthier, and Alexander L. Gaeta, "Applications of Slow Light in Telecommunications", Opt. Photon. News **17**, 18 (2006).

[30]S. Residori, U. Bortolozzo, and J. P. Huignard, "Slow and Fast Light in Liquid Crystal Light Valves", Phys. Rev. Lett. **100**, 203603 (2008).

[31]R. W. Boyd and D. J. Gauthier, "Controlling the Velocity of Light Pulses", Science **326**, 1074–1077 (2009).

[32]Robert W. Boyd, "Slow and fast light: fundamentals and applications", J. Mod. Opt. **56**, 1908–1915 (2009).

[33]B. Megyeri, G. Harvie, A. Lampis, and J. Goldwin, "Directional Bistability and Nonreciprocal Lasing with Cold Atoms in a Ring Cavity", Phys. Rev. Lett. **121**, 163603 (2018).

[34]Evgeny V. Anikin, Natalya S. Maslova, Nikolay A. Gippius, and Igor M. Sokolov, "Enhanced excitation of a driven bistable system induced by spectrum degeneracy", Phys. Rev. A **100**, 043842 (2019).

[35]Leonard Mandel and Emil Wolf, *Optical coherence and quantum optics* (Cambridge university press, 1995).

[36]A. Szöke, V. Daneu, J. Goldhar, and N. A. Kurnit, "Bistable Optical Element and Its Applications", Appl. Phys. Lett. **15**, 376–379 (1969).

[37]T. N. C. Venkatesan and S. L. McCall, "Optical bistability and differential gain between 85 and 296 °K in a Fabry-Perot containing ruby", Appl. Phys. Lett. **30**, 282–284 (1977).

[38]H. M. Gibbs, S. L. McCall, and T. N. C. Venkatesan, "Differential Gain and Bistability Using a Sodium-Filled Fabry-Perot Interferometer", Phys. Rev. Lett. **36**, 1135–1138 (1976).

[39]R. Bonifacio and L. A. Lugiato, "Optical bistability and cooperative effects in resonance fluorescence", Phys. Rev. A **18**, 1129–1144 (1978).

[40]A. T. Rosenberger, L. A. Orozco, H. J. Kimble, and P. D. Drummond, "Absorptive optical bistability in two-state atoms", Phys. Rev. A **43**, 6284–6302 (1991).

[41]Jing Wu, Xin-You Lü, and Li-Li Zheng, "Controllable optical bistability and multistability in a double two-level atomic system", J. Phys. B **43**, 161003 (2010).

[42]M. Kitano, T. Yabuzaki, and T. Ogawa, "Optical Tristability", Phys. Rev. Lett. **46**, 926–929 (1981).

[43] S. Cecchi, G. Giusfredi, E. Petriella, and P. Salieri, "Observation of Optical Tristability in Sodium Vapors", Phys. Rev. Lett. **49**, 1928–1931 (1982).

[44] C. M. Savage, H. J. Carmichael, and D. F. Walls, "Optical multistability and self oscillations in three level systems", Opt. Commun. **42**, 211–216 (1982).

[45] W. Harshawardhan and G. S. Agarwal, "Controlling optical bistability using electromagnetic-field-induced transparency and quantum interferences", Phys. Rev. A **53**, 1812–1817 (1996).

[46] Amitabh Joshi, Andy Brown, Hai Wang, and Min Xiao, "Controlling optical bistability in a three-level atomic system", Phys. Rev. A **67**, 041801 (2003).

[47] Amitabh Joshi and Min Xiao, "Optical Multistability in Three-Level Atoms inside an Optical Ring Cavity", Phys. Rev. Lett. **91**, 143904 (2003).

[48] R. J. Cook, "Atomic motion in resonant radiation: An application of Ehrenfest's theorem", Phys. Rev. A **20**, 224–228 (1979).

[49] J. P. Gordon and A. Ashkin, "Motion of atoms in a radiation trap", Phys. Rev. A **21**, 1606–1617 (1980).

[50] Yohai Roichman, Bo Sun, Yael Roichman, Jesse Amato-Grill, and David G. Grier, "Optical Forces Arising from Phase Gradients", Phys. Rev. Lett. **100**, 013602 (2008).

[51] J. E. Bjorkholm, R. R. Freeman, A. Ashkin, and D. B. Pearson, "Observation of Focusing of Neutral Atoms by the Dipole Forces of Resonance-Radiation Pressure", Phys. Rev. Lett. **41**, 1361–1364 (1978).

[52] Richard Fitzpatrick, *Oscillations and waves: an introduction*, First (CRC Press, Boca Raton, Fla., 2013).

[53] Léon Brillouin, *Wave propagation and group velocity*, Vol. 8, Pure and Applied Physics (Elsevier, New York, 1960).

[54] Alexander M Akulshin and Russell J McLean, "Fast light in atomic media", J. Opt. **12**, 104001 (2010).

[55] C. G. B. Garrett and D. E. McCumber, "Propagation of a Gaussian Light Pulse through an Anomalous Dispersion Medium", Phys. Rev. A **1**, 305–313 (1970).

[56]Raymond Y. Chiao, "Superluminal (but causal) propagation of wave packets in transparent media with inverted atomic populations", Phys. Rev. A **48**, R34–R37 (1993).

[57]Eric L. Bolda, John. C. Garrison, and Raymond Y. Chiao, "Optical pulse propagation at negative group velocities due to a nearby gain line", Phys. Rev. A **49**, 2938–2947 (1994).

[58]Michael D. Stenner, Mark A. Neifeld, Zhaoming Zhu, Andrew M. C. Dawes, and Daniel J. Gauthier, "Distortion management in slow-light pulse delay", Opt. Express **13**, 9995–10002 (2005).

[59]Peter W. Milonni, *Fast light, slow light and left-handed light*, Series in Optics and Optoelectronics (Taylor & Francis, New York, NY, 2005).

[60]Robert W. Boyd and Paul Narum, "Slow- and fast-light: fundamental limitations", J. Mod. Opt. **54**, 2403–2411 (2007).

[61]Lene Vestergaard Hau, S. E. Harris, Zachary Dutton, and Cyrus H. Behroozi, "Light speed reduction to 17 metres per second in an ultracold atomic gas", Nature **397**, 594–598 (1999).

[62]Michael M. Kash, Vladimir A. Sautenkov, Alexander S. Zibrov, L. Hollberg, George R. Welch, Mikhail D. Lukin, Yuri Rostovtsev, Edward S. Fry, and Marlan O. Scully, "Ultraslow Group Velocity and Enhanced Nonlinear Optical Effects in a Coherently Driven Hot Atomic Gas", Phys. Rev. Lett. **82**, 5229–5232 (1999).

[63]D. Budker, D. F. Kimball, S. M. Rochester, and V. V. Yashchuk, "Nonlinear Magneto-optics and Reduced Group Velocity of Light in Atomic Vapor with Slow Ground State Relaxation", Phys. Rev. Lett. **83**, 1767–1770 (1999).

[64]D. Walls, P. Zoller, and M. Steyn-Ross, "Optical bistability from three-level atoms", IEEE J. Quantum Electron. **17**, 380–384 (1981).

[65]M A Antón and Oscar G Calderón, "Optical bistability using quantum interference in V -type atoms", J. Opt. B **4**, 91–98 (2002).

[66]M.A. Antón, Oscar G. Calderón, and F. Carreño, "Optical bistability in V-type atoms driven by a coherent field in a broadband squeezed vacuum", Phys. Lett. A **311**, 297–312 (2003).

[67] Amitabh Joshi, Wenge Yang, and Min Xiao, "Effect of quantum interference on optical bistability in the three-level V-type atomic system", Phys. Rev. A **68**, 015806 (2003).

[68] K. I. Osman, "Effects of the control field on the optical multistability in V-type three-level atomic system", Opt. Commun. **259**, 194–199 (2006).

[69] Jiahua Li, "Coherent control of optical bistability in a microwave-driven V-type atomic system", Physica D **228**, 148–152 (2007).

[70] Zhiping Wang and Miaocun Xu, "Control of the switch between optical multistability and bistability in three-level V-type atoms", Opt. Commun. **282**, 1574–1578 (2009).

[71] S M Mousavi, L Safari, M Mahmoudi, and M Sahrai, "Effect of quantum interference on the optical properties of a three-level V-type atomic system beyond the two-photon resonance condition", J. Phys. B **43**, 165501 (2010).

[72] Ya-Nan Li, Yu-Yuan Chen, and Ren-Gang Wan, "All-optical switching and flip-flop based on dynamically controlled bistability in a V-type atomic system", J. Opt. Soc. Am. B **36**, 1799 (2019).

[73] S. E. Harris, J. E. Field, and A. Kasapi, "Dispersive properties of electromagnetically induced transparency", Phys. Rev. A **46**, R29–R32 (1992).

[74] G. S. Agarwal, Tarak Nath Dey, and Sunish Menon, "Knob for changing light propagation from subluminal to superluminal", Phys. Rev. A **64**, 053809 (2001).

[75] Mostafa Sahrai, Habib Tajalli, Kishore T. Kapale, and M. Suhail Zubairy, "Tunable phase control for subluminal to superluminal light propagation", Phys. Rev. A **70**, 023813 (2004).

[76] Kyoungdae Kim, Han Seb Moon, Chunghee Lee, Soo Kyoung Kim, and Jung Bog Kim, "Observation of arbitrary group velocities of light from superluminal to subluminal on a single atomic transition line", Phys. Rev. A **68**, 013810 (2003).

[77] Jiepeng Zhang, Gessler Hernandez, and Yifu Zhu, "Copropagating superluminal and slow light manifested by electromagnetically assisted nonlinear optical processes", Opt. Lett. **31**, 2598 (2006).

[78]Parvendra Kumar and Amarendra K. Sarma, "Optical dipole force on ladderlike three-level atomic systems induced by few-cycle-pulse laser fields", Phys. Rev. A **86**, 053414 (2012).

[79]Daniel A Steck, *Quantum and Atom Optics*, available online at http://steck.us/teaching, Sept. 2020.

[80]Peter W. Milonni and Joseph H. Eberly, *Laser physics* (Wiley, Hoboken, NJ, 2010).

[81]Robert W Boyd, *Nonlinear Optics*, Fourth (Elsevier, 2020).

[82]L. J. Wang, A. Kuzmich, and A. Dogariu, "Gain-assisted superluminal light propagation", Nature **406**, 277–279 (2000).

[83]M. H. Anderson, J. R. Ensher, M. R. Matthews, C. E. Wieman, and E. A. Cornell, "Observation of Bose-Einstein Condensation in a Dilute Atomic Vapor", Science **269**, 198–201 (1995).

[84]Harold J. Metcalf and Peter van Straten, *Laser cooling and trapping*, Second, Graduate Texts in Contemporary Physics (Springer, New York Berlin Heidelberg, 2002).

[85]J. Ignacio Cirac and Peter Zoller, "New Frontiers in Quantum Information With Atoms and Ions", Physics Today **57**, 38–44 (2004).

[86]Yuqiang Jiang, Tetsuya Narushima, and Hiromi Okamoto, "Nonlinear optical effects in trapping nanoparticles with femtosecond pulses", Nature Phys **6**, 1005–1009 (2010).

[87]Markus Aspelmeyer, Tobias J. Kippenberg, and Florian Marquardt, "Cavity optomechanics", Rev. Mod. Phys. **86**, 1391–1452 (2014).

[88]Parvendra Kumar and Amarendra K. Sarma, "Optical force on two-level atoms by few-cycle-pulse Gaussian laser fields beyond the rotating-wave approximation", Phys. Rev. A **84**, 043402 (2011).

[89]Thomas Brabec and Ferenc Krausz, "Intense few-cycle laser fields: Frontiers of nonlinear optics", Rev. Mod. Phys. **72**, 545–591 (2000).

[90]Parvendra Kumar and Amarendra K. Sarma, "Gaussian and sinc-shaped few-cycle-pulse-driven ultrafast coherent population transfer in Λ -like atomic systems", Phys. Rev. A **85**, 043417 (2012).

[91]Subhadeep Chakraborty and Amarendra K. Sarma, "Optical trap potential control in N-type four-level atoms by femtosecond Gaussian pulses", J. Opt. Soc. Am. B **32**, 270 (2015).

[92]Pawan Kumar, Parvendra Kumar, and Amarendra K. Sarma, "Simultaneous control of optical dipole force and coherence creation by super-Gaussian femtosecond pulses in Λ -like atomic systems", Phys. Rev. A **89**, 033422 (2014).

[93]Nikolay V Vitanov, Thomas Halfmann, Bruce W Shore, and Klaas Bergmann, "Laser-Induced Population Transfer by Adiabatic Passage Techniques", Annu. Rev. Phys. Chem. **52**, 763–809 (2001).

[94]Moshe Shapiro and Paul Brumer, "Coherent Control of Atomic, Molecular, and Electronic Processes", in *Advances In Atomic, Molecular, and Optical Physics*, Vol. 42, edited by Benjamin Bederson and Herbert Walther (Academic Press, Jan. 2000), pp. 287–345.

[95]Petr Král, Ioannis Thanopulos, and Moshe Shapiro, "Colloquium: Coherently controlled adiabatic passage", Rev. Mod. Phys. **79**, 53–77 (2007).

[96]Amitabh Joshi, Wenge Yang, and Min Xiao, "Effect of spontaneously generated coherence on optical bistability in three-level Λ-type atomic system", Phys. Lett. A **315**, 203–207 (2003).

[97]Dong-chao Cheng, Cheng-pu Liu, and Shang-qing Gong, "Optical bistability and multistability via the effect of spontaneously generated coherence in a three-level ladder-type atomic system", Phys. Lett. A **332**, 244–249 (2004).

[98]Hossein Jafarzadeh, Mostafa Sahrai, and Kazem Jamshidi-Ghaleh, "Controlling the optical bistability in a Λ-type atomic system via incoherent pump field", Appl. Phys. B **117**, 927–933 (2014).

[99]Zhen Wang, Ai-Xi Chen, Yanfeng Bai, Wen-Xing Yang, and Ray-Kuang Lee, "Coherent control of optical bistability in an open Λ-type three-level atomic system", J. Opt. Soc. Am. B **29**, 2891 (2012).

[100]Seyyed Hossein Asadpour, Hamid Reza Hamedi, and Hamid Rahimpour Soleimani, "Optical bistability and multistability in an open ladder-type atomic system", J. Mod. Opt. **60**, 659–665 (2013).

[101]Lü Xin-You, Li Jia-Hua, Liu Ji-Bing, and Luo Jin-Ming, "Optical bistability via quantum interference in a four-level atomic medium", J. Phys. B **39**, 5161–5171 (2006).

[102]Arijit Sharma, Tridib Ray, Rahul V. Sawant, G. Sheikholeslami, S. A. Rangwala, and D. Budker, "Optical control of resonant light transmission for an atom-cavity system", Phys. Rev. A **91**, 043824 (2015).

[103]Rahul Sawant and S. A. Rangwala, "Optical-bistability-enabled control of resonant light transmission for an atom-cavity system", Phys. Rev. A **93**, 023806 (2016).

[104]Pardeep Kumar and Shubhrangshu Dasgupta, "Optical switching and bistability in four-level atomic systems", Phys. Rev. A **94**, 023851 (2016).

[105]Seyyed Hossein Asadpour and Abdullah Eslami-Majd, "Controlling the optical bistability and transmission coefficient in a four-level atomic medium", J. Lumin. **132**, 1477–1482 (2012).

[106]Azar Vafafard, Hadisossadat Zaakeri, Lida Ebrahimi Zohravi, and Mohammad Mahmoudi, "Phase-controlled optical bistability via electromagnetically induced absorption", J. Opt. Soc. Am. B **31**, 1981 (2014).

[107]Xionghui Hu, Hongjun Zhang, Hui Sun, Yaohua Lei, Huijing Li, and Wei Liu, "Phase control of optical bistability and multistability in a tripod four-level atomic medium", Appl. Opt. **55**, 6263 (2016).

[108]Dinh Xuan Khoa, Le Van Doai, Le Nguyen Mai Anh, Le Canh Trung, Phan Van Thuan, Nguyen Tien Dung, and Nguyen Huy Bang, "Optical bistability in a five-level cascade EIT medium: an analytical approach", J. Opt. Soc. Am. B **33**, 735 (2016).

[109]Hannes Gothe, Tristan Valenzuela, Matteo Cristiani, and Jürgen Eschner, "Optical bistability and nonlinear dynamics by saturation of cold Yb atoms in a cavity", Phys. Rev. A **99**, 013849 (2019).

[110]C. D. Herold, V. D. Vaidya, X. Li, S. L. Rolston, J. V. Porto, and M. S. Safronova, "Precision Measurement of Transition Matrix Elements via Light Shift Cancellation", Phys. Rev. Lett. **109**, 243003 (2012).

[111]J. E. Sansonetti, "Wavelengths, Transition Probabilities, and Energy Levels for the Spectra of Rubidium (Rb I through Rb XXXVII)", J. Phys. Chem. Ref. Data **35**, 301–421 (2006).

[112]C. B. Alcock, V. P. Itkin, and M. K. Horrigan, "Vapour Pressure Equations for the Metallic Elements: 298–2500K", Can. Metall. Q. **23**, 309–313 (1984).

[113]Dong Sun, Hongjun Zhang, and Hui Sun, "Controllable optical bistability and multistability in asymmetric quantum wells via Fano-type interference", J. Phys. B **52**, 035501 (2019).

[114]Zhiping Wang and Benli Yu, "Switching from optical bistability to multistability in a coupled semiconductor double-quantum-dot nanostructure", J. Opt. Soc. Am. B **30**, 2915 (2013).

[115]G. Solookinejad, M. Jabbari, M. Nafar, E. Ahmadi, and S. H. Asadpour, "Incoherent control of optical bistability and multistability in a hybrid system: Metallic nanoparticle-quantum dot nanostructure", J. Appl. Phys. **124**, 063102 (2018).

[116]A. H. Safavi-Naeini, T. P. Mayer Alegre, J. Chan, M. Eichenfield, M. Winger, Q. Lin, J. T. Hill, D. E. Chang, and O. Painter, "Electromagnetically induced transparency and slow light with optomechanics", Nature **472**, 69–73 (2011).

[117]Qinghong Liao, Xing Xiao, Wenjie Nie, and Nanrun Zhou, "Transparency and tunable slow-fast light in a hybrid cavity optomechanical system", Opt. Express **28**, 5288 (2020).

[118]Luc Thévenaz, "Slow and fast light in optical fibres", Nature Photon. **2**, 474–481 (2008).

[119]E. Podivilov, B. Sturman, A. Shumelyuk, and S. Odoulov, "Light Pulse Slowing Down up to 0.025 cm/s by Photorefractive Two-Wave Coupling", Phys. Rev. Lett. **91**, 083902 (2003).

[120]Nacera Bouldja, Marc Sciamanna, and Delphine Wolfersberger, "Improved slow light performances using photorefractive two-wave mixing", Opt. Lett. **44**, 1496 (2019).

[121]C. Goyon, M. R. Edwards, T. Chapman, L. Divol, N. Lemos, G. J. Williams, D. A. Mariscal, D. Turnbull, A. M. Hansen, and P. Michel, "Slow and Fast Light in Plasma Using Optical Wave Mixing", Phys. Rev. Lett. **126**, 205001 (2021).

[122]Chien Liu, Zachary Dutton, Cyrus H. Behroozi, and Lene Vestergaard Hau, "Observation of coherent optical information storage in an atomic medium using halted light pulses", Nature **409**, 490–493 (2001).

[123]D. F. Phillips, A. Fleischhauer, A. Mair, R. L. Walsworth, and M. D. Lukin, "Storage of Light in Atomic Vapor", Phys. Rev. Lett. **86**, 783–786 (2001).

[124]Toshihiro Nakanishi and Masao Kitano, "Storage and retrieval of electromagnetic waves using electromagnetically induced transparency in a nonlinear metamaterial", Appl. Phys. Lett. **112**, 201905 (2018).

[125]Aephraim M. Steinberg and Raymond Y. Chiao, "Dispersionless, highly superluminal propagation in a medium with a gain doublet", Phys. Rev. A **49**, 2071–2075 (1994).

[126]G. S. Agarwal and Shubhrangshu Dasgupta, "Superluminal propagation via coherent manipulation of the Raman gain process", Phys. Rev. A **70**, 023802 (2004).

[127]Matthew S. Bigelow, Nick N. Lepeshkin, and Robert W. Boyd, "Observation of Ultraslow Light Propagation in a Ruby Crystal at Room Temperature", Phys. Rev. Lett. **90**, 113903 (2003).

[128]M. S. Bigelow, "Superluminal and Slow Light Propagation in a Room-Temperature Solid", Science **301**, 200–202 (2003).

[129]Hua Cao, A. Dogariu, and L.J. Wang, "Negative group delay and pulse compression in superluminal pulse propagation", IEEE J. Select. Topics Quantum Electron. **9**, 52–58 (2003).

[130]Charles M. Bowden and Jonathan P. Dowling, "Near–dipole-dipole effects in dense media: Generalized Maxwell-Bloch equations", Phys. Rev. A **47**, 1247–1251 (1993).

[131]Keyu Xia, Shangqing Gong, Chengpu Liu, Xiaohong Song, and Yueping Niu, "Near dipole-dipole effects on the propagation of few-cycle pulse in a dense two-level medium", Opt. Express **13**, 5913 (2005).

[132]K. B. Davis, M. -O. Mewes, M. R. Andrews, N. J. van Druten, D. S. Durfee, D. M. Kurn, and W. Ketterle, "Bose-Einstein Condensation in a Gas of Sodium Atoms", Phys. Rev. Lett. **75**, 3969–3973 (1995).

[133]J. E. Sansonetti, "Wavelengths, Transition Probabilities, and Energy Levels for the Spectra of Sodium (NaI–NaXI)", J. Phys. Chem. Ref. Data **37**, 1659–1763 (2008).

[134]Daniel Adam Steck, *Sodium D Line Data*, available online at `https://steck.us/alkalidata`, Nov. 2019.

[135]I. Sydoryk, N. N. Bezuglov, I. I. Beterov, K. Miculis, E. Saks, A. Janovs, P. Spels, and A. Ekers, "Broadening and intensity redistribution in the Na(3p) hyperfine excitation spectra due to optical pumping in the weak excitation limit", Phys. Rev. A **77**, 042511 (2008).

[136]Jiazhong Hu, Alban Urvoy, Zachary Vendeiro, Valentin Crépel, Wenlan Chen, and Vladan Vuletić, "Creation of a Bose-condensed gas of ^{87} Rb by laser cooling", Science **358**, 1078–1080 (2017).

[137]S. L. Campbell, R. B. Hutson, G. E. Marti, A. Goban, N. Darkwah Oppong, R. L. McNally, L. Sonderhouse, J. M. Robinson, W. Zhang, B. J. Bloom, and J. Ye, "A Fermi-degenerate three-dimensional optical lattice clock", Science **358**, 90–94 (2017).

[138]Simon Stellmer, Benjamin Pasquiou, Rudolf Grimm, and Florian Schreck, "Laser Cooling to Quantum Degeneracy", Phys. Rev. Lett. **110**, 263003 (2013).

[139]Mark Kasevich and Steven Chu, "Laser cooling below a photon recoil with three-level atoms", Phys. Rev. Lett. **69**, 1741–1744 (1992).

[140]Marshall T. DePue, Colin McCormick, S. Lukman Winoto, Steven Oliver, and David S. Weiss, "Unity Occupation of Sites in a 3D Optical Lattice", Phys. Rev. Lett. **82**, 2262–2265 (1999).

[141]A. Ashkin, "Acceleration and Trapping of Particles by Radiation Pressure", Phys. Rev. Lett. **24**, 156–159 (1970).

[142]A. Ashkin, J. M. Dziedzic, J. E. Bjorkholm, and Steven Chu, "Observation of a single-beam gradient force optical trap for dielectric particles", Opt. Lett. **11**, 288 (1986).

[143]Steven Chu, J. E. Bjorkholm, A. Ashkin, and A. Cable, "Experimental Observation of Optically Trapped Atoms", Phys. Rev. Lett. **57**, 314–317 (1986).

[144]Dongliang Gao, Weiqiang Ding, Manuel Nieto-Vesperinas, Xumin Ding, Mahdy Rahman, Tianhang Zhang, ChweeTeck Lim, and Cheng-Wei Qiu, "Optical manipulation from the microscale to the nanoscale: fundamentals, advances and prospects", Light Sci. Appl. **6**, e17039–e17039 (2017).

[145]A.M. Weiner, D.E. Leaird, J.S. Patel, and J.R. Wullert, "Programmable shaping of femtosecond optical pulses by use of 128-element liquid crystal phase modulator", IEEE J. Quantum Electron. **28**, 908–920 (1992).

[146]S. Witte, R. Th. Zinkstok, W. Hogervorst, and K. S. E. Eikema, "Generation of few-cycle terawatt light pulses using optical parametric chirped pulse amplification", Opt. Express **13**, 4903 (2005).

[147]Zhaoyang Li and Noriaki Miyanaga, "Simulating ultra-intense femtosecond lasers in the 3-dimensional space-time domain", Opt. Express **26**, 8453 (2018).

[148]A. Ashkin, "Optical trapping and manipulation of neutral particles using lasers", Proc. Natl. Acad. Sci. USA **94**, 4853–4860 (1997).

[149]Pierre Meystre, *Atom Optics*, Springer Series on Atomic, Optical, and Plasma Physics (Springer-Verlag, New York, 2001).

[150]Kishan Dholakia and Pavel Zemánek, "*Colloquium* : Gripped by light: Optical binding", Rev. Mod. Phys. **82**, 1767–1791 (2010).

[151]G. Juzeliūnas and P. Öhberg, "Optical Manipulation of Ultracold Atoms", in *Structured Light and Its Applications* (Elsevier, 2008), pp. 295–333.

[152]A. Ashkin, "Applications of Laser Radiation Pressure", Science **210**, 1081–1088 (1980).

[153]A. Goepfert, I. Bloch, D. Haubrich, F. Lison, R. Schütze, R. Wynands, and D. Meschede, "Stimulated focusing and deflection of an atomic beam using picosecond laser pulses", Phys. Rev. A **56**, R3354–R3357 (1997).

[154]Ivan Kozyryev, Louis Baum, Leland Aldridge, Phelan Yu, Edward E. Eyler, and John M. Doyle, "Coherent Bichromatic Force Deflection of Molecules", Phys. Rev. Lett. **120**, 063205 (2018).

[155]Z. Feng, S. Ebser, L. Ringena, F. Ritterbusch, and M. K. Oberthaler, "Bichromatic force on metastable argon for atom-trap trace analysis", Phys. Rev. A **96**, 013424 (2017).

[156]S. E. Galica, L. Aldridge, and E. E. Eyler, "Four-color stimulated optical forces for atomic and molecular slowing", Phys. Rev. A **88**, 043418 (2013).

[157]T. Lu, X. Miao, and H. Metcalf, "Bloch theorem on the Bloch sphere", Phys. Rev. A **71**, 061405 (2005).

[158]X. Miao, E. Wertz, M. G. Cohen, and H. Metcalf, "Strong optical forces from adiabatic rapid passage", Phys. Rev. A **75**, 011402 (2007).

[159]Yuan Sun and Harold Metcalf, "Nonadiabaticity in stimulated Raman adiabatic passage", Phys. Rev. A **90**, 033408 (2014).

[160]Christopher Corder, Brian Arnold, and Harold Metcalf, "Laser Cooling without Spontaneous Emission", Phys. Rev. Lett. **114**, 043002 (2015).

[161]Pidong Hu, Yueping Niu, Xiangxin Wang, Shangqing Gong, and Chengpu Liu, "Generation of attosecond pulse pair in polar media by chirped few-cycle pulses", J. Opt. **18**, 095504 (2016).

[162]S. Hamideh Kazemi and Mohammad Mahmoudi, "Phase-controlled optical trap potential in a closed-loop atomic system", J. Opt. Soc. Am. B **33**, 479 (2016).

Vita

Abdelsalam Hassan Muhammad Abdelaziz was born on 29th June, 1982 in Dakahliya, Egypt. He received his B.Sc. from Ain Shams University at Cairo in 2003. He joined Suez Canal University at Ismailia as a demonstrator in 2005, where he received his M.Sc. in 2013. Subsequently, he promoted to the position of an Assistant Lecturer. He awarded a PhD scholarship from the Indian council for cultural relations (ICCR). Then, he enrolled into the Ph.D program at the Indian Institute of Technology Guwahati in July, 2016. He now finds great joy in doing science!